Bij het afronden van dit proefschrift zou ik graag de volgende personen willen bedanken:

Prof. dr. J. Gelan en Prof. dr. D. Vanderzande die mij de mogelijkheid gegeven hebben deze interessante studie aan te vatten aan het LUC en voor het vertrouwen dat ze in me hadden voor het uitvoeren van dit toch wel dure onderzoek.
Prof. dr. J. Gelan voor zijn interesse in de evolutie van mijn solid state NMR onderzoek op de gelabelde polymeren en voor zijn hulp bij het interpreteren van de resultaten.
Prof. dr. P. Adriaensens voor het aanleren van de vele NMR technieken, voor zijn kritische ingesteldheid bij het nalezen van publicaties, voor het 'brainstormen' rond de bekomen resultaten en het sturen van dit onderzoek. Peter, ik heb veel van je geleerd!
Dr. L. Lutsen voor de feedback over de uitgevoerde optische en elektronische metingen op de gesynthetiseerde polymeren.
Anne, Liesbet, Robby en Koen die steeds klaarstonden voor het opvangen van mijn kleine NMR probleempjes en voor de gezellige babbels tussendoor.
Huguette, Iris, Lieve, Filip, Stijn, Joachim, Els, Veerle, Anja, Roel, Ine, Lien, Sofie en Kristof voor de toffe momenten in het labo, het delen van lief en leed op de bureau. Ik zal later met veel plezier terugdenken aan deze leuke jaren. Speciale dank aan Huguette voor de FT-IR en UV-Vis opnames, en aan Iris en Veerle voor de GPC analyses.
Het team van Prof. dr. R. Carleer voor de aangename middagpauzes en in het bijzonder Martine en Guy voor het uitvoeren van de DSC en rheologie analyses, en Jan voor het opnemen van de massaspectra.
Richard for teaching me the "step-by-step" fitting and for the WAXS measurements he carried out in Poland.
Jos die steeds klaar stond om het gebroken glaswerk te herstellen en wideline buisjes bij te maken.
Christel voor de nodige productbestellingen en het secretariaat van SBG voor alle administratieve taken.
Het Instituut voor de aanmoediging van Innovatie door Wetenschap en Technologie in Vlaanderen (IWT) voor de financiële steun.
Mijn ouders, die me de kans gegeven hebben om verder te studeren, voor hun aanhoudende steun en belangstelling. Mama en papa nogmaals bedankt, in al die jaren was niets jullie te veel!
Mijn zus An voor de gezellige weekend-babbels.
Stefan, ik had me geen betere en enthousiastere begeleider in tweede licentie kunnen wensen. Ook tijdens deze vier jaren stond je steeds voor me klaar. Ik hoop dat we samen nog lang onze passie voor scheikunde kunnen delen.

1. General introduction

2. The physical basis of NMR spectroscopy 23

3. Polymerization defects in sulphinyl and Gilch based polymers 39

1. General introduction

1.1 Conductive polymers – an interesting discovery

"Plastic electronics would seem to be an impossibility, for the simple reason that plastics do not conduct electric current, or do they?"

This view was changed when A. J. Heeger, A. G. MacDiarmid and H. Shirakawa discovered in 1977 that a polymer, polyacetylene, can be made conductive almost like a metal upon doping[1]. The "doped" form of polyacetylene had a conductivity of 10^5 Sm^{-1}, which was higher than that of any previously known polymer. As a comparison, teflon has a conductivity of 10^{-16} Sm^{-1} and silver and copper 10^8 Sm^{-1}. Since then, the field of plastic electronics has been moved rapidly from fundamental research to industrial R&D with many interesting and novel practical applications. The combination of electronic (e.g. the band gap E_g) and optical properties (electro- and photoluminescence efficiency) of semiconductors with the mechanical properties and processability of polymers make conjugated polymers unique and potentially useful for a wide range of applications. Moreover, the technological advantages of polymeric materials over conventional inorganic materials are the reduction of production costs by large scale production with the possibility to fabricate large area flexible devices. Also the diversity of synthetic methods (direct approach or precursor routes) leading to an unlimited structural variation and tunability of the band gap, make these polymers very attractive. Among the numerous applications are polymer light emitting diodes[2] (PLEDs), solar cells[3], field effect transistors[4] (FETs) and sensors[5] the most important and widely studied (see further). Therefore it is not surprising that the Royal Swedish

Academy of Sciences awarded in 2000 the three scientists mentioned above with the Nobel Prize in chemistry.

Conjugated polymers or semiconducting polymers consist of alternating single (σ bonds) and double bonds (π bonds). The π electrons are highly delocalized and easily polarizable, features that play important roles in the electrical and optical properties, making them rather different from conventional electronic systems. However, the alternating single and double bonds make the chains rather stiff. As a consequence, polyconjugated polymers are not as soluble and tractable, unless side groups are introduced in the main chain. Examples of polymers within this class include poly(*p*-phenylene vinylene) (PPV), polyacetylene, polyaniline, poly(ethylenedioxythiophene) and polythiophene. The polymer of interest in this study is the poly(2-methoxy-5-(3,7-dimethyloctyloxy)-1,4-phenylene vinylene), abbreviated MDMO-PPV or OC_1C_{10}-PPV. Some chemical structures are shown in Figure 1.

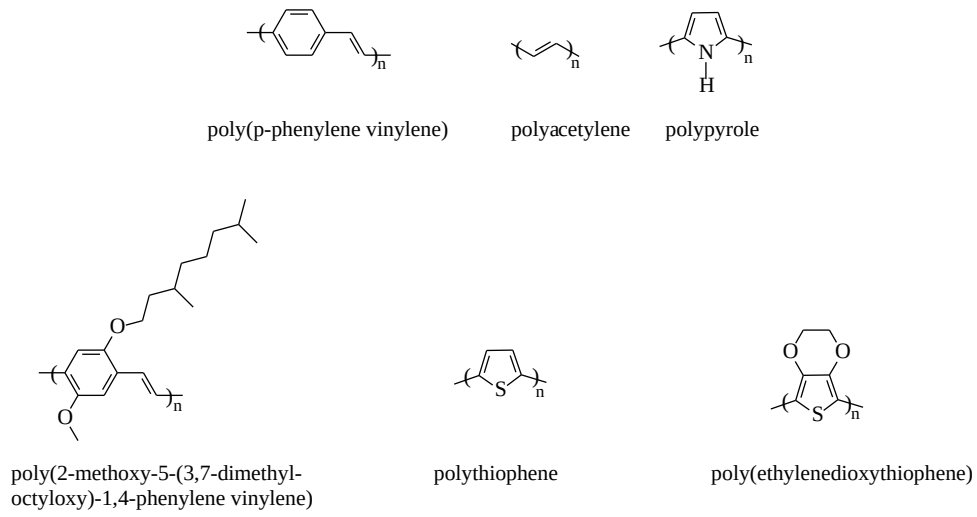

Figure 1 *The chemical structure of some conjugated polymers.*

1.2 Electrical and optical properties

1.2.1 Factors influencing the opto-electronic properties

An important issue for further advancements in the field of plastic electronics is a thorough understanding of the chemical structure – physical properties relationship. Such an understanding is not only of importance for the developments of new and better materials, but also for a reliable industrial manufacturing. In general, the conjugation length, the strength of the interchain interaction, the extent of both intra- and interchain delocalization of the π electrons, the extent of disorder, the number and type of chemical and conformational defects are some of the significant parameters that govern the physical properties of conjugated polymers. The influence of these parameters on the device performance (e.g. efficiency, operational lifetime, performance at elevated temperature) will be briefly discussed below, but will be discussed in more detail in the next chapters.

The main sources of disorder in conducting polymers are the sp^3 defects in the main chain, chain ends, chain entanglements, voids, morphological induced defects etc. Furthermore, it is known that higher degrees of interchain interactions[6] (formation of aggregates) enhance the mobility of the charge carriers at the expense of lower quantum efficiency for electroluminescence. Because of side reactions, conjugated polymers can contain structural defects e.g. single or triple bonds, sp^3 defects and carbonyl defects instead of normal double bonds. These polymerisation irregularities disrupt the conjugated π system and can act as boundaries for charge transport, thus limiting the length of the pathway for intramolecular charge transport[7]. Torsion in the polymer chain causes a breaking of the conjugation and might impede the transport of charges. Direct measurements of the intrachain mobility have shown that the hole-mobility on MEH-PPV, a polymer similar to MDMO-PPV was 0.43 $cm^2V^{-1}s^{-1}$ whereas for poly(3-hexylthiophene) a value of

0.02 $cm^2V^{-1}s^{-1}$ was obtained, indicating that the coplanar alignment was higher for MEH-PPV[8]. The regioregularity i.e. % head-to-tail additions of conjugated polymers, has also an important influence on the effective conjugation length and thus on the mobility of the charge carriers. For regioregular polythiophenes, the π conjugation length seems to be longer since the thiophene rings are less twisted relative to each other due to decreased steric hindrance[9]. Introduction of a head-to-head coupling namely dramatically alters the calculated conformation. The thiophene rings maintain a trans conformation, but they are now severely twisted approximately 40 ° from coplanarity[10] leading to poor electrical conductivity.

Finally, the complex morphology[11] of these polymers, which can be fully amorphous, fully crystalline or semicrystalline plays also a crucial role in the electric charge transport and optical performance. The creation of microcrystalline domains embedded in an amorphous matrix[12] results in complex microstructures which have important consequences for the electrical properties of these materials: charge transport is actually limited by the most difficult hopping processes and is therefore dominated by the disordered matrix, resulting in low charge carrier mobilities.

The relationship between chemical structure and band gap in conjugated polymers is another fundamental aspect that needs to be looked into for making progress in this direction. It is well known that the modification of side groups[13], steric hindrance, π conjugation length, etc. can vary the HOMO and LUMO levels and thus affect the band gap.

However, the chemical structure is not the only factor that determines the final electrical and optical performance of the devices. There is also a non-negligible contribution from the device preparation and architecture. It was found that both spincasting conditions and casting solvents affect the film nanomorphology, which must ensure an efficient charge transport[14,15]. Also a proper choice of the electrodes is required. It is preferred that the electrodes match the HOMO and LUMO of the

polymer, so that the barrier heights are close to zero. This gives the lowest operating voltage and maximum device efficiency. Moreover, the devices have to be protected from air and humidity to achieve high operational life times, otherwise degradations processes take place (see further).

1.2.2 What makes a polymer conductive?

It must be noted that conjugation is not the only condition that has to be fulfilled to make a polymer conductive. In addition, charge carriers i.e. electrons and holes, have to be injected into the polymer. A hole is a position where an electron is missing. When such a hole is filled by an electron jumping in from a neighbouring position, a new hole is created and so on, allowing charges to migrate over a long distance. These charge carriers can be generated by several processes like electrical stimulation, photo-excitation or chemical doping. Concerning the latter, the dopant ions can either oxidize the polymer chain to create a positive charge by removing an electron or reduce it to generate a negative charge on the polymer chain. An electrical transport based on a "hopping" mechanism is widely accepted for conjugated polymers. Hopping between conjugated parts of the chain (intrachain hopping) as well as between conjugated parts of different chains (interchain hopping) are possible.

The electronic properties of a material mainly depend on its electronic structure, which can be described by the molecular orbital theory[16]. According to this theory, the orbitals of the atoms overlap with the equivalent orbitals of their neighbouring atoms to form molecular orbitals. In general, from N atomic orbitals, N molecular orbitals can be formed. In the case of conjugated polymers, the overlap of adjacent atomic p_z-orbitals results in both bonding (π) and antibonding (π^*) molecular orbitals. When N is very large, many molecular orbitals are spaced together so that the π orbitals generate a virtually continuous, occupied valence band (VB) while the π^* orbitals form the conduction band (CB), each covering a range of energies.

The energy spacing between the highest occupied molecular orbital (HOMO) and the lowest unoccupied molecular orbital (LUMO) is called the band gap (E_g). At present, the band gap in conjugated polymers varies from 1 to 4 eV. By synthesizing the appropriate chemical structures, the desired band gap and other electronic and optical properties can be obtained.

1.2.3 Electroluminescence

Electroluminescence (EL) is the generation of light by electrical excitation. This process is depicted in Figure 2. EL devices have been extensively studied due to their potential application to full color flat panel displays since the first observation of EL in antracene in 1965[17]. In the late 1980s efficient EL on two-layer sublimated molecular film devices of organic fluorescent dyes was demonstrated by Tang and VanSlyke[18]. However, EL from conjugated polymers was first reported in 1990[2], using PPV as the single semiconducting layer between two electrodes. Since then, the development in this field was rapid, leading to prototype devices who meet now realistic specifications for industrial applications (see further).

1.3 Applications and current status

In this paragraph, the working and recent developments of some opto-electronic devices will be discussed. Within the scope of this thesis, stress is also put on the various factors determining the device performance.

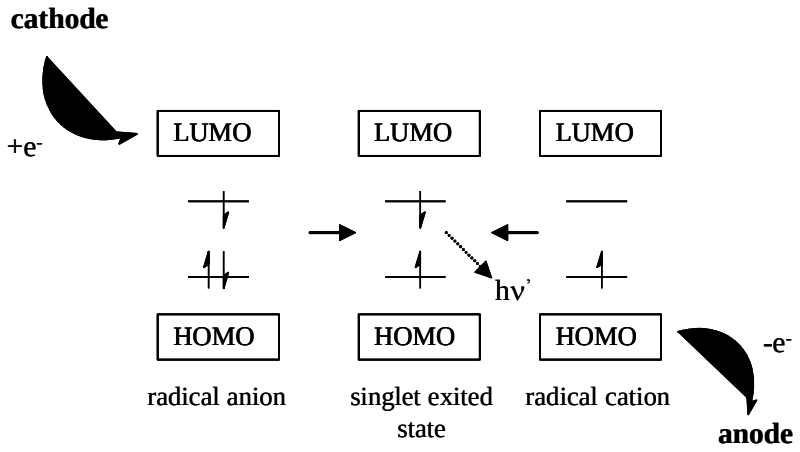

Figure 2 *From the cathode electrons are injected in the LUMO to form radical anions (negative polarons). The anode extracts electrons from the HOMO, or in other words injects holes to form radical cations (positive polarons). The resulting charges migrate within the polymer film under influence of an applied electric field. Somewhere in the bulk of the polymer, electron and hole recombine and form an exciton which can emit light by returning to the ground state***.**

1.3.1 Polymer light emitting diodes

Displays based on polymer light emitting diodes (PLEDs) have a high potential to be successful in a lot of applications e.g. backlights for liquid crystal display (LCD) screens, displays for mobile phones, flat screens etc. A typical device configuration consisting of a single conjugated polymer film, sandwiched between two electrodes, is illustrated in Figure 3. Starting from the bottom, a glass or polymer substrate e.g. polyethylene terephtalate (PET) is covered with a thin layer of indium tin oxide (ITO). The ITO acts as a transparent anode, allowing the generated light to go through the device. On top of this, a single polymer layer is spin casted. Then, the second electrode, a metal cathode (e.g. Al, Ca or Mg) is deposited via thermal evaporation. Finally, the device is encapsulated to protect it from air and moisture in order to prevent degradation (see further).

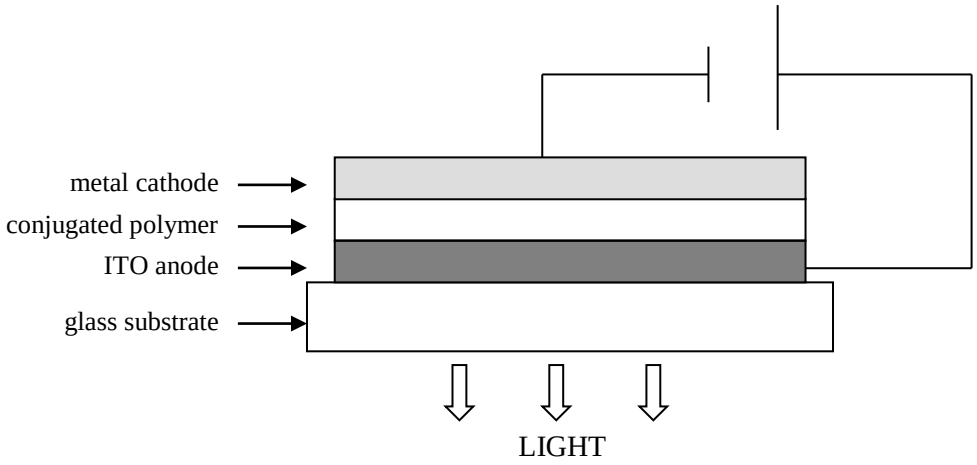

Figure 3 *Device structure of a single-layer polymer light emitting diode.*

As the ITO anode has a relative high work function, it is suitable for hole injection. The metal cathode, on the other hand, has a low work function and is responsible for the injection of electrons. LED operation is achieved when the device is biased sufficiently to inject holes and electrons. These charge carriers migrate toward each other into the polymer layer and recombine forming an excited state or exciton. When this exciton decays radiatively to the ground state, light is emitted.

The most important advantages of the PLED over its silicon counterpart are the higher contrast, the higher brightness, the low operating voltages and the solution processibility leading to a low-cost manufacturing. Moreover, the performance of screens based on PLEDs is independent of the viewing angle since light is emitted in all directions with the same intensity.

Since the discovery of EL from conjugated polymers, there has been significant progress in quantum efficiencies. The first polymers exhibit external quantum efficiencies below 0.1 % and lifetimes in the range of minutes, whereas now the external quantum efficiency up to 4 % and many thousand hours of operational lifetime can be achieved[2,19]. Up till now, the best LED performance, using MEH-PPV, is obtained at UNIAX Corporation[20,21]. A brightness of 100 Cd/m^2 at 2.4 V (the brightness of a color TV), an external quantum efficiency of 2.5 % photons per

electron (ph/el) and an operating lifetime of 10^4 h are detected. Philips and Hoechst have achieved comparable results with MDMO-PPV[22]. Both groups reported external quantum efficiencies of 2.1 % at 100 Cd/m^2. Note that it is difficult to compare results reported by various groups since measurements are done with different device architectures. Although the PLED technology has made an enormous progress over the last decade, the major obstacle towards commercialization is their relatively poor stability[23]. Several degradation mechanisms such as interface degradation of the highly reactive metal cathodes like Al or Mg, which are susceptible to rapid oxidation by water or oxygen[24] and photo-oxidation[25] of the electroluminescent layer itself, influence the performance of PLEDs in a negative way.

Furthermore, to achieve efficient luminescence, a good balance of electron and hole currents and optimal recombination in the emissive layer is a necessity since in PPV the injection of holes dominates. This can be realised by using multilayer devices[26] or by synthesizing copolymers with both hole and electron affinity units in the conjugated main chain[27]. Multicolor display applications require at least three colors: red, green and blue. By modification of the chemical structure (either main chain or side chain modification), the emission color (and also the band gap) can be varied over the whole visible spectrum. Scientists managed to synthesize polymers which emit green[28], orange[21,22,29] or red light. These polymers showed good processability, high quantum efficiency and long lifetimes. However, the search for a stable, highly efficient blue-light emitting polymer is still going on. A few blue-light emitting polymers[30] were obtained but they show rather poor processability and mechanical properties and had high operating voltages in PLEDs.

Although some serious efforts have to be made to optimize further the device characteristics, polymer LEDs are favored targets for market introduction.

1.3.2 Organic solar cells.

Over the last years, much attention has been paid to clean and renewable energy sources in which solar cells or photovoltaic cells play a prominent role. In contrast to inorganic solar cells based on crystalline silicon and gallium arsenide, organic solar cells consist of conjugated polymers. Low weight, mechanical flexibility and probably low manufacturing costs are the main stimulating factors for research in this area. The device structure of an organic solar cell is basically the same as for a PLED except that now light is converted into an electric current.

The discovery of photoinduced charge transfer in composites of conducting polymers (as donors) and buckminsterfullerenes (C_{60}) and its derivatives (as acceptors)[31] provided an approach to high efficiency photovoltaic conversion. Becauce the photoinduced electron transfer from the semiconducting polymer onto the C_{60} occurs in less than 1 ps, two orders of magnitude faster than competing radiative and non-radiative recombination processes, the quantum efficiency for charge separation is close to unity. Although this optimal photoinduced electron transfer in a donor/acceptor (D/A) pair, early devices fabricated from conjugated polymer/C_{60} bilayers[32] yielded low power conversion efficiencies ($\eta_c < 0.1\%$ under AM 1.5 illumination) due to insufficient interfacial contact area between donor and acceptor layers. This since efficient charge separation occurs only at the D/A interface, thus photo-excitations created far from the D/A junctions recombine prior to diffusing to the heterojunction. Significant improvement was achieved by using an interpenetrating phase separated D/A network or bulk heterojunction by controlling the morphology. In that way, a high interfacial area within a bulk material can be obtained since any point in the network is within a few nanometers of a D/A interface. It was found that the efficiency was dramatically increased by blending a soluble methanofullerene into the MEH-PPV[33]. This increase was also simultaneous observed by the Cambridge and Santa Barbara groups using two different conjugated polymers[34].

A key issue in these bulk heterojunction solar cells is to have an efficient transport of the charge carriers to the opposite electrodes and to prohibit recombination, both in which morphology will play an essential role. Until recently, very little was known about the active layer in bulk heterojunction solar cells. The presence of a fine bicontinuous network of nano-scale crystallites of C_{60} embedded in the amorphous MEH-PPV for a composite of 1:1 by weight was observed by transmission electron microscopy (TEM) and confirmed the formation of bulk heterojunctions[35]. By applying the same technique it was further found for a MDMO-PPV:PCBM blend in a 1:4 ratio by weight that a much finer film morphology can be obtained using chlorobenzene instead of toluene as casting solvent and by spincoating the films instead of using a slower drying process like dropcasting[14]. Devices with an active film spincoated from chlorobenzene show a nearly three times higher power conversion efficiency (η_c = 2.5 %) under AM 1.5 illumination than devices spincoated from toluene (η_c = 0.9 %). These findings were in agreement with previously reported AFM results[15]. The higher power conversion efficiency for chlorobenzene based devices can be explained by an increased mobilty for both holes and electrons. Clustering of PCBM, which happens in toluene, is expected to decrease the charge carrier mobility for electrons since the voids between the clusters present large barriers for the hopping process. The charge carrier mobility for holes is also affected by the morphology of the film, since the relative orientation[6] of the conjugated polymer chains which is influenced by the spincoating solvent, determines the degree of interchain interactions and thus the extent of the π delocalization. The presence of intermolecular interactions was already studied by means of photoluminescence excitation spectroscopy and scanning force microscopy for MEH-PPV, a polymer similar in structure to MDMO-PPV[6d]. The higher degree of interchain interactions in chlorobenzene can explain the higher mobility of the holes in this solvent compared to toluene. However, the exact influence of phase separation on the electron and hole mobility is still a topic of research.

Besides the film morphology also the purity of the chemical structure of the conjugated polymers will probably determine the photovoltaic performance. This was recently[36] shown by replacing the commonly used 'Gilch' MDMO-PPV[37] with a MDMO-PPV synthesized via the sulphinyl precursor route[38] leading to a power conversion efficiency of 2.9 % under AM 1.5 illumination, suggesting that different structural defects, inherent with a particular synthetic procedure, could be responsible for it (more about this in chapter 3).
These findings emphasize that further research between structural properties and photovoltaic performance is needed to enhance the efficiency of photovoltaic devices.

1.3.3 Organic thin film transistors

The impressive improvements in performance and efficiency of organic electro-optical devices during the last decade attracted the interest of industry and opened the way to practical applications for organic semiconductors. A schematic representation of an organic thin film transistors (OTFT) is shown in Figure 4.

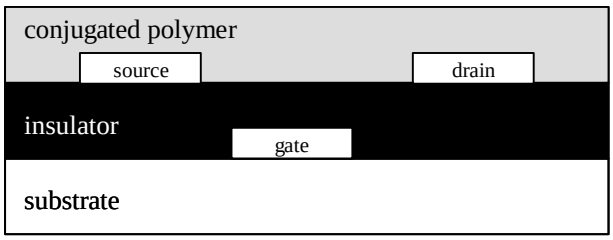

Figure 4 *Schematic view of an organic thin film transistor (OTFT).*
When a sufficiently high positive voltage is applied to the gate, an inversion layer forms at the insulator-semiconducting interface, providing a conducting channel between the source and drain electrodes.

As in traditional inorganic semiconductors, organic materials can either function as p-type or n-type semiconductors. In p-type semiconductors, like MDMO-PPV, the

majority of carriers are holes, while in n-type semiconductors electrons are the dominant charge carriers. Most of the work to date has focused on p-type organic materials such as pentacene[39], thiophene oligomers[40] and poly(3-alkylthiophene)s[41]. Because of the inherent instability of n-type semiconductors less development is made in this direction[42]. Due to the relative low charge carrier mobility of organic semiconductors, OTFTs cannot rival the performance of field effect transistors based on single crystalline inorganic semiconductors like Si, Ge and GaAs, of which the charge carrier mobility is three or more magnitudes higher[43]. Therefore, OTFTs are not suitable for use in applications requiring very high switching speeds. However, solution processed organic semiconductors, both polymers and oligomers, are a potential cost-advantage since expensive chemical vacuum deposited techniques can be eliminated. This unique processability makes OTFTs excellent candidates for existing or novel thin film transistor applications such as electronic paper displays[44], sensors[45], smart cards, radio frequency tags etc. In the near future also switching devices for active matrix flat panel displays based on liquid crystals or organic light emitting diodes will be possible.

It was found for chain molecules, for instance thiophene oligomers[40,41,46], that long π-conjugation length along the long axes of the molecule and close molecular packing (π-stacking) along the short axes are two important conditions for high carrier mobility. When regioregular[9,41,47] poly(3-hexylthiophene), consisting of 98.5 % or more head-to-tail linkages, was used to fabricate field effect transistors, a dramatic increase in mobility was observed relative to regiorandom[48] poly(3-alkylthiophene)s. This increase in mobility seems to be related to side chain induced self-organization into a well-ordered two-dimensional lamellar structure[49]. More recently mobilities in the range of 0.01 to 0.1 $cm^2V^{-1}s^{-1}$ have been achieved using solution processed substituted oligothiophenes[50]. The mobility was found to depend strongly on film morphology, which can be controlled by processing conditions such as solution concentration, solvent choice, substrate temperature during casting etc. These findings show that both synthesis of 'defect-free'

polymers, having the possibility to organize in well-ordered structures and a better control of the morphology during device fabrication are a prerequisite to improve further the charge transport in OTFTs.

1.4 Aim and outline of the thesis

A thorough knowledge of the chemical structure – physical properties relationship is the main objective of this research project. Understanding the factors influencing the opto-electronic properties especially the synthetic procedures used, may provide the means to enhance the efficiency of the opto-electronic devices.
In chapter two, the basic principles of nuclear magnetic resonance spectroscopy (NMR) are described. Throughout this work, NMR spectroscopy has proven to be a powerful and indispensable tool, not only to elucidate the polymer structure, but also to provide insight into the molecular ordering and dynamics of polymer chains. The type and amount of structural defects present in the ^{13}C-labeled MDMO-PPV synthesized according to the sulphinyl and Gilch precursor route are discussed in chapter three. In chapter four, the various solid state NMR techniques used to study the molecular chain mobility and ordering of the sulphinyl and Gilch MDMO-PPV polymers are explained. The chain dynamics of MDMO-PPV during the elimination reaction is examined by means of ^{1}H wideline NMR spectroscopy in chapter 5. The molecular ordering and dynamics of the Gilch and sulphinyl synthesized MDMO-PPVs are examined in chapter 6 by means of ^{2}H wideline, ^{13}C wideline, ^{1}H wideline and high-resolution ^{13}C CP/MAS with high power proton dipolar decoupling NMR spectroscopy. Furthermore, the morphology was studied by applying some WAXS, DSC and rheology measurements. The synthesis of the ^{13}C- and ^{2}H-labeled polymers, as well as the experimental conditions of the analytical techniques are mentioned in chapter seven. Finally, a short summary,

general conclusions and perspectives are given in English (chapter eight) and Dutch(chapter nine),respectively. In chapter 10, a list of abbreviations ismentioned.

1.5 References

[1] Shirakawa, J.; Louis E. J.; MacDiarmed A. G.; Chiang, C. K.; Heeger A. J. *J. Chem. Soc. Chem. Comm.* **1977**, 579.

[2] a) Burroughes, J. H.; Bradley, D. D. C.; Brown, A. R.; Marks, R. N.; Mackay, K.; Friend, R. H.; Burn, P. L. *Nature* **1990**, *347*, 539. b) Braun, D.; Heeger, A. J.; *Appl. Phys. Lett.* **1991**, *58*, 1982. c) May, P. *Physics World* **1995**, *8(3)*, 52.

[3] Brabec, J. C.; Sariciftci, N. S.; Hummelen, J. C. *Adv. Funct. Mater.* **2001**, *11*, 15-48.

[4] a) Roth, S., *One-dimensional metals* **1995**, Weinheim VCH, 209-231. b) Horowitz, G. *Adv. Mat.* **1998**, *10(5)*, 365. c) Dimitrakopoulos, C. D.; Malenfant, R.L. *Adv. Mat.* **2002**, *14(2)*, 99.

[5] Mac Diarmid, W.; Zhang, W.; Huang, Z.; Wang, P.C.; Huang, F.; Xie, S. *Polymer Prepr.* **1997**, *11 (5)*, 333.

[6] a) Samuel, I. D. W.; Rumbles, G.; Collison, C. J. ; Moratti, S. C. ; Holmes, A. B. *Chemical Physics* **1998**, *227*, 75. b) Nguygen, T. ; Doan, V. ; Schwarz, B. J. *J. Chem. Phys.* **1999**, *110(8)*, 4068. c) Shi, Y.; Liu, J.; Yang, Y. *Macromol. Symp.* **2000,** *154*, 187. d) Nguygen, T.; Martini, I. B.; Liu, J.; Schwarz, B. J. *J. Phys. Chem.* **2000**, *104*, 237.

[7] Grozema, F. C.; Van Duijnen, P. T.; Berlin, Y. A.; Ratner, M. A.; Siebbeles, L. D. A. *J. Phys. Chem. B* **2002**, *106*, 7791.

[8] Grozema, F. C.; Siebbeles, L. D. A.; Warman, J. M.; Seki, S.; Tagawa, S.; Scherf, U. *Adv. Mat.* **2002**, *14*, 228.

[9] a) Garnier, F.; Horowitz, G.; Peng, X.; Fichou, D. *Adv. Mat.* **1990**, *2*, 592. b) McCullough, R. D.; Lowe, R. D. *J. Chem. Soc. Chem. Comm.* **1992**, *70*, 1992. c) Sirringhaus, H.; Brown, P. J.; Friend, R. H.; Nielsen, M. M.; Bechgaard, K.; Langeveld-Voss, B. M. W.; Spiering, A. J. H.; Janssen, R. A. J.; Meijer, E. W.; Herwig, P.; de Leeuw, D. M. *Nature* **1999**, *401*, 685.

[10] McCullough, R. D.; Lowe, R. D.; Jayaraman, M.; Anderson, D. L. *J. Org. Chem.* **1993**, *58*, 904.

[11] a) Ezquerra, T. A.; Lopez-Cabarcos, E.; Balta-Calleja, F. J. ; Stenger-Smith, J. D. ; Lenz, R. W. ; *Polymer* **1991**, *32*, 781. b) Herold M. ; Gmeiner, J.; Schwoerer, M. *Acta Polym.* **1996**, *47*, 436. c) Greiner, A.; Schafer, O.; Pommerehne, J.; Guss, W.; Vestweber, H.; Tak, H. Y.; Bassler, H.; Schmidt, C.; Lussem, G.; Schartel, B.; Stumpflen, V.; Wendorff, J. H.; Spiegel, S.; Moller, C; Spiess, H. W. *Synth. Met.* **1996**, *82*,1. d) Brabec, C. J.; Winder, C.; Scharber, M. C.; Sariciftci, N. S.; Hummelen, J. C.; Svensson, M.; Andersson, M.R. *J. Chem. Phys.* **2001**, *115(15)*, 7235.

[12] Samuelsen, E.J.; Mardalen, J. *Handbook of Organic Conductive Molecules and Polymers Vol 3,* **1997**, Wiley, Chichester, UK, 87.

[13] Cornil, J.; Dos Santos, D. A.; Beljonne, D.; Brédas, J. L. *J. Phys. Chem.* **1995**, *99*

[14] Martens, T.; D'Haen, J.; Munters, T.; Goris, L.; Beelen, Z.; Manca, J.; D'Olieslaeger, M.; Vanderzande, D.; De Schepper, L.; Andriessen, R. *Mat. Res. Soc. Symp. Proc.* **2002**, *725*, 7.11.1.

[15] Shaheen, S. E., Brabec, C. J.; Saricifci, N .S. Padinger, F.; Fromherz, T.; Hummelen, J. C. *Appl Phys. Lett.* **2001**, *78 (6)*, 841.

[16] Shriver, D. F.; Atkins, P. W.; Langford, C. H. *Inorganic Chemistry - second edition*, Oxford University Press, **1994**, 91.

[17] Helfrich, W.; Schneider, W. G. *Phys. Rev. Lett.* B **1965**, *14*, 229.

[18] Tang, C. W.; VanSlyke, S. A. *Appl. Phys. Lett.* **1987**, *51*, 913.

[19] Kraft, A.; Grimsdale, A. C.; Holmes, A. B.; *Angew. Chem. Int. Ed.* **1998**, *37*, 402.

[20] *European Plastic News* march, **1998**, 21.

[21] Yu, G. *Synth. Met.* **1996**, *80*, 143.

[22] Salbeck, J. *Ber. Bunsenges. Phys. Chem.* **1996**, *100*, 1666.

[23] a) Cacialli, F.; Friend, R. H.; Moratti, S. C.; Holmes, A. B. *Synth. Met.* **1994**, *67*, 157. b) Cumpston, B. H.; Jensen, K. F. *Appl. Phys. Lett.* **1996**, *80*, 7. c) Aziz, H.;

Xu, G. *Synth. Met.* **1996**, *80*, 7. d) Service, R. F. *Science* **1996**, *273*, 878. e) Scott, J. C.; Kaufman, J. H.; Brock, P. J.; DiPietro, R.; Salem, J.; Goitia, J. A. *J. Appl. Phys.* **1996**, *79*, 2745. f) Karg, S.; Scott, J.C.; Salem, J. R.; Angelopoulos, M. *Synth. Met.* **1996**, *80*,111. g) Do, L. M.; Kim, K.; Zyung, T.; Shim, H. K.; Kim, J. J.; *Appl. Phys. Lett.* **1997**, *70*, 3470. h) Carter, S. A.; Angelopoulos, M.; Karg, S.; Brock, P. J.; Scott, J.C.; *Appl. Phys. Lett.* **1997**, *70*, 2067. i) Savvateev, V. N.; Yakimo, V.; Davidov, D.; Pogreb, P.; Neumann, R.; Avny, Y. *Appl. Phys. Lett.* **1997**, *71*, 3344.

[24] a) Do, L. M.; Han, E. M.; Niidome, Y. Fujihira, M.; Kanno, T.; Yoshida,S.; Maeda, A.; Ikushima, A. J. *J. Appl. Phys.* **1994**, *76*, 5118. b) Burrows, P.E.; Bulovic, V.; Forrest, S. R.; Sapochak, L. S.; McCarty, D. M.; Thompson, M. E. *Appl. Phys. Lett.* **1994**, *65*, 2922. c) McElvain, J.; Antoniadis, H.; Hueschen M. R.; Miller, J. N. Roitman, D. M.; Sheats, J. R.; Moon, R. L.; *J. Appl. Phys.* **1996**, *80*, 6002. d) Do, L. M.; Oyamada, M.; Koike, A.; Han, E. M.; Yamamoto, N.; Fujihira, M.; *Thin Solid Films* **1996**, *273*, 209.

[25] a) Kuzina, S. I.; Mikhailov, A. I.; *Eur. Polym. J.* **1993**, *29*, 1589. b) Cumpston, B. H.; Jensen, K. F. *Synth. Met.* **1995**, *73*, 195. c) Cumpston, B. H.; Parker, I. D.; Jensen, K. F.; *J. Appl. Phys.* **1997**, *81*, 3716.

[26] a)Brown, A. R.; Bradley, D. D.; Burroughes, D. D. C., Friend, J. H.; Greenham, R. H.; Burn, N .C.; Holmes, A. B.; Kraft, A. *Appl. Phys. Lett.* **1992**, *61 (23)*, 2793. b) Yoshida, M.; Fujii, A.; Ohmori, Y.; Yoshino, K. *Appl. Phys. Lett.* **1996**, *69*, 734.

[27] Song, S.; Jang, M. S.; Shim, H.; Hwang, D.; Zyung, T. *Macromolecules* **1999**, *32*, 1482.

[28] a) Hwang, D. H.; Kim, S. T.; Shim, H. K.; Holmes, A. B.; Moratti, S. C.; Friend, R. H. *Chem. Commun.* **1996**, 2241. b) Carter, J. C.; Grizzi, I.; Heeks, S. K.; Lacey, D. J.; Latham, S. G.. May, P. G.. de los Panos, O. R.; Pichler, K.; Towns, C. R.; Wittmann, H. F. *Appl. Phys. Lett.* **1997**, *71*, 34. c) Andersson, M. R.; Yu, G.; Heeger, A.J. *Synth. Met.* **1997**, *85*, 1275. d) Lee, J.; Yu, H.; Kim, W.; Gal, Y.; Park, J.; Jin, S. *J. Polym. Sc.:Part A: Polymer Chemistry* **2000**, *38*, 4185. e) Jin, S.;

Park, H.; Kim, J. Y.; Lee, K.; Lee, S.; Moon, D.; Lee, H.; Gal, Y. *Macromolecules* **2002**, *35*, 7532.

[29] a) Heeger, A. J.; Braun, D. (UNIAX *WO-B92/16023* **1992**), (*Chem. Abstr*. **1993**, *118*, 157401j). b) Greenham, N. C.; Friend, R. H.; Bradley, D. D. C. *Adv. Mat.* **1994**, *6*, 491. c) Baigent, D. R; Greenham, N. C.; Grüner, J.; Marks, R. N.; Friend, R. H.; Moratti, S.C.; Holmes, A. B. *Synth. Met.* **1994**, *67*, 3. d) Chen, F.; Mehta, P. G.; Takiff, L.; McCullough, R. D.; *J. Chem. Mat.* **1996**, *6*, 1763.

[30] a) Ohmori, Y.; Udicha, M.; Muro, K.; Yoshino, K. *Jpn. J. Appl. Phys.* **1991**, *30*, L1941.b) Burn, P. L.; Holmes, A. B.; Kraft, A.; Bradley, D. D. C.; Brown, A. R.; Friend, R. H. *J. Chem. Soc. Chem. Commun.* **1992**, *55*, 936. c) Grem, G.; Leditzky, G.; Ullrich, B.; Leising, G. *Synth. Met.* **1992**, *51 (1-3)*, 383. d) Sokolik, I. ; Yang, Z. ; Karasaz, F. E. ; Morton, D. C. *J. Appl. Phys.* **1993**, *74 (5)*, 3584.e) Grem, G.; Martin, V.; Meghdadi, F.; Paar, C.; Stampfl, J.; Sturm, J.; Tasch, S.; Leising, G. *Synth. Met.* **1995**, *71*, 2193. f) Yang, Y. ; Pei, Q. ; Heeger, A. J. *J. Appl. Phys.* **1996**, *79*, 934. g) Remmers, M. ; Neher, D. ; Grüner, J. ; Friend, R. H. ; Gelinck, G. H. ; Warman, J. M. ; Quattrocchini, C. ; dos Santos, D. A. ; Brédas, J. L. *Macromolecules* **1996**, *29*, 7432. h) Bigerson, J. ; Kaeriyama, K. ; Barta, P. ; Broms, P. ; Fahlman, M. ; Granlund, T. ; Salaneck, W. R. *Adv. Mat.* **1996**, *8*, 982. i) Klaerer, G. ; Miller, R. D. *Macromolecules* **1998**, *31*, 2007. j) Ahn, T. ; Jang, M. S. ; Shim, H. ; Hwang, D.; Zyung, T. *Macromolecules* **1999**, *32*, 3279. k) Cho, H. N.; Kim, J. K.; Kim, D. Y.; Song, N. W.; Kim, D. *Macromolecules* **1999**, *32*, 1476.

[31] a) Sariciftci, N. S.; Smilowitz, L.; Heeger, A. J.; Wudl, F. *Science* **1992**, *258*, 1474. b) Sariciftci, N. S.; Heeger, A. J. *Int. J. Mod. Phys., Part B* **1994**, *8*, 237.

[32] a) Sariciftci, N. S.; Baun, D.; Zhang, C.; Srdaov, V. I.; Heeger, A. J.; Stucky, G.; Wudl, F. *Appl. Phys. Lett.* **1993**, *62*, 585. b) Halls, J. J. M.; Pickler, K.; Friend, R. H.; Morati, S. C.; Holmes, A. B. *Appl. Phys. Lett.* **1996**, *68*, 3120.

[33] Yu, G.; Cao, J.; Hummelen, J. C.; Wudl, F.; Heeger, A. J. *Science* **1995**, *270*,1789.

[34] a) Halls, J. J. M.; Walsh, C. A.; Greenham, N. C.; Marseglia, E. A.; Friend, R. H.; Moratti, S. C., Holmes, A. B. *Nature* **1995**, *376*, 498. b) Yu, G.; Heeger, A. J. *J. Appl. Phys.* **1995**, *78*, 4510. c) Granstom, M.; Petritsch, K.; Arias, A. C.; Lux, A.; Andersson, M. R.; Friend, R. H. *Nature* **1998**, *395*, 257.

[35] Yang, C. Y.; Heeger, A. J. *Synth. Met.* **1996**, *83*, 85.

[36] Munters, T.; Martens, T.; Goris, L.; Vrindts, V.; Manca, J.; Lutsen, L. De Ceuninck, W.; Vanderzande, D.; De Schepper, L.; Gelan, J.; Sariciftci, N.S.; Brabec, C.J. *Thin Solid Films* **2002**, *403-404*, 247-251.

[37] Gilch, H. G.; Wheelwright, W. L. *J. Polym. Sci.: A* **1966**, *4*, 1337.

[38] Issaris, A.; Vanderzande, D.; Gelan, J. *J. Polymer* **1997**, *38*, 2571.

[39] a) Horowitz, G.; Peng, X. Z.; Fichou, D.; Garnier, F. *J. Mol. Electron.* **1991**, *7*, 85. b) Dimitrakopoulos, C. D.; Brown, A. R.; Pomp, A. *J. Appl. Phys.* **1996**, *80*, 2501. c) Gundlach, D. J. ; Lin, Y. Y. ; Jackson, T. N.; Nelson, S. F.; Schlom, D. G.; *IEEE Electron Device Lett.* **1997**, *18*, 87.

[40] Horowitz, G.; Fichou, D.; Peng, X .Z.; Xu, G. ; Garnier, F. *Solid State Commun.* **1989**, *72*, 381.

[41] McCullough, R. D. *Adv. Mater.* **1998**, *10*, 93.

[42] a) Xie, R.; Karim, A.; Douglas, J. F.; Han, C. C.; Weiss, R. *Phys. Rev. Lett.* **1998**, *81*, 1251. b) Sferrazza, M. et al. *Phys. Rev. Lett.* **1998**, *81*, 5173. c) Reiter, G. *Phys. Rev. Lett.* **1992**, *68*, 75.

[43] Taur, Y.; Ning, T. H.; *Fundamentals of Modern VLSI* Devices **1998**, Cambridge University Press, 11.

[44] Wisnieff, R. *Nature* **1998**, *394*, 225.

[45] Crone, B; Dodabalapur, A.; Gelperin, A.; Torsi, L.; Katz, H. E.; Lovinger, A. J.; Bao, Z. *Appl. Phys. Lett.* **2001**, *78*, 2229.

[46] a) Horowitz, G.; Peng, X.; Fichou, D.; Granier, F. *Synth. Met.* **1992**, *51*, 419. b) Granier, F. ; Yasser, A.; Hajlaoui, R.; Horowitz, G.; Dellofre, F.; Servet, B.; Reis, S.; Alnot, P. *J. Am. Chem. Soc.* **1993**, *115*, 8716. c) Servet, B.; Horowitz, G.; Ries, S.; Lagorsse, O.; Alnot, P.; Yassar, A.; Deloffre, F.; Srivastava, P.; Hajlaoui, R.;

Lang, P.; Garnier, F.; *Chem. Mat.* **1994**, *6*, 1809. d) Dodabalapur, A.; Torsi, L; Katz, H. E. *Science* **1995**, *268*, 270. e) Katz, H. E.; Dodabalapur, A.; Torsi, L; Elder, D. *Chem. Mat.* **1995**, *7*, 2238.

[47] a) McCullough, R. D.; Lowe, R. D. *J. Chem. Soc. Chem. Commun.* **1992**, 70. b) Chen, T. A.; Rieke, R. D.; *J. Am. Chem. Soc.* **1992**, *114*, 10087. c) Chen, T. A.; Wu, X.; Rieke, R. D. *J. Am. Chem. Soc.* **1995**, *117*, 233. d) McCullough, R. D. *Adv. Mater.* **1998**, *10*, 93.

[48] Bao, Z.; Dodabalapur, A.; Lovinger, A. J. *Appl. Phys. Lett.* **1996**, *69*, 4108.

[49] a) Prosa, T. J.; Winokur, M. J.; Moulton, J.; Smith, P.; Heeger, A. J. *Macromolecules* **1992**, *25*, 4364. b) McCullough, R. D.; Tristram-Nagle, S.; Williams, S. P.; Lowe, R. D.; Jayaraman, M. *J. Am. Chem. Soc.* **1993**, *115*, 4910. c) McCullough, R. D.; Williams, S. P.; Jayaraman, M.; Reddinger, J.; Miller, L.; Tristram-Nagle, S. *Electrical, Optical, and Magnetic properties of Organic Solid State Materials* **1994**, Materials Research Society, Pittsburg PA, Vol. 328, 215. d) Prosa, T. J.; Winokur, M. J.; McCullough, R. D.; *Macromolecules* **1996**, *29*, 3654.

[50] a) Katz, H. E.; Laquindanum, J. G.; Lovinger, A. J. *Chem. Mat.* **1998**, *10*, 633. b) Granier, F.; Hajlaoui, R.; Kassmi, A. E.; Horowitz, G.; Laigre, L. Porzio, W.; Amanini, M.; Provasoli, F. *Chem. Mat.* **1998**, *10*, 3334. c) Katz, H. E.; Li, W.; Lovinger, A. J.; Laquindanum, J. G. *Synth. Met.* **1999**, *102*, 897. d) Katz, H. E.; Lovinger, A. J.; Johnson, J.; Kloc, C.; Siegrist, T.; Li, Y.; Lin, Y.; Dodabalapur, A. *Nature* **2000**, *404*, 478.

2. The physical basis of NMR spectroscopy

The pioneering experiments of Bloch[1] and Purcell[2] have ushered in a new era in which nuclear magnetic resonance (NMR) spectroscopy has become a well established and indispensable tool for structure elucidation in the field of chemistry, biochemistry and medicine. The necessary information is obtained by the still going on developments in high-resolution liquid NMR techniques in the first and second dimension, 1D and 2D respectively, and now even in higher dimensions. The availability of higher magnetic field strengths, more powerful computers and sensitive electronics has encouraged this evolution. Although most NMR experiments are performed on liquid state samples, solid state NMR spectroscopy has also emerged rapidly as a powerful method for the study of solid systems ranging from catalyst and glasses to polymers. It provides information about the structure of solid materials, the morphology of blends and block copolymers[3] and, the molecular dynamics and chain orientation[4].

Throughout this work, these different facets of NMR spectroscopy have been proven to be very useful to unravel not only the polymer structure, but also to gain insight into the molecular ordering and dynamics of the polymer chains. Furthermore, the complementary nature of solid state proton, carbon and deuterium NMR experiments has pointed out that a complete picture of the chain dynamics and orientation of polymers can only come from many experiments designed to probe these aspects.

The basic concepts of nuclear relaxation, which underlie the study of polymer motion and phase morphology, will be discussed below.

2.1 Basic concepts of NMR spectroscopy[5,6,7]

The phenomenon of nuclear magnetic resonance is based on the fact that nuclei possess a nuclear angular momentum P:

$$P = (I\,(I+1))^{1/2}\,h/2\pi \qquad (2.1)$$

Where I is the angular momentum quantum number, usually called the nuclear spin and h is Planck's constant. The nuclear spin is quantized and in different nuclei it may have values of 0, 1/2, 1, 3/2 etc. The nuclei of interest in this work are proton (^{1}H), deuterium (^{2}H) and carbon thirteen (^{13}C), of which both ^{1}H and ^{13}C have a nuclear spin I = 1/2, whereas I = 1 for ^{2}H. Table 1 lists the NMR parameters and relative detectability of the considered nuclei in this work.

The angular momentum P has associated with it a magnetic moment μ:

$$\mu = \gamma\,P \qquad (2.2)$$

where γ is the gyromagnetic ratio, a characteristic constant for each nucleus and a measure for the detection sensitivity in the NMR experiment.

nucleide	spin *I*	natural abundance (%)	gyromagnetic ratio γ (10^7 rad T^{-1} s^{-1})	magnetic moment μ[a]
^{1}H	1/2	99.98	26.7519	2.7927
^{2}H	1	0.016	4.1066	0.8574
^{13}C	1/2	1.108	6.7283	0.7022

Table 1 *Nulear spin properties for the studied nuclei. [a]Magnetic moment in units of the nuclear magneton.*

From equation 2.1 and 2.2, it can be concluded that nuclei with I = 0 have no angular magnetic moment P and thus are not detectable.

When placed in an external, static magnetic field B_o aligned along the z-axis the angular moment is quantized and will adopt one of the (2I + 1) orientations with respect to B_o:

$$P_z = m\, h/2\pi \qquad (2.3)$$

Here m is the magnetic quantum number and can take any of the values of m = I, I-1, …, -I. In the following, we will only consider nuclei with I = 1/2 (the properties of nuclei with I = 1 will be discussed elsewhere). For protons and ^{13}C nuclei which have both I =1/2, this results in two m values (+1/2 and -1/2); however for deuterium with I = 1 there are three values (1, 0, -1). This is shown in Figure 1.

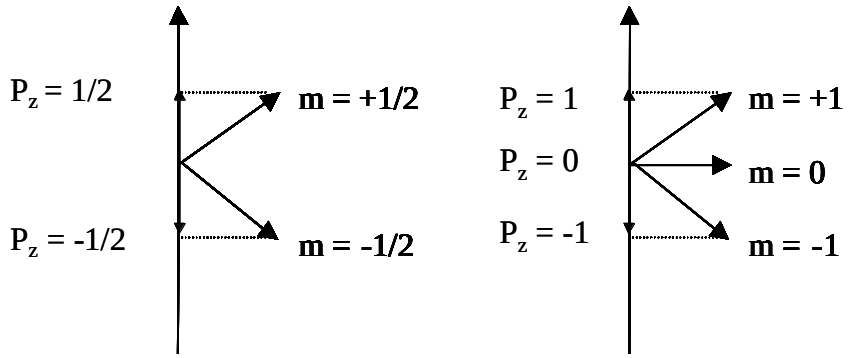

Figure 1 *Directional quantization of the angular momentum P (in units of ħ) in the magnetic field for nuclei with I = ½ and 1.*

With these 2I+1 orientations correspond of course 2I+1 energy levels of which the energy is:

$$E = - m \gamma h B_o/2\pi \qquad (2.4)$$

Thus, nuclei with I = 1/2 can take up two orientations, a low-energy orientation aligned with the applied field and a high-energy orientation opposed to the applied field. In the absence of a uniform magnetic field B_o, these states all have the same energy.

When a nucleus with a magnetic moment μ is brought into a homogenous magnetic field B_o, it starts to precess around B_o. The precession frequency ω_L is called the Larmor frequency and depends on B_o and the nature of the nucleus.

$$\omega_L = \gamma B_o \qquad (2.5)$$

Since there is a slight excess (Boltzmann excess) of nuclei having spins aligned with the field, they give rise to a resultant magnetization vector M_o which lies in the direction of B_o i.e. in the positive direction of the z-axis as shown in Figure 2.

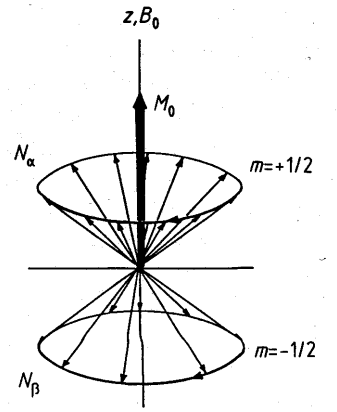

Figure 2 *Distribution of the precessing nuclear dipoles around the double cone. As there is a slight excess of nuclear dipoles in the lower energy state (N_α) there is a resultant macroscopic magnetization M_o.*

In a nuclear magnetic resonance experiment transitions are only induced between adjacent energy levels ($\Delta m = 0$) by irradiating the nuclei with a superimposed alternating radiofrequency field B_1, applied perpendicular to the applied field B_o i.e. the x-axis. Transitions can only occur if the frequency ω_1 of the radiofrequency transmitter matches the Larmor frequency. This is the so called *resonance condition.*

$$\omega_1 = \omega_L = \gamma B_o \qquad (2.6)$$

To describe the complex motions of the magnetic field vectors B_o and B_1, a *rotating coordinate system x', y', z'=z* in which the x' and y' axis rotate around the z-axis at the Larmor frequency ω_L instead of a stationary coordinate system *x, y, z* is used. In the rotating coordinate system the B_1 field appears as static, i.e. the orientation and magnitude of B_1 are fixed. The B_1 field causes the vector M_o, which was previously stationary and along z, to tip and to start rotating about the

x'-axis i.e. in the y'z-plane. The angle θ through which M_o is tipped away is called the pulse angle:

$$\theta = \gamma B_1 \tau_p \qquad (2.7)$$

This angle increases with the amplitude of B_1 when applied during a fixed time or depends on the length of time τ_p of the pulse. During the subsequent period, the vector M_0 splits into three components: M_x, M_y and M_z which specify its orientation at any instant.

If the direction of B_1 coincides with that of the x'-axis, a $90°_{x'}$ or $180°_{x'}$ pulse can be distinguished. From the vector diagrams it can be seen that the transverse magnetization $M_{y'}$ is maximal immediately after a $90°_{x'}$ pulse (Figure 3a) and is zero after a $180°_{x'}$ pulse (Figure 3b).

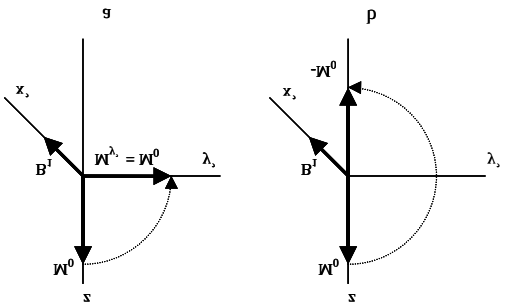

Figure 3 *The position of the magnetization vector after applying a $90°_{x'}$ (a) and a $180°_{x'}$ pulse (b).*

The transverse magnetization $M_{y'}$ is important for the observation of the NMR signal since the receiver coil is oriented along the y'-direction. Immediately after the $90°_{x'}$ pulse, the magnetization vector M_o is deflected from its equilibrium position and relaxation processes begin which allow the nuclei to relax back to their equilibrium position. The macroscopic magnetization M_o is subjected to two different relaxation processes. In the first, termed spin-lattice or longitudinal

relaxation, M_z grows back to its original value M_o. In the second, known as spin-spin or transverse relaxation, $M_{x'}$ and $M_{y'}$ tend to approach zero due to the gradual loss of the phase coherence. The decay of $M_{y'}$ will be that of an oscillating exponential decreasing function as a function of time, also called the free induction decay (FID). Due to the presence of different resonance frequencies and spin-spin coupling, the FIDs of the different transverse magnetization components will be superimposed and interference will occur. The resulting interferogram is still in the time domain, which is difficult to analyze, and therefore is converted to the frequency domain by a fast Fourier transformation.

2.2 Nuclear relaxation

2.2.1 Different types of relaxation

Spin-lattice relaxation

After applying a pulse, the equilibrium of the spin system is disturbed since the population ratio has been changed. A $90°_{x'}$ pulse equalizes the populations of the two energy levels, whereas a $180°_{x'}$ pulse inverts the population ratio. After this perturbation, the equilibrium position $M_z = M_o$ reasserts itself. The rate at which this occurs is determined by the *spin-lattice or longitudinal relaxation time* T_1 and described as follows:

$$\frac{dM_z}{dt} = - \frac{M_z - M_o}{T_1} \qquad (2.8)$$

Spin-lattice relaxation is associated with a change in the energy since the energy absorbed from the pulse must be given up again to the surroundings, or the lattice.

Spin-spin relaxation

After the $90°_{x'}$ pulse, the z-component of the macroscopic magnetization M_z is zero and instead of M_z there are now transverse magnetization components ($M_{y'} = M_o$, $M_{x'} = 0$) of which the evolution is given by:

$$\frac{dM_{y'}}{dt} = -\frac{M_{y'}}{T_2} \text{ and } \frac{dM_{x'}}{dt} = -\frac{M_{x'}}{T_2} \qquad (2.9)$$

The time constant T_2 is the *spin-spin or transverse relaxation time* and determines how rapidly the transverse magnetization components decay. This means that the precessing spins which are bunched together gradually lose their phase coherence, i.e. the bunch fans out and $M_{y'}$ becomes smaller and with it the induced signal in the receiver coil. Figure 4 shows this process in the form of a vector diagram. In contrast to spin-lattice relaxation, spin-spin relaxation is an energy conserving process.

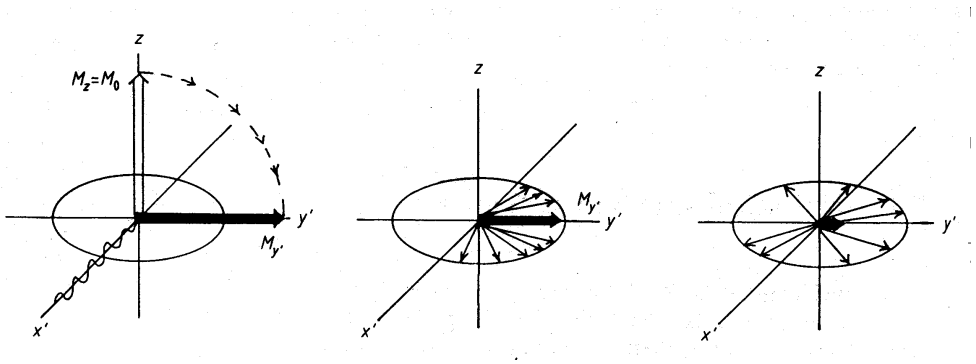

Figure 4 *Decay of the transverse magnetization $M_{y'}$ after a $90°_{x'}$ pulse, the precessing bunched spins fan out as a result of magnetic field inhomogeneities.*

T_2 determines also the line width of the signals in the frequency spectrum. For a homogenous field B_o this line width at half-height is given by

$$\Delta\nu_{1/2} = \frac{1}{\pi T_2} \qquad (2.10)$$

However, the magnetic field is rarely homogeneous. The magnetic field inhomogeneities cause even nuclei that are chemically equivalent to precess with slightly different Larmor frequencies, some faster and some slower than the resultant transverse magnetization $M_{y'}$. This leads to the fanning-out with time.

The true line width at half-height therefore is given by the following expression:

$$\Delta\nu_{1/2} = \frac{1}{\pi T_2^*} = \frac{1}{\pi(T_2 + T_2')} \qquad (2.11)$$

where the additional term $1/\pi T_2'$ is due to the field inhomogeneities. The intrinsic spin-spin relaxation time T_2 can be determined by the 'Carr-Purchell-Meiboom-Gill' (CPMG) pulse sequence[8,9].

Spin-lattice relaxation in the rotating frame

If in a pulse sequence a classical $90°_{x'}$ pulse is immediately followed by a 90° phase shift of the transmitter B_1, we get a situation where the B_1 vector and the M_o vector are both directed along the y'-axis. The magnetization vector M_o is said to be spin-locked by B_{1y}. Spin-locking tries to stabilize M_o along the y'-axis making relaxation more difficult. However, as M_o is developed in B_o which is several orders of magnitude longer than B_1, M_o will re-establish along the z-axis during the relaxation process governed by the relaxation time in the rotating frame $T_{1\rho}$. As for T_1, $T_{1\rho}$ is also affected by molecular motions of the surrounding. In fact, $T_{1\rho}$ depends on the spectral density governed by $\omega_1 = \gamma B_1$ (which is in the order of tens of kHz) while T_1 is governed by the spectral density at $\omega_0 = \gamma B_0$ (which is in the order of tens of MHz). This causes T_1 and $T_{1\rho}$ to be influenced by different

molecular motions which offers the possibility to study different polymer mobilities (see further).

According to the definitions of T_1 and T_2 relaxation, T_2 can never be longer than T_1. This is because it is possible for the transverse magnetization $M_{y'}$ to have already decayed completely by relaxation before the longitudinal magnetization M_z has reached the equilibrium value M_o. Conversely M_z cannot grow to M_o before $M_{y'}$ has completely disappeared.

2.2.2 Relaxation mechanisms

The most important mechanism for spin-lattice relaxation is dipole-dipole relaxation, however, within this study we have to consider other relaxation pathways that contribute strongly or dominate in particular circumstances, namely the quadrupolar relaxation and the relaxation by paramagnetic species.

Dipole-dipole relaxation[10]

This relaxation arises between nuclei that are close to each other in space. Each nucleus is surrounded by other magnetic nuclei in the same or adjacent molecules which are in motion. Their motions cause fluctuating magnetic fields at the position of the nucleus being observed. To the degree that these local fluctuating fields have components at the Larmor frequency ω_L, they will induce nuclear spin transitions between the energy levels so that relaxation takes place.

Quadrupolar relaxation[10,11,12,13,14]

This relaxation mechanism only occurs for nuclei with a nuclear spin I longer than 1/2 such as deuterium and ^{14}N. These nuclei possess electric quadrupole moments Q and show a nonspherical charge distribution. The electric quadrupole moments can interact with the electric field gradient created by the surroundings. As this

interaction fluctuates with molecular tumbling, energy can be exchanged between the spins and the lattice (environment) so that relaxation takes place. The quadrupolar relaxation dominates over all other mechanisms and therefore simplifies the interpretation of molecular dynamics which becomes important in the solid state (see further). However, in liquid state NMR, the resonances may be so broad to be difficult or impossible to observe especially for large molecules.

Relaxation by paramagnetic species[10]

Interaction with unpaired electrons is another efficient relaxation mechanism. The unpaired electron generates very large fluctuating magnetic fields due to the fact that the magnetic moment of the electron is about 1000 times greater than that of a proton. This leads to very short T_1 and T_2 relaxation times. Chromium (III) acetylacetonate is a common reagent used for this purpose. Adding such a paramagnetic substance is not only time saving as the experiment can be speed up but the accuracy of quantitative measurements will also be increased (see chapter 3).

2.2.3 Relaxation times as a function of the correlation times and the magnetic field

The relaxation times are affected by molecular motions (see before) but also by the internuclear distances and the magnetic field. The dipole-dipole interaction is a through-space interaction and is the most important relaxation mechanism for nuclei with a nuclear spin I = 1/2. The local field B_{loc} felt by a nuclei I as a result of the magnetic moment μ_S of nuclei S nearby, can be expressed by the following equation:

$$B_{loc} = \pm \mu_S \frac{1}{r^3_{I,S}} (3 \cos^2 \theta_{I,S} - 1) \qquad (2.10)$$

hereby is $r_{I,S}$ the internuclear distance (< 10 Å) and $\theta_{I,S}$ the angle between the internuclear vector and the main magnetic field B_o. The ± sign corresponds to the fact that the local field may add to or subtract from B_o depending upon whether the neighbouring dipole is aligned with or against the applied field B_o. Molecular motions cause modulations of $\theta_{I,S}$ so that relaxation can take place. The relaxation times are strongly dependent on the way that the dipole-dipole interactions are varied by molecular motions, which are characterized by a correlation time τ_c. The correlation time of a molecule or parts of it (e.g. side chain rotation) corresponds roughly to the time interval between two successive reorientations or positional changes (by vibration, rotation or translation). In Figure 5 the relationship between the relaxation times T_1, $T_{1\rho}$ and T_2 and the correlation time τ_c is presented. Notice that when B_o increases, the T_1 minimum increases and moves to shorter values of τ_c.

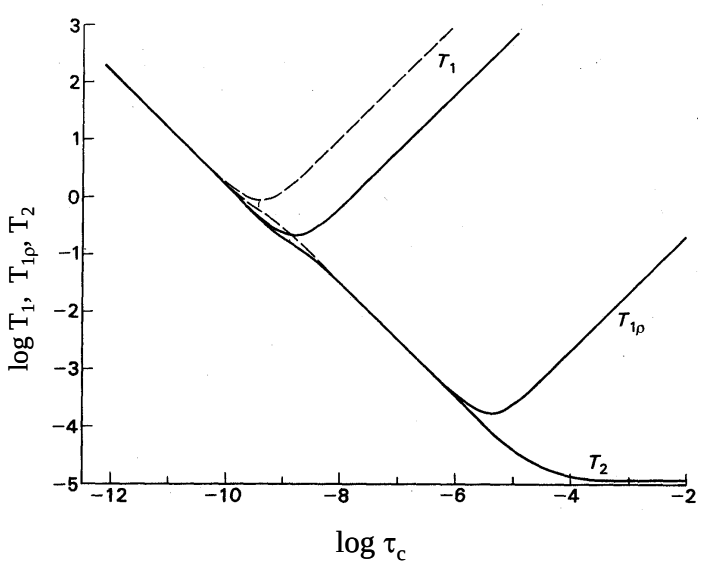

Figure 5 *The dependence of T_1, $T_{1\rho}$ and T_2 on the correlation time τ_c of molecular motions. The solid lines are calculated for ω_L = 100 Hz and the dashed lines for ω_L = 400 Hz.*

As these reorientations or motions in the bulk are random, they will be spread over a broad range of frequencies and their distribution is given by a spectral density function defined by:

$$J(\omega) = \frac{2\tau_c}{1+\omega^2\tau_c^{\,2}} \qquad (2.11)$$

In Figure 6 this function is shown for the three main regions of τ_c.

1) For short τ_c or when $\tau_c^2\omega_L^2<1$, $J(\omega)$ is low for all frequencies of molecular motions, including the Larmor frequency ω_L and have low probability. Therefore, none of the relaxation processes are efficient (Figure 6a). This region is known as the *extreme narrowing region* and is occupied by very fast motions as those of molecules in solution. In Figure 5 one can see that T_1, $T_{1\rho}$ and T_2 are equal in this region and change linearly as a function of the correlation time τ_c. This implies that the decay times will decrease as τ_c increases, thus as the molecular motions are slowing down.

2) If $\tau_c^2\omega_L^2\sim1$ the spectral density $J(\omega)$ is high at or near the Larmor frequency ω_L (Figure 6b). In this region, the T_1 relaxation is most efficient and has its shortest decay time (minimum in the curve). This is occupied by the elastomers and by motions of flexible side chains and end groups of rigid macromolecules.

3) For long τ_c or when $\tau_c^2\omega_L^2>1$, there is a high spectral density of low frequency motions. The spectral density at ω_L is low and the T_1 relaxation of rigid macromolecules is not efficient (Figure 5 and 6 c). In this region, only T_2 relaxation of rigid macromolecules is efficient since only the very low frequency motions contribute as can be derived from the equations developed by Bloembergen, Purcell and Pound[15].

For all three spectral density curves, the total area is equal, only the distribution is different. Concerning the $T_{1\rho}$ relaxation, the picture is similar to the T_1 relaxation, except that it has its minimum at $\tau_c = \omega_1^{-1}$ for which ω_1 is determined by the strength of the spin lock field B_1 ($B_1 = \omega_1/\gamma$) which is in the order of several kHz.

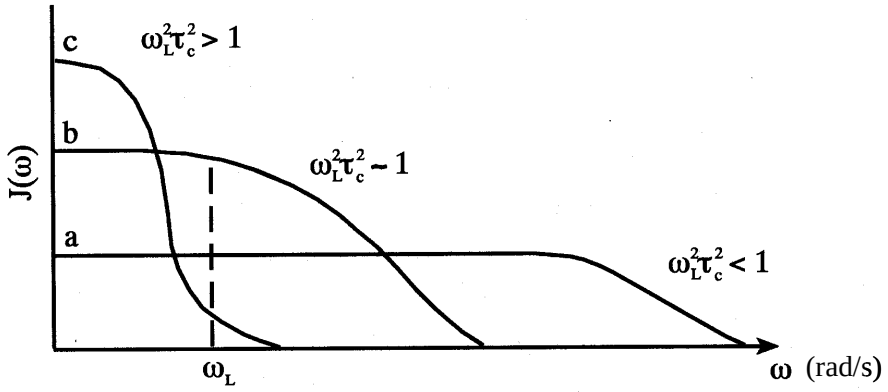

Figure 6 *Plot of spectral density J(ω) as a function of the molecular motions for (a) the extreme narrowing region, as for solutions, (b) moderate mobility as for elastomers and (c) for rigid molecules.* ω_L *is the Larmor frequency.*

2.3 References

[1] Bloch, F.; Hansen, W. W.; Packard, M. E. *Phys. Rev.* **1946**, *69*, 127.

[2] Purcell, E. M.; Torrey, H. C.; Pound, R. V. *Phys. Rev.* **1946**, *69*, 37.

[3] Schmidt-Rohr, K.; Spiess, H. W. *Multidimensional solid state NMR and polymers* **1996**, Academic Press, 402.

[4] Fyfe, C. A. *Solid State NMR for chemists* **1983**, C.F. C. Press, Canada.

[5] Atta-ur-Rahman, *Nuclear Magnetic Resonance-basic principles* **1986**, Springer-Verlag New York, Inc.

[6] Bovey, F. A. *Nuclear Magnetic Resonance spectroscopy* **1988**, Academic Press, London.

[7] Friebolin, H. *Basic One- and two-dimensional NMR spectroscopy* **1991**, VCH Verslags-gesellschaft, Weinheim.

[8] Carr, H. Y.; Purcell, E. M. *Phys. Rev.* **1954**, *94*, 630.

[9] Meiboom, S.; Gill, D. *Rev. Sci. Instr.* **1958**, *29(8)*, 688.

[10] Bovey, F. A. *Nuclear Magnetic Resonance spectroscopy* **1988**, Academic Press, second edition, London, 255.

[11] Harris, R. K. Nuclear *Magnetic Resonance Spectrosopy – A Physicochemical View* **1983**, Pitmann Publishing, Massachusettes, 130.

[12] Komoroski, R. A. *High Resolution NMR spectroscopy of Synthetic Polymers in Bulk* **1986**, VCH Publishers, Florida, 335.

[13] Ibbett, R. N. *NMR spectroscopy of Polymers* **1993**, Chapman & Hall, London, 275.

[14] Mathias, L. *Solid State NMR of Polymers* **1991**, Plenum Press, New York, 23.

[15] Bloembergen, N.; Purcell, E. M.; Pound, R.V. *Phys. Rev.* **1948**, *73*, 679.

3. Polymerization defects in Gilch and sulphinyl based polymers[a]

3.1 Introduction

Although considerable research has been concentrated on discovering new polymers and device improvement, only little effort has been made on a fundamental understanding of the interplay between polymer synthesis, polymer defects and device performance. This relationship will be examined in the next paragraphs since it is of utmost importance that high quality polymers can be synthesized which fulfill the desired physical properties. First, a general idea of the consequences of structural defects on the working of opto-electronic devices will be given. Next, the structural defects present in the MDMO-PPV synthesized according to the Gilch and sulphinyl precursor route, which use both a totally different chemistry, will be elucidated and related to the outcome of preliminary measurements in organic thin film transistors and solar cells.

It is important to realize that the conjugated polymer backbone is not simply a planar monomer unit replicated to macroscopic dimensions as the structure inherently includes defects. Some of these defects in PPV were already postulated by Schoo and Demandth[1]. In fact, the term "defects" is broad since there are several kinds of defects: structural defects due to photo-oxidation or due to the synthesis itself or the presence of aggregates due to interchain interactions etc. As the defects are an integral part of the polymer structure, they are hard to remove.

[a] *Part of this chapter is published in Macromolecules **2003**, 46 (15), 5613.*

Firstly, we will briefly discuss the impact of some of the structural defects on the device performance.

A way to improve the opto-electronic properties is to lower the concentration of head-to-head and tail-to-tail linkages in the polymer chain which interrupt the π-conjugation. This might be possible if a polymerization method with a minimum of side reactions can be found or optimized. Aliphatic hydrocarbon (-CH_2-CH_2-) incorporation by the fragmentation of the monomer during the pyrolysis step into PPV, prepared by chemical vapor deposition, was detected before using X-ray photoelectron spectroscopy (XPS), Raman spectroscopy and temperature dependent IR spectroscopy[2]. Recently, longer operational lifetimes for PLEDs (up to 30 times) have been achieved for phenyl-substituted PPVs by decreasing the formation of head-to-head and tail-to-tail couplings from 6 % to 3 %[3]. Furthermore, lower polymerization temperatures have yielded polymers with a lower content of structural defects which was reflected in a much higher PL and EL efficiency[4]. The introduction of methoxy groups on the phenylene rings also reduces the formation of these defects[3]. The same conclusion could be drawn when a combination of both was made[5]. Head-to-head and tail-to-tail linkages as well as enchainment in the 2,4 instead of the 2,5 position in poly(3-alkylthiophenes) (PATs)[6] have been studied by means of NMR spectroscopy as well. It was found that the number of defects strongly depends on the polymerization method and consequently heavily influences the physical properties. By optimizing the polymerization method, an almost complete regioregular head-to-tail PAT was obtained[7] which gives rise to a higher conductivity compared to polymers with a much lower degree of regioregularity.

The presence of sp^3 defects, interrupting the π-conjugation, was also found to effect the physical properties. For conjugated/non-conjugated PPV based copolymers[8] a strong increase of the quantum efficiency of both photo-luminescence (PL) and electroluminescence (EL) was found. This effect has been

explained by trapping of the radiative exciton on the conjugated segments, hindering their diffusion to structural defects, which can act as quenching sites where non-radiative relaxation to the ground state occurs[9]. Nevertheless, it seems that EL efficiency reaches an optimum for a certain number of non-conjugated units as too high concentrations of nonconjugated segments impede electron and hole transport along the chain, thereby prohibiting exciton formation which result in a drop of EL efficiency. Furthermore, it was found for a copolymer of poly(p-phenylene) (PPP) and polyethylene that the mobility is reduced by a factor 2 if the π-conjugation is disrupted every tenth phenyl unit and the PL efficiency is increased significantly[10] .

Polyacetylene films with fewer sp^3 defects lead also to a large improvement in conductivity[11]. By partial oxidation of the sulphinyl groups a precursor polymer containing both sulphinyl and sulphonyl groups was obtained. Careful tuning of the elimination conditions leads to a selective removal of the sulphinyl groups. The resulting partially conjugated polymer shows an enhanced EL efficiency compared to standard PPV[12]. Furthermore, it was observed by means of the pulse radiolysis time-resolved microwave technique (PR – TMRC) that the presence of saturated ethylene units in the polymer backbone of an isolated alkoxy-substituted phenylene-vinylene/ethylene copolymer decreases markedly the conductivity to a factor of 20 for 40 % ethylene units[13]. This is mainly due to a lower rate of intrachain charge transport caused by the single bonds. However, a detrimental effect of sp^3 hybridization on chain alignment and interchain π-π interactions may also play a role.

Thermal oxidation or photo-oxidation results in the formation of carbonyl defects, which act as exciton dissociation sites leading to a quenching of the photoluminescence[14]. It was found that the incorporation of one carbonyl defect per 400 phenylenevinylene units is enough to quench the PL by a factor 2[15]. Thermal oxidation[16] happens mainly in Wessling polymers since the residual hydroxygroups

are oxidized to ketones at elevated temperatures in the presence of traces of oxygen. Photo-oxidations[17] on the other hand are likely to occur at the vinylene bond and are independent of the synthetic procedure used. This results in chain scission with formation of aldehydes[18] thus shortening the average conjugation length of the polymer chains. Moreover, it was found that also the chemical structure plays a role in the photodegradation process. XPS measurements showed that extra oxygen can be built in into the side chains of alkoxy substituted PPV[18] giving rise to the formation of esters. Recently, the optical properties of three PPV derivatives with a different amount of head-to-head and tail-to-tail couplings, known as the tolane-bisbenzyl (TBB) defect, were studied[19]. It was found that the PPV with the largest amount of TBB units is most sensitive to oxygen uptake. Also side chains consisting of phenylene groups are more reactive with oxygen. However, the presence of carbonyl defects does not only quench the PL but increases also the photoconductivity[20]. A similar process namely the splitting of the exciton, occurs also in photovoltaic devices where C_{60} is mixed with PPV[21] in order to transport the charge carriers to the opposite electrodes.

Secondly, the conformational state of the polymer chain and thus the final morphology of the film is also determined by defects that alter the spatial direction of the polymer backbone. Improved EL efficiency by more than one order of magnitude was obtained through partial disruption of the main chain π-conjugation by incorporating 2,3,5,6-tetramethyl-1,4-phenylenevinylene (TMPV) units in PPV compared to the PPV homopolymer[22]. The TMPV units force the phenylene or vinylene structure to twist out of the planar structure in order to prevent the steric repulsion between the methyl and vinylene protons of the TMPV units. Restriction of the π-conjugation length by inclusion of metasubstituted units along the backbone causing improved PL and EL efficiency was also mentioned[23]. Furthermore, it was shown theoretically for PPV and MEH-PPV that both chemical saturation defects (single bonds) and cis defects produce a kink in the polymer

backbone and are reasonably thermodynamically accessible during synthesis and film preparation[24]. As a result, the PL spectra are slightly blue shifted with respect to the linear (all trans) chain. PPV synthesized via the xanthate precursor route[25] showed an internal quantum efficiency of 0.22 % which is considerably higher than the 0.01 % mentioned for a LED prepared with Wessling PPV[26]. This increase is attributed to the presence of both cis and trans double bonds in the latter route, making the PPV more amorphous. Moreover, IR studies indicated that the cis content decreases as the conversion temperature increases leading to a lower efficiency. This suggests that at higher elimination temperatures a transition from an amorphous to a crystalline structure takes place, which was also observed by others for Wessling PPV.[27]

Separation of the polymer backbones by the presence of lengthy alkoxy substituents on the phenylene rings prevents also interchain exciton transfer resulting in an enhanced EL efficiency[28]. However, too large a separation must be avoided since this causes too low mobility of the charge carriers in LEDs.

Finally, the formation of interchain species (aggregates) was also found to influence the physical properties in that the mobility of the charge carriers increases while the EL luminescence decreases[29]. The degree of interchain interaction can be controlled by varying the solvent and polymer concentration of the solution from which films are cast. This provides possibilities to tune the amount of interchain interactions as a function of the device-type for which the polymer will be used. Thus, for photovoltaic devices where efficient charge transport is required and luminescence is undesirable, casting the films from a solvent that maximizes the interchain interactions can optimize the device. For polymer based LEDs on the other hand, the ideal situation would be to force the current through the single polymer chains so that recombination can take place in an environment free of aggregation.

These findings show that depending on the application for which the polymers will be used some defects definetely must be avoided while others have to be built in deliberately in order to obtain high device performance.

3.2 Sulphinyl versus Gilch precursor route

There are several approaches toward the preparation of PPV and its derivatives which can be classified as direct and precursor methods[30]. The advantage of soluble precursor polymers is that they can be easily processed into devices and make therefore the use of precursor routes very attractive. Well known precursor routes are the Wessling route[26], the Gilch route[31], the xanthate route[25] and the sulphinyl route[32]. In all these precursor routes, the monomer undergoes a base-induced elimination step which leads to the "real monomer", a *p*-quinodimethane system. In the next step, a soluble and processable precursor polymer is formed which finally is eliminated to a conjugated polymer by thermal or chemical treatment (see Figure 1).

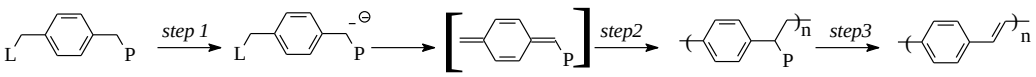

Figure 1 *General scheme for p-quinodimethane based polymerizations. Wessling: L = P = $SR_2^+Cl^-$, Gilch: L = P= Cl, xanthate: L = P = SC(S)OR, sulphinyl: L = Cl, P = S(O)R.*

A suitable leaving group is needed to obtain the *p*-quinodimethane intermediate, whereas a polarizer has to stabilize the formed anion. Besides from this, the polarizer should also polarize the monomer in such a way that regular head-to-tail addition is guaranteed. Finally, the polarizer needs to offer a specific chemistry

allowing the formation of a double bond in order to obtain the fully conjugated PPV.

The use of symmetrical monomers i.e. chemically identical leaving groups and polarizers as in the Wessling and Gilch precursor route, will lead inevitable to the formation of unstable precursor polymers (e.g. partial elimination) and a number of side reactions[33] (solvent substitution, branching and crosslinking, gelation, head-to-head and tail-to-tail additons etc). To avoid many of these drawbacks, the sulphinyl route was developped in our laboratory. It is distinguished from the other routes in that it starts from an asymmetric monomer i.e. leaving group (Cl) and polarizer group (S(O)R) are different. This chemical differentiation allows full control over both the stability of the precursor polymers and the polymerization reaction. Halides were used as leaving groups because of their good leaving group capacities and since they do not enhance the acidity of the benzylic positions. Sulphinyl groups were opted as polarizer for several reasons: firstly, sulphinyl groups show no leaving group properties versus nucleophilic reagents. Secondly, they allow thermal conversion to the double bond[34] and finally, the alkyl side chain of the sulphoxide group provides the opportunity to control the solubility[35].

An open question is still whether this chemical differentiation will have an influence on the polymer microstructure and final device performance. Previous studies[36] already indicated that there was indeed a difference in luminescence efficiency, gelation temperature and current-voltage characteristics between polymers obtained via the Gilch and sulphinyl routes. This despite the fact that the ^{13}C spectra of unlabeled sulphinyl and Gilch polymers are the same at first glance. Moreover, a recent comparison[37] between state-of-the-art Gilch and sulphinyl synthesized MDMO-PPV/PCBM bulk hetero-junction solar cells pointed out that a power conversion efficiency η_c of nearly 3% is reached for the sulphinyl based device compared with 2.5% for the Gilch one. This feature of sulphinyl MDMO-PPV/PCBM bulk hetero-junction solar cells is a consequence of a higher fill factor,

incident photon per converted electron value and a short circuit current. This finding can be attributed to a different microstructure resulting from the higher chemical selectivity during polymerization. The microstructure is expected to be responsible for the different device characteristics as illustrated before. Recently, Becker et al.[38] elucidated the microstructure of Gilch-MDMO-PPV by introducing ^{13}C labels into the polymer chain. In that way, the defect signals –whose concentration is expected to be very low- can be clearly detected as their intensity will be blown up by a factor 100. As main structural defects they found the presence of single and triple bonds, the so called tolane-bisbenzyl (TBB) moieties (structure see p 57). After signal assignment by means of qualitative ^{13}C spectroscopy, they could roughly estimate the amount of the tolane-bisbenzyl moieties from the ^{1}H spectrum as being 1.5-2.2%. They further assumed a similar amount of single bonds (bisbenzyl moiety) and triple bonds (tolane moiety), which means that in total 3-4.4% of the vinylene bonds were replaced by irregular bonds in the main chain. This approach has inspired us to compare Gilch (Covion procedure[38]) and sulphinyl polymers, but based on more chemical shift selective quantitative ^{13}C NMR spectroscopy. In this way, a deeper insight into the type and amount of structural irregularities in the polymer chain will be obtained. The starting point toward a straightforward assignment of these structural defects can be found in the polymerization mechanism of both routes (see Figure 2). The first step -a base induced 1,6-elimination- leads to the formation of intermediate *p*-quinodimethane moieties. These species are the actual reactive monomers. Next, a free radical polymerization mechanism[35,39] is claimed for both the sulphinyl precursor route and Gilch precursor route[39]. In the radical mechanism, a diradical acts as the initiating moiety (step 1). Both sides of the diradical can propagate (step 2) independently by reaction with *p*-quinodimethane intermediates. One assumes that this mainly happens via a head-to-tail addition, leading to a regular polymer chain. Defects in the 'regular' polymer chain such as cross-links, CH_2-CH_2 bond formation (head-to-head addition) in connection with CHS(O)R-CHS(O)R or

CHCl-CHCl bond formation (tail-to-tail addition) can be introduced into this step. Currently, the nature of the termination reaction (step 3) remains undetermined, but two pathways are proposed. Either a hydrogen atom transfer or carbonyl formation by oxygen can take place (see below). Finally, the resulting precursor polymer is converted to the conjugated form. In this study, we were able to identify and quantify structural irregularities present in the corresponding conjugated polymers, by synthesizing the ^{13}C-labeled monomers **(2+5)** and corresponding polymers (**7)** (Figure 3) according to the sulphinyl[40] and Gilch procedures (see Experimental Section).

Step 1: formation of p-quinodimethane systems and subsequent initiation

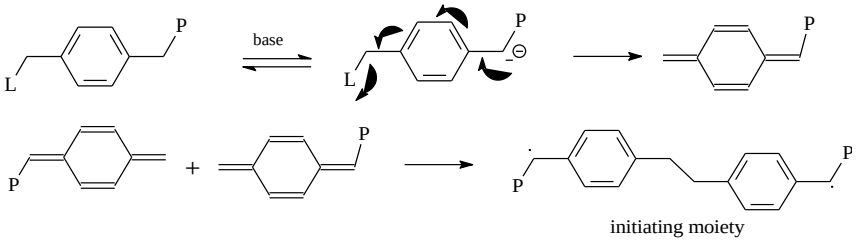

Step 2: propagation

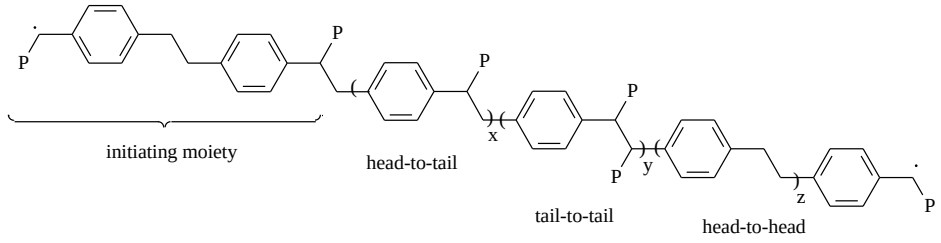

x >> y,z

note: only one propagation chain end is mentioned

Step 3: termination

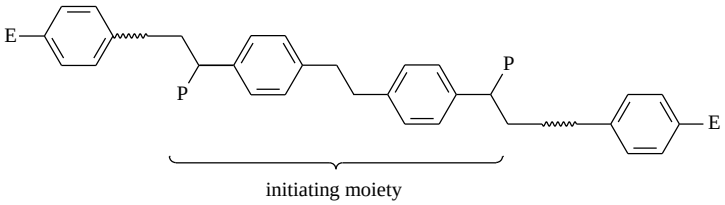

L = Cl, P = Cl (Gilch); P = S(O)R (sulphinyl) sulphinyl); E = C(O)H, C(O)OH, $CH_2S(O)R$ or CH_2Cl

Figure 2 *Radical precursor polymerization mechanism for MDMO-PPV.*

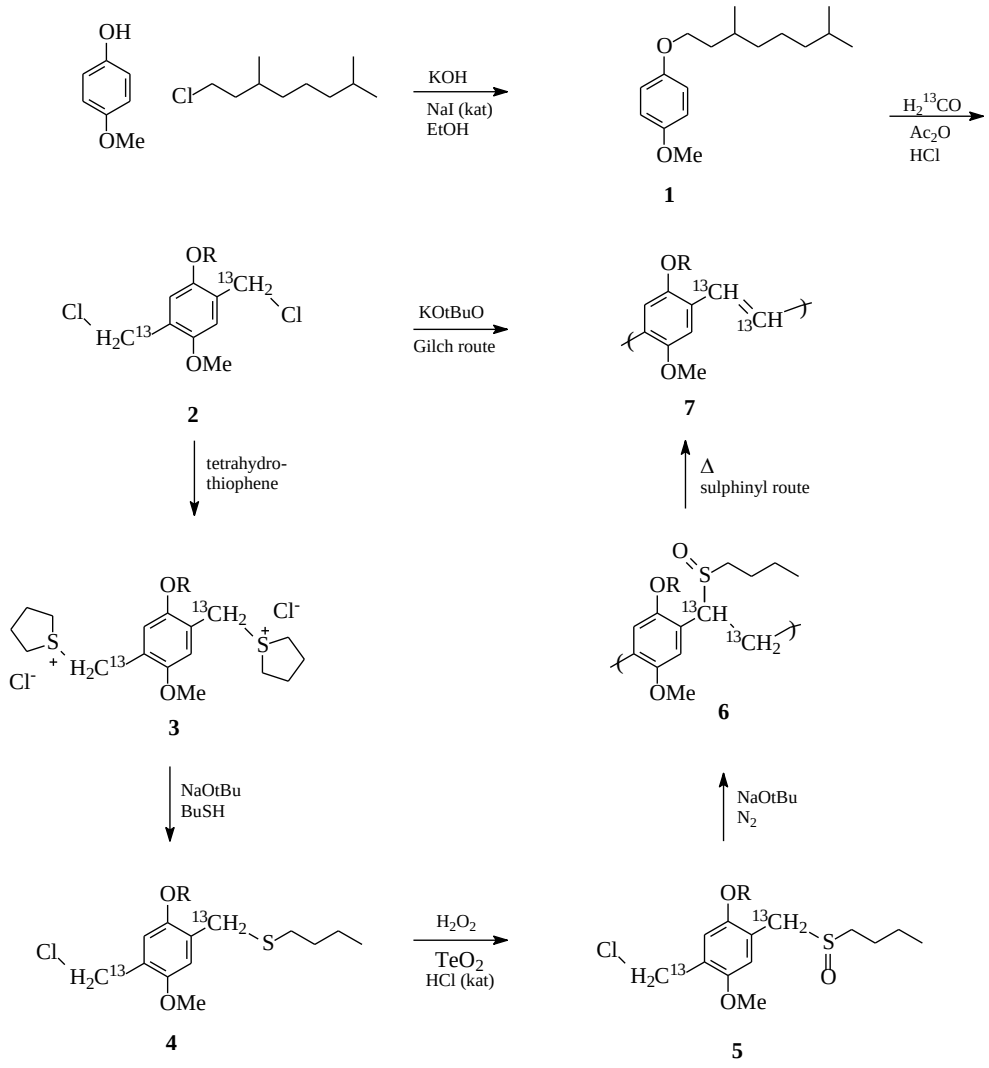

R = $C_{10}H_{21}$

Figure 3 *Preparation of the ^{13}C-labeled monomers and polymers.*

3.3 Quantitative ^{13}C liquid state NMR spectra

To obtain the nature and amount of structural defects from a ^{13}C NMR spectrum, fully quantitative NMR spectra are a prerequisite. In this way, our approach is different from the one of Becker et al.[38], since they estimated the amount of defects from the less chemical shift selective ^{1}H NMR spectra. Another drawback of ^{1}H NMR is that several functionalities e.g. internal triple bonds and carbonyl groups are not observed and their quantification is not possible. To acquire quantitative ^{13}C spectra, a preparation delay of five times the longest T_1 relaxation decay time has to be respected between consecutive pulses in order to let the magnetization return to equilibrium. Therefore the T_1 decay times of all carbon resonances were determined by means of the inversion recovery technique (Table 1). Since the longest T_1 decay times are on the order of 2.7 s, a preparation delay of at least 13.5 s is required (total experiment time of 21 h for 4300 repetitions). The influence of the paramagnetic relaxation agent chromium(III) acetylacetonate on the T_1 relaxation decay times was examined (see also 2.2.2). The addition of chromium(III) acetylacetonate however has to be made cautiously since too high concentrations can reduce the T_2 decay time significantly (increased line width). Therefore, the effect of varying concentrations of chromium(III) acetylacetonate on the T_1 relaxation decays was evaluated. Table 1 shows that the longest T_1 relaxation decay in the presence of 25 mM of chromium(III) acetylacetonate is 1.0 s, allowing acquisitional quantitative data with a preparation delay of 5.0 s (total experiment time 7 h for 4300 scans). Moreover, NOE effects which are classically removed by inverse gated decoupling are further suppressed by chromium(III) acetylacetonate. Paramagnetic relaxation agents mainly provide an additional relaxation mechanism that dominates the C-H dipole-dipole relaxation responsible for the NOE enhancement[41]. An increase of the filter bandwidth equal to the spectral width was also applied to improve quantification of the peaks at the edges of the spectrum.

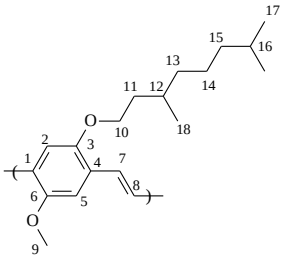

		T_1 (s)		
carbon atom	δ (ppm)	native	20 mM Cr (III)	25 mM Cr(III)
3+6	151.4	2.40	0.90	0.76
4+1	127.0	1.89	1.00	0.53
7+8	123.3	0.38	/	0.16
2+5	110.5	0.12	0.10	0.23
10	67.9	/	0.35	0.29
9	56.4	0.93	0.31	0.30
15	39.2	1.10	0.77	0.67
13	37.4	0.44	0.41	0.37
11	36.6	0.35	0.24	0.30
12	30.2	0.75	0.60	0.44
16	27.9	2.68	1.30	1.02
14	24.6	0.75	0.54	0.52
17	22.6	1.67	1.03	0.79
18	19.8	0.82	0.57	0.49

Table 1 *Chemical shift assignments of the carbon atoms of MDMO-PPV in $CDCl_3$ and T_1 relaxation decay times as a function of the concentration of chromium(III) acetylacetonate.*

3.4 Study of the structural defects in the polymers obtained via the Gilch route

By analyzing the ^{1}H NMR spectrum of 100 % ^{13}C-labeled Gilch MDMO-PPV two major differences are obviously present as compared to the ^{1}H NMR spectrum of

the unlabeled polymer: a broad resonance line centered at 7.5 ppm and a small signal at 2.9 ppm (Figure 4). Both appear as doublets with a $^1J_{CH}$ = 150 Hz and 130 Hz, respectively. The signal around 7.5 ppm clearly represents the vinylic bond. The resonance at 2.9 ppm represents an aliphatic, non-conjugated structure as will be revealed later.

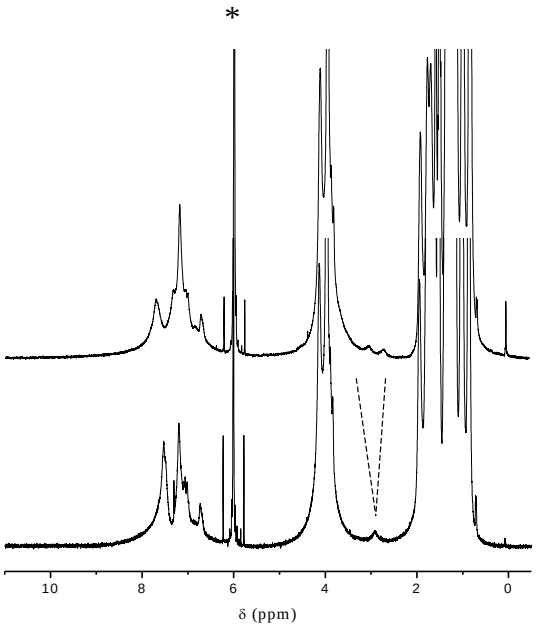

Figure 4 *^{1}H spectra of unlabeled (bottom) and 100 % Gilch MDMO-PPV (top) recorded in CD_2Cl_4. The resonance line marked with an asterisk originates from $C_2D_2Cl_4$.*

The signals between 3.7 and 4.5 ppm, and those between 0.5 and 2.0 ppm represent the protons of the alkoxy side chains. The resonance line at 7.1 ppm is attributed to the aromatic protons. The signals between 6.7 and 7.2 ppm are most likely from the aromatic protons in the neighbourhood of the defect signals.

More information about the type of structural defects present in the polymer backbone was found in the ^{13}C NMR spectra. By comparing the ^{13}C NMR spectra of the unlabeled (Figure 5) and labeled (Figure 6) eliminated conjugated polymers, it is obvious that some additional resonances can be detected upon labeling.

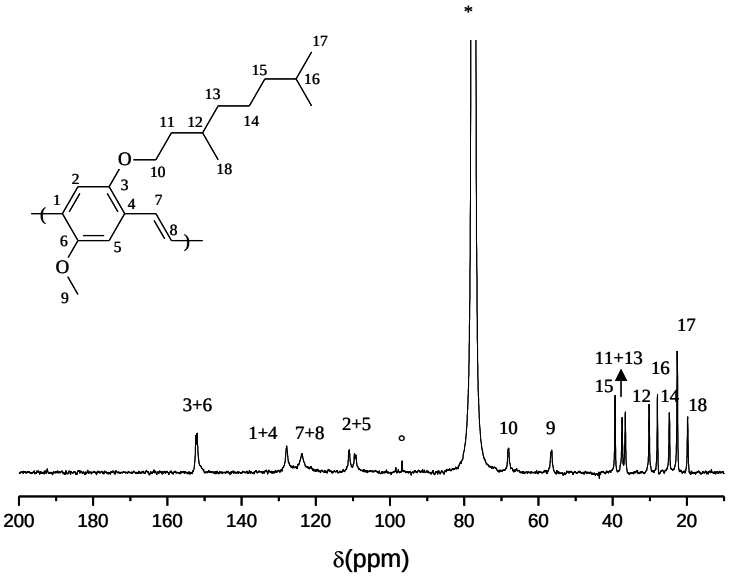

Figure 5 *^{13}C NMR spectrum of unlabeled sulphinyl and Gilch conjugated polymer at 40 °C. The resonances marked with an asterisk and an open circle result from $CDCl_3$ and the transmitter offset, respectively.^{13}C NMR (100 MHz, $CDCl_3$), δ = 151.4 (C_{3+6}, 2C); 127.0 (C_{1+4}, 2C), 123.3 (C_{7+8}, 2C); 110.5 (C_2, 1C); 108.8 (C_5, 1C); 67.9 (C_{10}, 1C); 56.4 (C_9, 1C); 39.2 (C_{15}, 1C); 37.4 (C_{13}, 1C); 36.6 (C_{11}, 1C); 30.2 (C_{12}, 1C); 27.9 (C_{16}, 1C); 24.6 (C_{14}, 1C); 22.6 (C_{17}, 2C); 19.8 (C_{18}, 1C).*

These resonances are situated at 31.0, 33.6, 38.3, 58.6, 90.4, 165.2 and 188.9 ppm. While the resonances at 31.0, 90.4, 165.2 and 188.9 ppm were also observed by Becker et al[38], some new resonances appear in our spectra. All of these signals are broadened due to the scalar $^{1}J_{CC}$ coupling and because they arise from carbons of the polymer backbone. The resonances mentioned above were not detected in the spectrum of the unlabeled polymer, indicating that they are present in an amount less than 5 %.

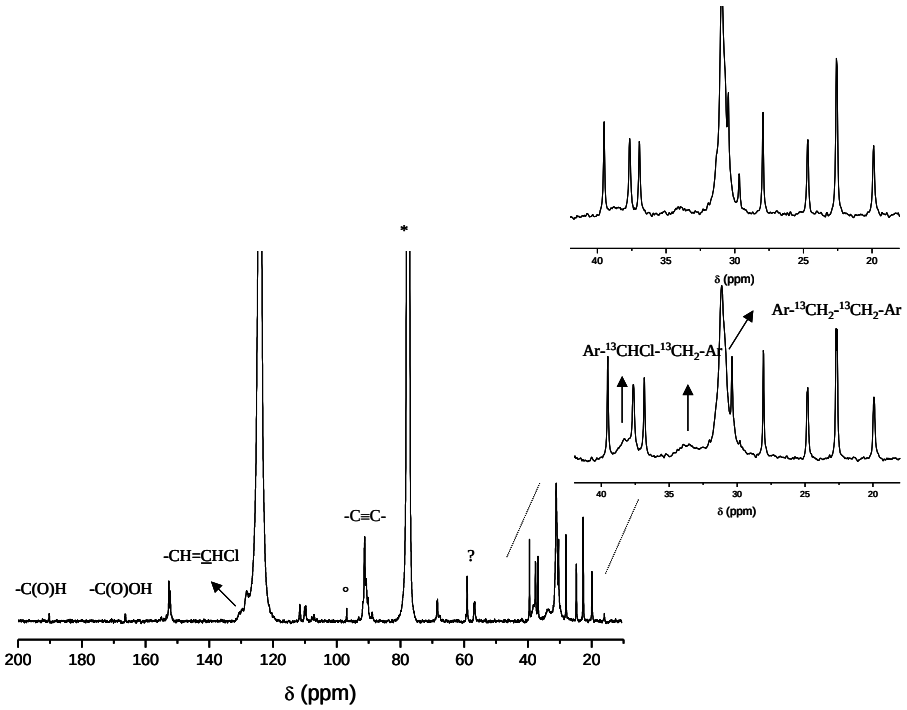

Figure 6 *^{13}C NMR spectrum of 100 % ^{13}C-labeled Gilch MDMO-PPV at 40 °C. Expanded region – bottom: ^{13}C NMR spectrum recorded in $CDCl_3$ at 40 °C. Top: ^{13}C NMR spectrum recorded in $C_2D_2Cl_4$ at 90 °C. The resonances marked with an asterisk and an open circle result from $CDCl_3$ and the transmitter offset, respectively.*

The very intense resonance signal at 123.2 ppm originates from the ^{13}C labeled double bond atoms of the conjugated backbone. The corresponding proton lines

(7.7 and 7.3 ppm) were assigned by means of one-bond HETCOR spectra and appear as doublets in the proton spectra with a typical $^{1}J_{CH}$ value of 151 Hz. To calculate the amount of structural defects from the ^{13}C NMR spectra, the summed integration of some non labeled and defect free signals (carbon atom 3, 6, 17 and 18) was taken as an internal reference to which the other resonances were normalized. For spectral regions containing both defect and regular signals, reduction of the total intensity with the intensity of the regular signals (based on the normalized integrals) allows quantification of the structural defects.

The main structural defects are clearly represented by the signal of the triple bond (90.4 ppm), which is a product of a tail-to-tail addition, as well as by the signal of the bisbenzyl unit (31.0 ppm), which originates from a head-to-head addition (cf. Figure 2). By means of DEPT, the resonances at 31.0 ppm and 90.4 ppm were shown to arise from a methylene carbon and a quaternary carbon atom, respectively. Furthermore, it was proven by an one-bond HETCOR spectrum that the proton resonance at 2.9 ppm and carbon resonance at 31.0 ppm are related, indicating that both represent the same structural moiety i.e. the bisbenzyl unit. By applying the proposed procedure, it was found that the tolane moiety (triple bond) appears in an amount of 4.2 %, while the bisbenzyl unit (single bond) was present for 5.6 %. The higher defect level of the bisbenzyl unit as compared to the tolane unit, will be explained later.

By DEPT the resonances at 33.6 ppm and 38.3 ppm were assigned to a methylene and a methine carbon atom, respectively. These resonances are present in equal amounts (1.8 %) and are attributed to the noneliminated groups (-CH_2-CHCl-), which was confirmed by a 2D INADEQUATE spectrum as both resonances have a $^{1}J_{CC}$ of 34 Hz. We remark that this defect was not observed in the ^{13}C NMR spectrum of the polymer synthesized by Becker et al.[38] recorded in $C_2D_2Cl_4$ at 90 °C. Therefore, a ^{13}C NMR spectrum of our Gilch polymer was acquired under the

same experimental conditions ($C_2D_2Cl_4$, 90 °C and a pulse preparation delay of 15 s since no chromium(III) acetylacetonate was used to reduce the T_{1C} decay times). Under these conditions, the resonances in question appear more broadend and are clearly more difficult to detect (Figure 6–expanded region, top). Note that it took about 80 h to acquire this high signal to noise (*S/N)* spectrum. An explanation why Becker et al. did not observe these resonances can most probably be found in the experimental conditions used and the much weaker *S/N* ratio of their spectra.

It is further assumed that the peak at 129.0 ppm arises from a successor of the tail-to-tail addition namely the chloro-vinyl bond. Although it is impossible to determine the exact amount due to overlap with the signals of the aromatic and olefinic carbons, it looks fair to state that the amount covers the difference in amount between tolane and bisbenzyl units (~1.4%). This implies that according to our procedure, based on fully quantitative ^{13}C spectra, 11.2 % of the vinylene bonds in Gilch MDMO-PPV are replaced by tolane-bisbenzyl moieties. This result is in disagreement with Becker's[38]. Using ^{1}H NMR as determination method, they found 10-12% and 3-4.4% of tolane-bisbenzyl moieties in poly(2-methoxy-5-(2'-ethylhexyloxy)-1,4-phenylene vinylidene) (MEH-PPV)[42] and MDMO-PPV, respectively.

The signals at 188.9 and 165.2 ppm were attributed to aldehyde and carboxylic functionalities present at a level of 0.1 and 0.2%, respectively. Until now, their origin is not clear, but since MDMO-PPV is stable up to about 175°C,[43] they probably are related to the end groups of the polymer as mentioned before. So far, no reasonable explanation for the peak at 58.6 ppm can be offered. In Figure7, the assignments of the structural defects and their fractions are reported.

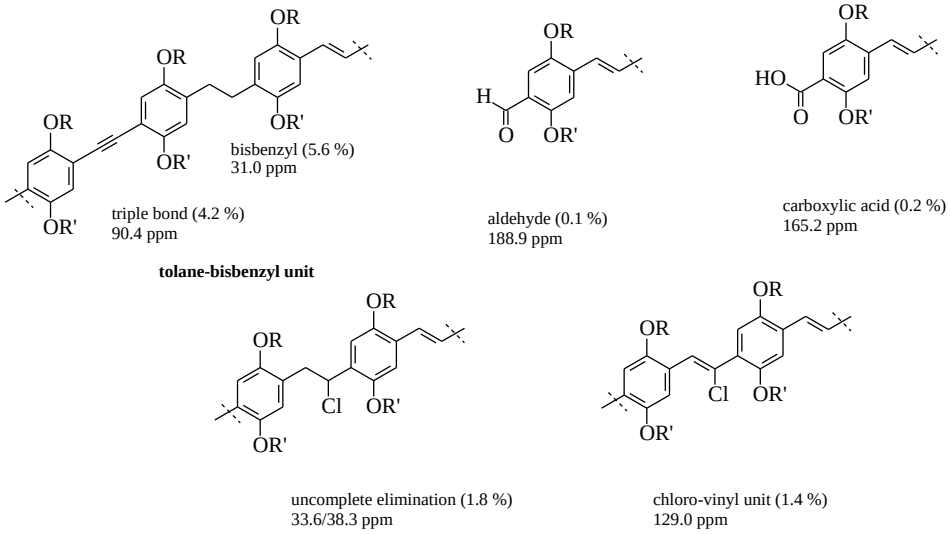

R = $C_{10}H_{21}$ and R' = CH_3

Figure 7 *Overview of the type and amount of the structural defects present in the MDMO-PPV obtained via the Gilch precursor route.*

3.5 Study of the structural defects in the polymers obtained via the sulphinyl route

By comparing the ^{1}H NMR spectrum of the unlabeled and the 100 % ^{13}C-labeled conjugated sulphinyl MDMO-PPV (Figure 8), synthesized by starting from a 50/50 mixture of isomers, it is clear that two resonances are strongly influenced by labeling: the resonance line centered at 7.5 ppm and the small peak at 5.1 ppm. For the labeled polymer, these resonances appear as doublets due to the $^{1}J_{CH}$ coupling with the labeled carbons with a typical value of 151 Hz and 134 Hz, respectively. While the signal at 7.5 ppm represents the protons of the vinylic bond, the resonance line at 5.1 ppm obviously reflects an aliphatic, non-conjugated unit within the polymer chain as will be explained later. All other resonances can be assigned to side chain and aromatic protons (cf. Experimental section).

With respect to the unlabeled eliminated polymer (Figure 5), new resonances appear around 29.0 and 31.0 ppm, 57.3 and 58.4 ppm, and at 188.9 ppm (Figure 9) for the sulphinyl polymer. A combination of APT and DEPT measurements reveals the nature of the two resonances around 57.3 and 58.4 ppm as being methine carbons, while those at 31.0 and 29.0 ppm can be attributed to methylene carbons. Starting from the resonances at 58.4 and 57.3 ppm and at 31.0 and 29.0 ppm, a comparison of the carbon spectrum of the precursor (Figure 10) and conjugated polymer (Figure 9) indicates that the two groups of signals are related and represent the noneliminated groups (CH_2- CHS(O)R).

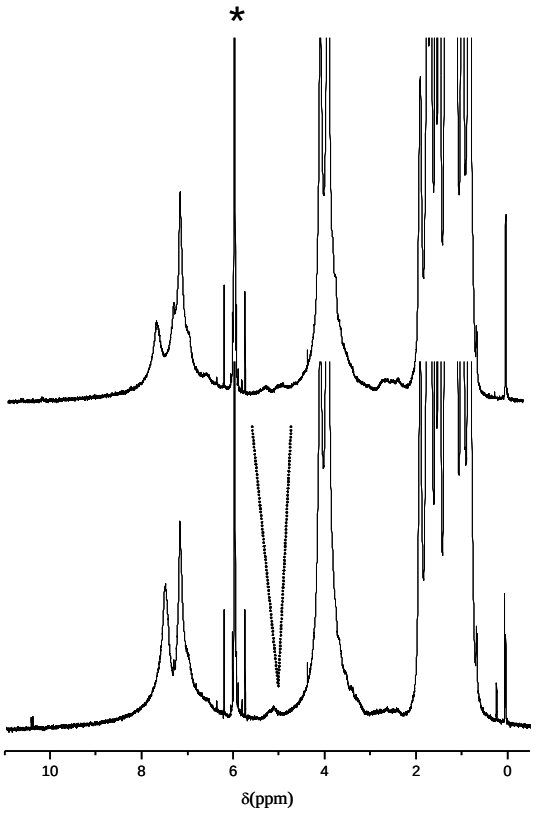

Figure 8 *^{1}H spectra of unlabeled (bottom) and 100 % ^{13}C-labeled sulphinyl MDMO-PPV (top) in $C_2D_2Cl_4$. The resonance line marked with an asterisk originates from $C_2D_2Cl_4$.*

The carbon spectrum of the precursor polymer clearly shows both groups of resonances assigned to the carbons 7 and 8 in Figure 10. The presence of the asymmetric carbon atom 8 in combination with the asymmetric sulphoxide group results in four diastereomers of which two pairs, *RR* and *SS* on one hand, and *RS* and *SR* on the other hand, can be differentiated by NMR.[44] The splitting of the carbon 8 (58.4 and 57.3 ppm) represents the population distribution of these two pairs of isomers and explains the resultant splitting of the carbon 7 resonance (31.0 and 29.0 ppm) in equal (integration) parts. The corresponding proton resonances

were assigned by means of an one-bond optimized HETCOR experiment on the eliminated polymer (Figure 11), which shows that the resonances of carbon atom 8 are correlated with a proton signal around 5.2 ppm, while the resonances of carbon 7 are correlated with a proton resonance around 3.7 ppm. These protons manifest themselves as doublets with a $^{1}J_{CH}$ value of 134 Hz due the coupling with the labeled carbons. It should be noted, no correlation was found between the proton resonance at 2.6 ppm and a ^{13}C resonance because the corresponding carbon atom is not labeled. This resonance arises from methylene protons of the non-eliminated sulphoxide groups i.e. -S(O)C$\underline{H}_2$-$(CH_2)_2CH_3$. After the thermal elimination, one can clearly observe a dramatic decrease of the intensity of both carbon resonances 7 and 8 (compare Figure 10 with Figure 9).

By this, we have proven that the sulphinyl polymer is free from structural defects due to head-to-head and tail-to-tail additions but is characterized by an uncomplete elimination. According to the standard elimination procedure used, i.e., 3 h refluxing in toluene at 110 °C, 6.9 % of noneliminated groups remain. In the following, we will refer to this polymer as the standard sulphinyl MDMO-PPV. These noneliminated groups will act as sp^3-defects, and definitely will disrupt the conjugation of the backbone p-orbitals. Since polymer chain organisation is without doubt coupled to the mechanical and electro-optical properties, these defects probably will also influence the final performance in the devices (see paragraph 2.6).

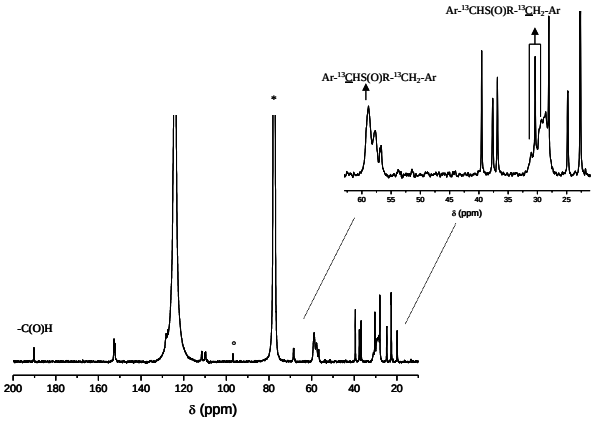

Figure 9 *^{13}C NMR spectrum of 100 % ^{13}C-labeled sulphinyl MDMO-PPV at 40 °C. The resonances marked with an asterisk and open circle result from $CDCl_3$ and the transmitter offset, respectively.*

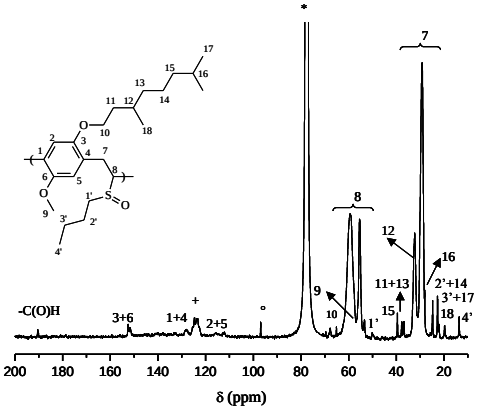

Figure 10 *^{13}C NMR spectrum of 100 % ^{13}C-labeled sulphinyl precursor polymer at 40 °C. The resonances marked with an asterisk and open circle result from $CDCl_3$ and the transmitter offset, respectively. The resonance marked with (+) is due to initial elimination.^{13}C NMR (100MHz, $CDCl_3$), δ = 151.4 (C_{3+6}, 2C); 127.0 (C_{1+4}, 2C); 110.5 (C_{2+5}, 1C); 67.9 (C_{10}, 1C); 59.1-55.1 (C_8, 1C); 56.4 (C_9, 1C); 39.2 (C_{15}, 1C); 37.4 (C_{13}, 1C); 36.6 (C_{11}, 1C); 32.1-29.1 (C_7, 1C); 30.2 (C_{12}, 1C); 27.9 (C_{16}, 1C); 24.6 (C_{14}, 1C); 22.6 (C_{17}, 2C); 19.8 (C_{18}, 1C); 49.7 ($C_{1'}$, 1C); 24.6 ($C_{2'}$, 1C); 21.9 ($C_{3'}$, 1C); 13.5 ($C_{4'}$, 1C).*

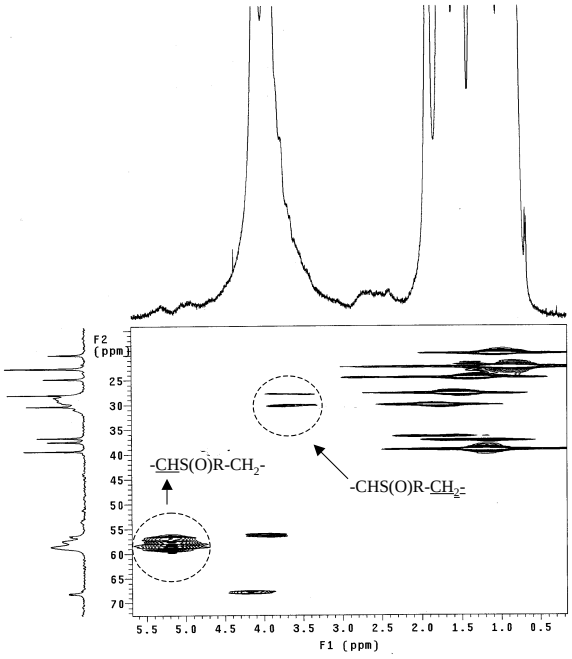

Figure 11 *One bond optimized HETCOR spectrum of ^{13}C-labeled MDMO-PPV.*

To reduce the amount of noneliminated groups further, both the elimination time and temperature were investigated in more detail. By prolonging the elimination time from 3 h to 7 h, the amount of noneliminated groups could be further reduced to 2.0 %. To increase the elimination temperature the solvent had to be changed from toluene to dichlorobenzene (boiling point 170 °C). This increase in reaction temperature resulted in a reduction in the noneliminated groups to 2.4 %. A solution to shift the equilibrium further in the direction of the elimination products in toluene at 110 °C was found in a two-step elimination procedure. After the first elimination step, performed during a 3 h reaction time, the polymer was precipitated, then refluxed in fresh toluene for another 4 h (second elimination). This so called two-step elimination procedure gave rise to a MDMO-PPV with less than 0.5 % of noneliminated groups referred to as two-step eliminated MDMO-PPV in the next chapters (Figure 12).

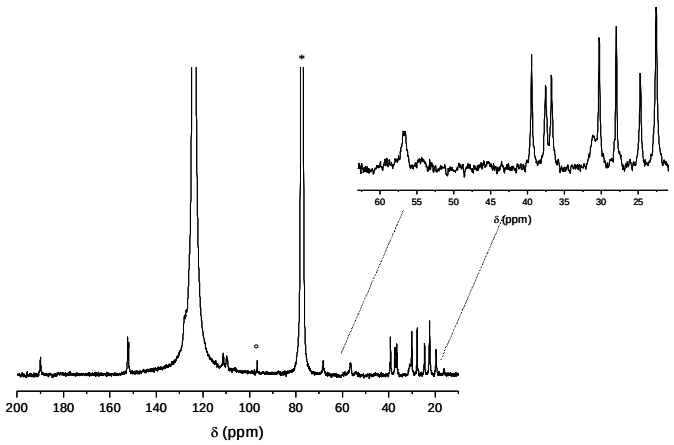

Figure 12 *^{13}C NMR spectrum of 100 % ^{13}C-labeled sulphinyl OC_1C_{10}-PPV prepared by the two-step elimination procedure at 40 °C. The resonances marked with an asterisk and open circle result from $CDCl_3$ and the transmitter offset, respectively.*

As a consequence, the average conjugation length will somewhat larger. However, this slightly increase ($\Delta\lambda_{max}$ = 17 nm), as confirmed by means of solid state UV/Vis spectroscopy, is neglibible since λ_{max} is calculated over approximately 7 to 10 monomer units. Therefore, the defect level is too low to cause a red shift (see Figure 13).

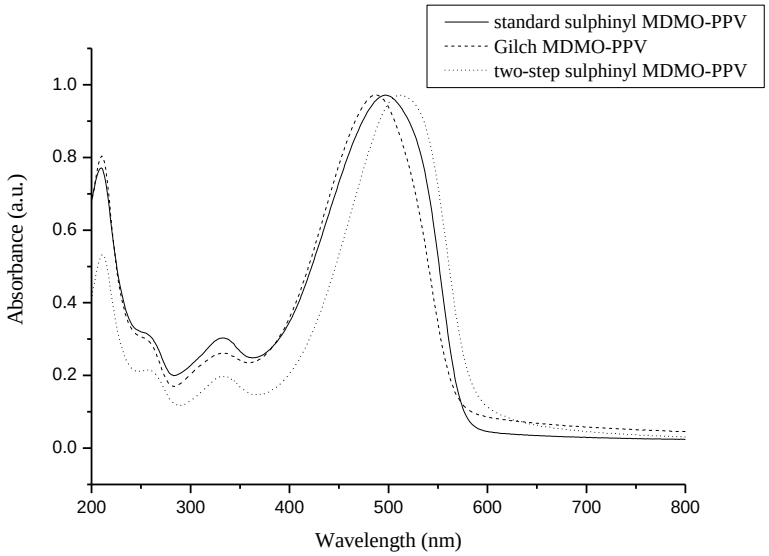

Figure 13 *UV/Vis spectrum of Gilch MDMO-PPV (solid line), standard sulphinyl MDMO-PPV (dashed line) and two-step eliminated sulphinyl MDMO-PPV (dotted line).*

Also note the small resonance at 31.0 ppm which is supposed to be the initiating moiety since no degradation occurs at 110 °C. The ^{13}C labels reveal resonances from this initiating moiety, which normally can not be detected since the amount present in the polymer chain is too low.

The most notable distinction between the sulphinyl and Gilch polymers is the absence of tolane-bisbenzyl moieties in sulphinyl-MDMO-PPV. This is supported by comparing the ^{13}C chemical shifts of a tail-to-tail addition model compound **11** (Figure 14 and Experimental section). Since only oligomers were formed due to steric hindrance of the two sulphoxide groups, we were able to observe the end group resonances ($-CH_2S(O)R$) for these noneliminated oligomers. If we take the influence of electron donating ether substituents on the aromatic system of MDMO-PPV into account[10], the complete absence of signals in the region between

52 and 40 ppm for the sulphinyl polymer, is a strong confirmation that in the sulphinyl route no tail-to-tail additions occur.

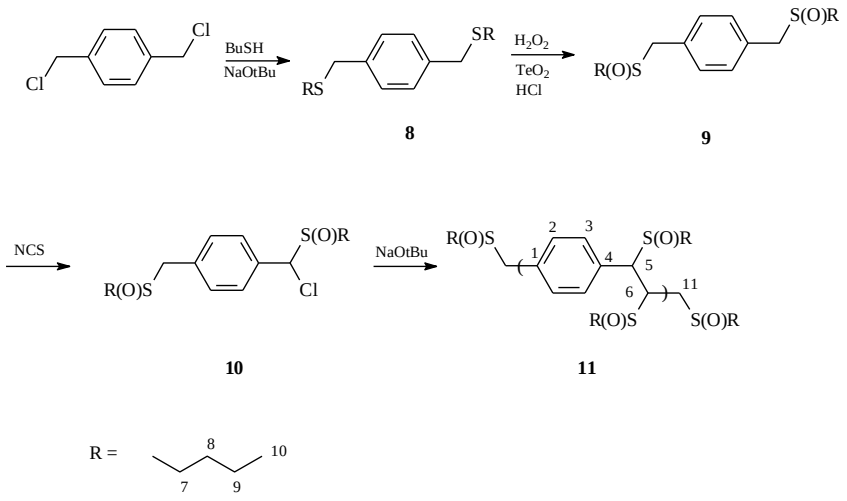

Figure 14 *Preparation of a tail-to-tail model compound.*

Concerning the carbonyl resonances, it must be noticed that the Gilch polymer has two carbonyl functionalities, an aldehyde resonance at 188.9 ppm and a carboxylic acid resonance at 165.2 ppm, while the sulphinyl polymer has only one carbonyl resonance at 188.9 ppm. The latter is present in an amount of 0.3 %. Although it is generally suggested that carbonyl groups are most likely related to degradation of the conjugated polymer chain in the presence of oxygen or heat, strong indications were found that they represent the polymer end groups, at least for those prepared by the sulphinyl route. This since the aldehyde resonance is already observed in the spectrum of ^{13}C-labeled sulphinyl precursor polymer (Figure 10): the intensity ratio of the quaternary carbons 3 and 6 to the aldehyde functionality was found to be identical for both the precursor and eliminated polymer (compare Figure 9 and 10). It is assumed that it originates from the reaction between oxygen and the radical ends of the polymer chain. This leads to the formation of a hydroperoxide, which

by rearrangement can be converted to an aldehyde group. If so, then oxygen acts as a radical scavenger and subsequently terminates the growing polymer chain (Figure 2, step 3).

sample	polymerization atmosphere	yield precursor	Elimination atmosphere	yield	M_w^*	M_n^*	DP^*
1	N_2	70	N_2	89	560000	118000	4.7
2	N_2	61	N_2	80	551000	244000	2.3
3	N_2	78	N_2	85	465000	204000	2.3
4	N_2	65	N_2	90	560000	109000	5.1
5	O_2	16	O_2	81	163000	32000	5.0
6	O_2	20	O_2	87	172000	33000	5.2

Table 2 *Influence of oxygen on the polymerization and elimination (3h in toluene at 110 °C) reactions of MDMO-PPV.* * *molecular weights determined for the eliminated polymer.*

Hence, by polymerizing the unlabeled monomer in an oxygen rich atmosphere (both monomer and base solution were flushed with oxygen at 30°C instead of nitrogen), we expected a decrease in the molecular weight of the polymers as well as the appearance of aldehyde resonances in the ^{1}H spectrum. As expected, a decrease of the molecular weight as well as a reduction of the yield of the precursor polymer was observed (Table 2). While no aldehyde functions could be detected in the ^{1}H NMR spectrum of the polymer fraction because the molecular weights are still too high, the ^{1}H spectrum of the residual fraction, which mainly consists of monomer and oligomers, clearly shows the resonances of a conjagated aldehyde functionality at 10.2 ppm. Performing the polymerization under an oxygen atmosphere has also proven to cause no blue shift in the UV/Vis spectra. In the IR spectra, on the other hand, the aldehyde C(O) stretch is clearly visible. This experiment confirms that oxygen terminates a significant part of the growing

oligomers, although a small fraction of polymer is still formed. In Figure 15 the assignments of the structural irregularities and their fractions are given.

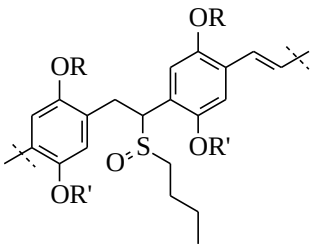

uncomplete elimination (6.9 %)
32.0-29.0 and 58.4-57.3 pmm

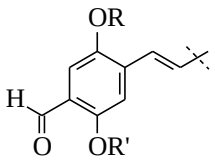

aldehyde (0.3 %)
188.9 ppm

R = $C_{10}H_{21}$ and R' = CH_3

Figure 15 *Overview of the type and amount of the structural defects present in the sulphinyl polymer synthesized according to the standard elimination procedure.*

3.6 Preliminary measurements in opto-electronic devices

3.6.1 Organic thin film transistors [(b)]

The bulk mobility of the charge carriers has been measured in organic thin film transistors using standard and two-step eliminated sulphinyl MDMO-PPV as active layer. The results are represented in Table 3. Although the difference is not significant, a trend can be observed: the mobility decreases slightly upon increasing the amount of sp^3 defects. As the overall mobility is limited by the slowest process i.e. the hopping between the polymer chains, the measured mobility will depend to a large extent to the morphology of the polymers and less to the amount of structural defects. This probably explains the little difference between both polymers. However, the amount of structural defect will definetely play a role when the conductivity in an isolated polymer chain is measured (see further).

sulphinyl MDMO-PPV	mobility $\mu_{corr}/10^{-4}$ cm^2 V^{-1} s^{-1}
standard	2.2
two-step	3.0

Table 3 *The field effect mobility corrected for the presence of a contact resistance for standard and two-step eliminated sulphinyl MDMO-PPV. The standard deviation is 4.4 10^{-5} and 3.4 10^{-5} cm^2 V^{-1} s^{-1} for standard and two-step eliminated sulphinyl MDMO-PPV, respectively.*

[b] The measurements have been carried out at the Institute of Material Research, Physical Department, Diepenbeek by T. Munters.

3.6.2 Solar cells [b]

The power conversion efficiency η_c under AM 1.5 illumination for standard and two-step eliminated sulphinyl MDMO-PPV is depicted in Table 4. As an efficient transport of the charge carriers to the opposite electrodes is a prerequisite to achieve high performance organic solar cells, the slightly higher η_c for the two-step MDMO-PPV can be understood on the basis of its higher bulk mobility (see 3.6.1). Notice that the obtained power conversion efficiencies are on the limit of reproducibility.

sulphinyl MDMO-PPV	power conversion efficiency η_c (%)
standard	1.4
two-step	1.6

Table 4 *The power conversion efficiency under AM1.5 illumination (80 mW cm-^{2}) was measured for a significant population of standard and two-step eliminated sulphinyl MDMO-PPV/PCBM bulk heterojunction solar cells. The standard deviation is 0.4 and 0.3 for standard and two-step eliminated sulphinyl MDMO-PPV, respectively.*

3.6.3 Pulse radiation time-resolved microwave conductivity [(c)]

In contrast to the measurements of the bulk mobility of MDMO-PPV, the pulse radiation time-resolved microwave conductivity technique (PR-TRMC) offers the possibility to study the intrachain mobility of isolated polymer chains. More information about the relation between molecular structure i.e. structural defects, and mobility of the charge carriers can be obtained since no intermolecular interactions take place. The hole mobility for both an isolated standard and two-

[c] The measurements have been carried out at the Radiation Chemistry Department, IRI, Delft University of Technology by P. Prins and L.D.A. Siebbeles.

step eliminated sulphinyl MDMO-PPV chain, dissolved in benzene (concentration 0.1 mM), was measured. The results are represented in Table 5. As a comparison, the hole mobility for a sulphinyl MDMO-PPV, eliminated for 2 h in toluene, is also mentioned.

sulphinyl MDMO-PPV	intrachain hole mobility ($cm^2\ V^{-1}\ s^{-1}$)
standard	0.75
two-step	1.20
eliminated for 2h	0.52

Table 5 *The intrachain hole mobility for standard and two-step eliminate sulphinyl MDMO-PPV.*

From table 5, it can be concluded that the intrachain hole mobility for two-step MDMO-PPV is higher compared to standard sulphinyl MDMO-PPV. This can be explained by the higher amount of sp^3 defects in the standard sulphinyl MDMO-PPV which will limit the hole mobility. As the sulphinyl MDMO-PPV eliminated for 2 h has the lowest intrachain hole mobility, it is assumed that the amount of sp^3defects will be higher.

3.7 Conclusions

The aim of this study was to examine the nature and amount of the structural irregularities in MDMO-PPV obtained by two different precursor routes, namely the Gilch and the sulphinyl route, to clarify the role of the synthesis in their introduction. Gilch and sulphinyl polymers were therefore selectively ^{13}C-labeled in the main chain and examined by liquid state 1D and 2D NMR techniques. The amount of structural 'defects' was derived from quantitative ^{13}C NMR spectra. A tolane-bisbenzyl unit (11.2 %) was found to be the major defect in eliminated Gilch polymers. Also the presence of non-eliminated locations (1.8 %) as well as chloro-vinyl bonds (ca 1.4%), which is a product due to the tail-to-tail addition, was demonstrated. In contrast, only a considerable amount of noneliminated groups (6.9 %) was found in the conjugated sulphinyl polymers. The amount of noneliminated groups could be reduced by increasing the elimination time (2.0 %) or temperature (2.4 %). However, a two-step elimination procedure was shown to be the most efficient and results in a polymer with less than 0.5 % of noneliminated groups. Strong indications were further presented to assign the observed aldehyde functionalities to the end groups: oxygen clearly affects the termination reaction of the growing oligomers. In general, we can conclude that in contrast to the Gilch route the polymerization reaction via the sulphinyl route is characterized by a very regular propagation step, due to the difference in chemistry used in both routes.

3.8 References

[1] Schoo, H. F. M.; Demandt, R. J. C. E. *Philips J. Res.* **1998**, *51*, 527.

[2] Vaeth, K. M.; Jensen, K. F. *Macromolecules* **1998**, *31*, 6789.

[3] Becker, H.; Spreitzer, H.; Kreuder, W.; Kluge, E.; Schenk, H.; Parker, I.; Cao, Y. *Adv. Mat.* **2000**, *12(1)*, 42.

[4] Johansson, D. M.; Theander, M.; Srdanov, G.; Yu, G.; Inganäs, O.; Andersson, R. *Macromolecules* **2001**, *34*, 3716.

[5] Johansson, D. M.; Wang, X.; Johansson, T.; Inganäs, O.; Yu, G.; Srdanov, G.; Andersson, R. *Macromolecules* **2002**, *35*, 4997.

[6] a)Botta, C.; Stein, P. C.; Bolognesi, A.; Catellani, M.; Geng, Z. *J. Phys. Chem.* **1995**, *99*, 3331. b) Mucci, A.; Schenetti, L. *Macromol. Chem. Phys.* **1995**, *196*, 2687.

[7] Chen, T.A.; Wu, X.; Rieke, R. D. *J. Am. Chem. Soc.* **1995**, *117*, 233.

[8] a) Burn, P. L.; Holmes, A. B.; Kraft, A.; Bradley, D. D. C.; Brown, A. R.; Friend, R. H.; Gymer, R. W. *Nature* **1992**, *356*, 47. b) Staring, E. G. J.; Demandt, R. C.; Braun, D.; Rikken, G. L. J.; Kessener, Y. A.; Venhuizen, A. H. J.; Wynberg, H.; ten Hoeve, W.; Spoelstra, K. J. *Adv. Mat.* **1994**, *6*, 934. c) Braun, D.; Staring, E. G. J.; Demandt, R. C.; Rikken, G. L. J.; Kessener, Y. A.; Venhuizen, A. H. J. *Synth. Met.* **1994**, *66*, 75. d) Burn, P. L.; Kraft, A.; Baignent, D. R.; Bradley, D. D. C.; Brown, A. R.; Friend, R. H.; Guymer, R.; Holmes, A. B.; Jackson, R. W. *J. Am. Chem. Soc.* **1993**, *115*, 10117. e) Malliaras, G. G.; Herrema, J. K.; Wildeman, J.; Wieringa, R. H.; Gill, R. E.; Lampoura, S. S.; Hadziioannou, G. *Adv. Mat.* **1993**, *5*, 721. f) Zhang, C.; Braun, D.; Heeger, A. J.; *J. Appl. Phys.* **1993**, *73*, 5177.

[9] a)Brown, A. R.; Greenham, N. C.; Burroughes, J. H.; Bradley, D. D. C.; Friend, R. H.; Burn, P. L.; Kraft, A.; Holmes, A. B. *Chem. Phys. Lett.* **1992**, *200*, 46. b) Brown, A. R.; Bradley, D. D. C.; Burn, P. L.; Burroughes, J. H.; Friend, R. H.; Greenham, N. C.; Holmes, A.B.; Kraft, A. *Appl. Phys. Lett.* **1992**, *61*, 2793.

[10] Remmers, M.; Neher, D.; Grüner, J.; Friend, R. H.; Gelinck, H. G.; Warman, J. M.; Quattrocchi, C.; dos Santos, D. A.; Brédas, J. *Macromolecules* **1996**, *29*, 7432.

[11] Basescu, N.; Liu, Z. X.; Moses, D.; Heeger, A. J.; Naarmann, H.; Theophilou, N. *Nature* **1987**, 327, 403.

[12] De Kok, M. M. *Ph. D. Dissertation* **1999**, Limburgs Universitair Centrum, Diepenbeek, België.

[13] Gelinck, G. H.; Warmann, J. M. *J. Phys. Chem.* **1996**, *100*, 20035.

[14] Rothberg, L. J.; Yan, M.; Papadimitrakopoulos, F.; Galvin, M. E.; Kwock, E. W.; Miller, T. M. *Synth. Met.* **1996**, *80*, 41.

[15] Rothberg, L. J.; Yan, M.; Son, S.; Galvin, M. E.; Kwock, E. W.; Miller, T. M.; Katz, H. E.; Haddon, R. C.; Papadimitrakopoulos, F. *Synth. Met.* **1996**, *78*, 231.

[16] a) Papadimitrakopoulos, F.; Yan, M.; Rothberg, L. J.; Katz, H. E.; Chandross, E. A.; Galvin, M. E. *Mol. Cryst. Liq. Crys.* **1994**, *256*, 663. b) Papadimitrakopoulos, F.; Konstadinidis, K.; Miller, T. M.; Opila, R. ; Chandross, E. A.; Galvin, M. E. *Chem. Mat.* **1994**, *6*, 1563.

[17] Hale, G. D.; Oldenburg, S. J.; Halas, N. J. *Appl. Phys. Lett.* **1997**, *71(11)*, 1483.

[18] a) Cumpston, B. H.; Jensen, K. F. *Synth. Met.* **1995**, *73*, 167. b) Cumpston, B. H.; Parker, I. D.; Jensen, K. F. *J. Appl. Phys.* **1997**, *81(8)*, 3716.

[19] Janssen, F. J. J.; Yzendoorn, L. J.; Schoo, H. F. M.; Sturm, J. M.; Andersson, G. G.; Denier van der Gon, A. W.; Brongersma, H. H.; De Voight, M. J. A. *Synth. Met.* **2002**, *131*, 167.

[20] Antoniadis, H.; Rothberg, L. J.; Papadimitrakopoulos, F.; Yan, M.; Galvin, M. E.; Abkowitz, M. A. *Phys. Rev.* **1994**, *50*, 14911.

[21] a) Sariciftci, N. S.; Smilowitz, L.; Heeger, A. J.; Wudl, F. *Science* **1992**, *258*, 1474. b) Sariciftci, N. S.; Heeger, A. J. *Int. J. Mod. Phys., Part B* **1994**, *8*, 237.

[22] Chung, S. J.; Lee, D. W.; Oh, D. K.; Lee, C. E.; Jin, J. L. *Acta Polym.* **1999**, *50*, 298.

[23] Cho, H. N. ; Kim, D. Y.; Kim, Y. C.; Lee, J. Y.; Kim, C. Y. *Adv. Mat.* **1997**, *9*, 326.

[24] Wong, K. F.; Skaf, M. S.; Yang, C-Y.; Rossky, P. J.; Bagchi, B.; Hu, D.; Yu, J; Barbara, P.F. *J. Phys. Chem. B.* **2001**, *105*, 6103.

[25] Son, S.; Dodabalapur, A.; Lovinger,A. J.; Galvin, M.E. *Science* **1995**, *269*, 376.

[26] Wessling, R. A. J. Polym. Sci., Polym. Symp. **1985**, *72*, 55.

[27] Herold, M.; Gmeiner, J.; Schwoerer, M. *Acta Polym.* **1996**, *47*, 436.

[28] a) Heeger, A. J.; Parker, I. D.; Yang, Y. *Synth. Met.* **1994**, *67*, 23. b) Yan, M.; Rothberg, L. J.; Kwock, E. W.; Miller, T. M. *Phys. Rev. Lett.* **1995**, *75*, 1992. c) Chung, S. J.; Jin, J. I.; Lee, C. H.; Lee, C. E. *Adv. Mat.* **1998**, *10*, 684.

[29] a) Samuel, I. D. W.; Rumbles, G.; Collison, C. J. ; Moratti, S. C. ; Holmes, A. B. *Chemical Physics* **1998**, *227*, 75. b) Nguygen, T. ; Doan, V. ; Schwarz, B. J. *J. Chem. Phys.* **1999**, *110(8)*, 4068. c) Shi, Y.; Liu, J.; Yang, Y. *Macromol. Symp.* **2000**, *154*, 187. d) Nguygen, T.; Martini, I. B.; Liu, J.; Schwarz, B. J. *J. Phys. Chem.* **2000**, *104*, 237.

[30] Kiebooms, R.; Menon, R.; Lee, K.; *Handbook of advanced electronic and photonic materials and devices* **2001**, Academic Press, vol. 8, 1.

[31] Gilch, H. G.; Wheelwright, W. L. *J. Polym. Sci.: A* **1966**, *4*, 1337.

[32] a) Louwet, F.; Vanderzande, D.; Gelan, J.; Mullens, J. *Macromolecules* **1995**, *28*, 1330. b Issaris, A.; Vanderzande, D.; Gelan, J. *J. Polymer* **1997**, *38*, 2571.

[33] a) Garay, R. G.; Lenz, R. W. *Makromol. Chem. Suppl.* **1989**, *15*, 1. b) Yamada, S.; Tokito, S.; Tsutsui, T.; Saito, S. *J. Chem. Soc. Chem. Commun.* **1987**, 1448.

[34] Trost, B. M.; Salzmann, T. N.; Hiroi, K. *J. Am. Chem. Soc.* **1976**, *98*, 4887.

[35] Vanderzande, D.; Issaris, A.; Van Der Borght, M.; van Breemen; A.; de Kok, M.; Gelan, J. *Macromol. Symp.***1997**, *125*, 189.

[36] Lutsen, L.; Adriaensens, P.; Becker, H.; Van Breemen, A. J.; Vanderzande, D.; Gelan, J. *Macromolecules* **1999**, *32*, 6517-6525.

[37] Munters, T.; Martens, T.; Goris, L.; Vrindts, V.; Manca, J.; Lutsen, L. De Ceuninck, W.; Vanderzande, D.; De Schepper, L.; Gelan, J.; Sariciftci, N.S.; Brabec, C.J. *Thin Solid Films* **2002**, *403-404*, 247-251.

[38] Becker, H.; Spreitzer, H.; Ibrom, K.; Kreuder, W. *Macromolecules* **1999**, *32*, 4925-4932.

[39] Hontis, L.; Vrindts, V.; Vanderzande, D.; Lutsen, L. *Macromolecules* **2003**, *36*, 3035.

[40] Van Breemen, A. J.; Vanderzande, D.; Adriaensens, P.; Gelan, J. *J. Org. Chem.* **1999**, *64*, 3106-3112.

[41] Sanders, J. K. M.; Hunter, B.K. *Modern NMR spectroscopy* **1987**, Oxford University press, 181.

[42] Becker, H.; Spreitzer, H.; Kreuder, W.; Kluge, E.; Schenk, H.; Parker, I.; Cao, Y. *Adv. Mat.* **2000**, *12, No.1*, 42-48.

[43] Kesters, E.; Lutsen, L.; Vanderzande, D.; Gelan, J.; Nguyen, T. P.; Molinié, P. *Thin Solid Films* **2002**, *403-404*, 120-125.

[44] Van Breemen, A.; De Kok, M.; Adriaensens, P.; Vanderzande, D.; Gelan, J. *Macromol. Chem. and Phys.* **2001**, *202*, 354-361.

4. NMR Spectroscopy in the solid state

It is one of the key goals of material science to understand the structure-property relationship, in order to improve known and design new materials. This means in particular for polymers, whose material properties depend on both the molecular structure and the organization of the macromolecules in the solid state, as it is commonly used, their phase structure, morphology, molecular order and molecular dynamics[1]. The dynamic behaviour of polymers in the solid state is of significant practical importance with much interest focused on the relationship between structure and molecular motions, and the mechanical performance of these materials. In this work, we are interested in potential differences in the molecular ordering and dynamics of the sulphinyl and Gilch based MDMO-PPVs caused by the different types of defects (see chapter 3). This since the presence of ordered and more disordered domains can have serious consequences toward the final device performance. Among the various methods to study molecular dynamics, NMR spectroscopy has the advantage of being non-destructive and more structurally specific since the kind of nucleus being observed gives the possibility to study specific atoms of a monomer unit or chain segment.

A detailed overview of the molecular chain mobility and ordering of the Gilch and sulphinyl MDMO-PPV has been achieved by applying several solid state NMR techniques including ^{13}C high-resolution cross-polarization and magic angle spinning (CP/MAS) NMR with high-power proton dipolar decoupling (DD), ^{1}H wideline NMR, ^{13}C wideline NMR and ^{2}H wideline NMR spectroscopy, all of which have proven to be complementary (more about this in chapter 6).

Examination of the line shape and line width provides insight into the chain dynamics and ordering. Depending on the experimental approach, the line shape reflects either dipole-dipole interactions[2] or chemical-shift anisotropy[2] or in some cases a combination of both, or quadrupolar interactions[3]. Whatever the interaction, the observed line shape depends on the orientation of the monomer unit to the external, applied field. If molecular motions are present, the orientations and the line shape become partially averaged. These line shape changes are very distinctive and allow the assignment of motions characteristic for a given polymer system.
Besides line shape studies, the measurement of relaxation times gives information about local molecular dynamics in many frequency regimes[4]. A number of relaxation parameters can be studied, probing different motions over a wide range of frequencies since each relaxation time is characteristic for motions in a different range of frequencies. This chapter describes the spectral characteristics of the different solid state techniques used to examine the chain ordering and dynamics of sulphinyl and Gilch MDMO-PPV in the solid state.

4.1 The utility of some relaxation decay times

The different relaxation times are affected by molecular motions in a certain frequency range as mentioned before. The spin-lattice relaxation time T_1[5] (in the order of seconds) is dominated by the spectral density of motions in the MHz region, while the spin-lattice relaxation time in the rotating frame $T_{1\rho}$[6] (in the order of milliseconds) is affected by motions in the kHz region. For rigid systems, the spin-spin relaxation time T_2 (in the order of microseconds)[7] is mainly determined by very slow molecular motions in the order of 100-1000 Hz. As the interpretation of the relaxation times is often very complex and specific for a particular polymer, a reasonable explanation will be given when discussing the experimental results (see chapter 5 and 6) rather than defining them generally.

4.2 Spin diffusion

It must be noted that the proton spin relaxation times of solid polymers are not only determined by dynamic processes. Below the glass transition temperature, T_g, also the process of spin diffusion[8] contributes to the proton relaxation times T_{1H} and $T_{1\rho H}$. The strong proton dipole-dipole interactions are on the basis of it. Spin diffusion is the spatial propagation of spin magnetization by energy conserving "spin flips", and gives all abundant nuclei of the same type within the solid phase the same relaxation behavior. The presence of spin diffusion complicates the interpretation of proton spin-relaxation behaviour considerably. In contrast, spin diffusion is less efficient for ^{13}C and ^{2}H nuclei due to their low natural abundance which leads to large internuclear distances, so that spin diffusion and homonuclear coupling become negligible. Due to spin diffusion all abundant nuclei of the same type (e.g. proton spins) can show the same volume averaged T_{1H} and $T_{1\rho H}$ decay time. The maximum path length L, over which proton-proton spin diffusion can occur is approximately given by

$$L = \sqrt{6DT_i}$$

where D is the spin diffusion coefficient (~ 10^{-16} m^2/s for rigid polymers) and T_i is the relaxation time T_{1H} or $T_{1\rho H}$[9]. The decay time T_{1H}, in the order of seconds, is averaged out over a large distance (in the order of tens of nanometers). The proton decay time $T_{1\rho H}$, on the other hand, in the order of milliseconds, will be averaged out over a shorter distance (1–2 nm), making it a more local property. For blends and block-copolymers, both proton decay times allow to measure the degree of phase separation and the size of the phase separated molecular domains[10]. The decay time T_{2H} is not influenced by spin diffusion since this decay time is too short for solid polymers to allow magnetization transfer.

4.3 The ^{13}C CP/MAS experiment

^{13}C High-resolution solid state NMR permits the study of structures and molecular dynamics of solid materials as the resonances of chemically distinct carbons are separated. Consequently, simultaneously relaxation time studies of several specific groups (e.g. carbonyl groups, double bond carbons) can be undertaken since the relaxation of each nucleus can be studied individually. In the solid state, however, the resonance lines which were very sharp in the liquid state NMR spectrum, are replaced by extremely broad, featureless peaks, so that useful structural information (e.g. chemical shifts, scalar couplings) cannot be obtained. These line broadening effects are primarily the result of the strong dipole-dipole couplings and the chemical shift anisotropy (CSA) that are also present in the liquid state. However, these interactions do not lead to line broadening there because they are averaged out by the rapid and isotropic motions of the molecules. As motional averaging is incomplete in solids, the resultant broadening must be eliminated to obtain liquid-like spectra. In the following, the underlying mechanism of dipole-dipole coupling and CSA as well as methods for dealing with them will be briefly discussed.

4.3.1 The dipole-dipole interaction and the chemical shift anisotropy[11,12,13,14,15,16]

The *dipole-dipole interaction or dipolar coupling* has already been mentioned in paragraph 2.2.3 as a through-space interaction since the magnitude of the coupling between two nuclear spins depends on the internuclear distance (equation 2.10). For protons, the major contribution of this dipolar interaction arises from the protons themselves due to their high abundance and gyromagnetic ratio. ^{13}C nuclei

observed at natural abundance on the other hand, are dipolar coupled to the abundant and nearby ^{1}H nuclei (Figure 1a) resulting in a splitting D.

$$D = \frac{h\gamma_C\gamma_H}{4\pi^2 r^3}(3\cos^2\theta - 1) \qquad (4.1)$$

This splitting is illustrated in Figure 1b and its magnitude is several tens of kHz. In polycrystalline or glassy materials, the orientation of ^{13}C nuclei versus nearby protons is randomly arranged and their C-H vectors assume all possible angles with respect to the applied external magnetic field. This results in a Pake pattern[17] of ^{13}C resonances as shown in Figure 1c, if all C-H vectors are of the same distance r. In addition, the ^{13}C nuclei in a rigid, polymer sample are dipolar coupled to protons located at more than a single internuclear distance r. When the dipolar interaction between ^{13}C and ^{1}H nuclei is spread out over both the distance and orientation, a broad Gaussian line shape as presented in Figure 1d is obtained. The ^{13}C-^{13}C dipolar coupling can be ignored because the dipolar interaction among the ^{13}C nuclei is weak due to their large internuclear distances and small magnetic moments.

High-power ^{1}H dipolar decoupling[18] (DD) is used to remove the effects of the dipole-dipole interaction in solids. By constantly applying radio-frequency pulses that rotate the proton nuclear spins between their “spin-up” and “spin-down” states, the average orientation of the ^{1}H magnetic moments tends to zero, and the dipolar coupling is essentially averaged away. For the averaging to be effective, the irradiation obviously must be powerful enough to average ^{13}C-^{1}H couplings. This means that decoupling fields of 60 kHz or more are needed. The spectrum is still not solution-like as it contains broadening from the chemical shift anisotropy (CSA).

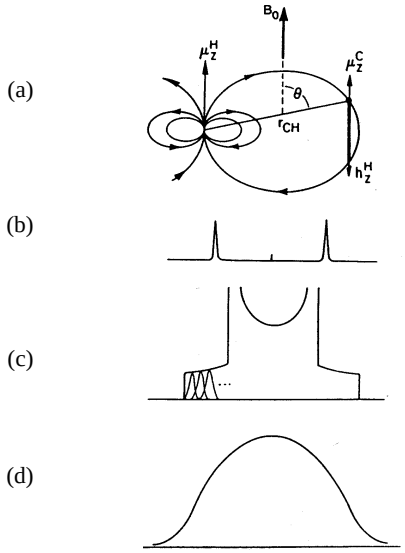

Figure 1 *(a) Dipolar interaction between a ^{13}C and proton spin. The μ_z are the z components of the magnetic moments, and h^{H}_{z} is the z component of the proton dipolar field at the ^{13}C nucleus. (b) Dipolar splitting of isolated C-H pairs at one angle relative to the magnetic field. (c) Pake pattern expected for isolated C-H pairs distributed at all angles as in polycrystalline or glassy materials. Several components from specific angles are illustrated schematically (d) Gaussian line shape observed for non-isolated C-H pairs, where all angles and nuclear distance are possible.*

The resonance frequency or chemical shift of a particular nucleus depends both on the type of nucleus (e.g. ^{1}H, ^{13}C) and the electronic environment of that nucleus i.e. the arrangement of electrons and other nuclei. The surrounding electrons shield the nucleus from the external magnetic field. Because the electronic environment is usually different in different directions in the molecule (anisotropic), the nucleus sees a different shielding and hence has a different chemical shift in different

directions. This orientation dependence of the chemical shift is also called *chemical shift anisotropy (CSA)*. In solution, the three-dimensional electronic shielding is averaged by the rapid molecular tumbling and a sharp, isotropic line is produced. In solids, in contrast, there are no rapid molecular motions and because the shielding is not identical along all directions, a broad resonance pattern or *chemical shift tensor powder pattern* is formed. When several chemical shift tensor powder patterns from chemically distinct nuclei are present in the spectrum, severe overlap occurs and most information is obscured. Because nuclear shielding is a field-dependent phenomenon, the width of the CSA pattern in frequency units increases linearly with the static field.

Magic angle spinning[19] (MAS) reduces the line broadening caused by the chemical shift anisotropy. By spinning the sample rapidly with the spinning axis inclined at 54.74° with respect to the static magnetic field B_o the broad chemical shift powder pattern is reduced to a single peak at the isotropic chemical shift.

4.3.2 Sensitivity enhancement by cross-polarization

In principal, high-resolution ^{13}C NMR spectra in the solid state can be generated for solids by applying both high-power proton decoupling and magic angle spinning. In practice, however, the pulse repetition rate is determined by the spin-lattice relaxation time T_1 values of the ^{13}C nuclei. Solids often have little molecular motion in the MHz frequency regime and thus have long carbon T_1 values. Other drawbacks of directly detecting nuclei with low gyromagnetic ratio such as ^{13}C are low isotopic abundances, low spin polarization and low signal intensity. These disadvantages can be circumvented by the *cross-polarization*[20] technique that combines both the high polarization and short relaxation times that are typical for ^{1}H NMR spectroscopy. This is realized by transferring the polarization of the abundant ^{1}H nuclei with short T_1 values to the rare ^{13}C nuclei. Although ^{1}H and ^{13}C

have Larmor frequencies different by a factor of four, Hartmann and Hahn[21] showed that energy can be transferred between them in the rotating frame of reference when

$$\gamma_C B_C = \gamma_H B_H \qquad (4.2)$$

This is the so called Hartmann-Hahn condition and results in a match of the rotating frame energies for ^1H and ^{13}C. The match is produced when the applied carbon RF field (B_{1C}) is four times the strength of the applied proton RF field (B_{1H}). By bringing the ^{13}C and ^1H spins in contact for a time t_c under the Hartmann-Hahn condition, cross-polarization to the carbon spins is achieved. The cross-polarization transfer is characterized by a growth rate of carbon intensity with a corresponding cross-polarization decay time T_{CH}. For fully quantitative ^{13}C NMR spectra recorded with CP/MAS/DD, a contact time study needs to be performed to ensure that all ^{13}C nuclei are in equilibrium with the abundant protons. For relaxation experiments, the contact time t_c is mostly set to about 5 times T_{CH}. Based upon these theoretical considerations, one might expect that carbon atoms polarize at the following relative rates: CH_3 (static) > CH_2 > CH ≥ CH_3 (mobile) > C (non-protonated).

In conclusion, the advantages of cross-polarization are twofold. First, the proton T_1 decay time dictates the repetition rate of the experiment, rather than the much larger carbon T_1 decay time. Second, the carbon shows an enhancement in signal intensity, which can be as large as the ratio of γ_C/γ_H or a factor of 4.

4.4 ^{1}H wideline NMR spectroscopy[11,16,22,23,24]

^1H solid state NMR spectra consist typically of one single broad peak with a line width in the order of 50 kHz due to the strong homonuclear ^1H-^1H dipolar

couplings (in the order of 100 kHz) and high natural abundance of protons. The presence of this strong coupling in addition to the very limited chemical shift range yields spectra with extensive overlap of resonances from chemically inequivalent protons and no structural information is available. The advantage of this technique compared to the ^{13}C CP/MAS technique described above, is the gain in time since it only takes a few minutes instead of hours or even days as in the ^{13}C CP/MAS experiment. Although no information about the chemical structure can be obtained from ^{1}H wideline NMR spectra, the technique provides an interesting tool for characterizing the chain dynamics and chain organization in solid polymers. By selecting the proper pulse sequences, the different relaxation times (T_{1H}, $T_{1\rho H}$ and T_{2H}) can be determined to gain more insight into the evolution of the chain dynamics and organization in the solid state. It must be noted that in contrast with ^{13}C , the strong dipolar coupling between protons in the solid state allows rapid spin diffusion (see before) below the glass transition temperature. As a result, the proton spin relaxation times T_1 and $T_{1\rho}$ are not only influenced by dynamic processes.

4.5 ^{13}C wideline NMR spectroscopy[25]

The line shape of the ^{13}C chemical shift powder pattern can be used to study molecular ordering and dynamics in a manner analogous to deuterium line shape analysis (see further).

The shapes are largely determined by the chemical shift anisotropy since no MAS is used, but also by the dipole-dipole interactions which unfortunately can not be removed. In that way, the line shape is less selective compared to deuterium solid state NMR. Whatever the interaction, the observed line shape depends on the orientation of the polymer chains relative to the external, applied field. If the polymer is oriented, the broad powder pattern will partially collapse. Molecular

motions can also partially average the powder pattern when the frequency of the motion becomes rapid with respect to the frequency separation between the points of the line shape[26]. For high molecular weight polymers, the motions will mainly consists of bond rotations in parts of the polymer backbone or side group rotations rather than an overall chain mobility. When the exact motion can not be specified, the width of the powder pattern and asymmetry can be used to infer the polymer chain dynamics. A complication in the use of powder patterns is that the overlapping signals from the many different carbons may make analysis impossible due the CSA and dipole-dipole interactions. A solution can be found in working with ^{13}C enriched materials in which the signal from a particular carbon atom is so enhanced relative to the rest of the spectrum that it can be treated individually. Notice that the effect of the dipolar coupling can be excluded by recording ^{13}C NMR spectra using cross-polarization and high-power proton decoupling fields so that only the CSA contributes to the line shape.

4.6 ^{2}H wideline NMR spectroscopy[27,28,29,30,31]

Although solid state deuterium NMR is not a high-resolution technique, deuterium wideline NMR is a unique probe for investigating molecular motions and alignment or orientation of polymer chains[32] based on the line shape and the quadrupole splitting. The main drawback of deuterium NMR is the fact that labeled materials are needed, but this is also an advantage, in that molecular order and dynamics can be examined at specific sites. The use of specifically labeled polymers can give detailed information regarding individual groups, or segments of microscopic domains of the polymer.

The deuterium nucleus has a nuclear spin of 1, resulting in three quantized energy levels, +1, 0, -1 (see 2.1). The allowed transitions are (m = -1) $\leftrightarrow$ (m = 0) and (m =

0) ↔ (m = +1). In addition, the deuterium nucleus is quadrupolar and there is a nonspherical charge distribution at the nucleus. The interaction of the quadrupole moment with the electric field gradient which originates from the electrons in the C-D bond (the quadrupolar interaction) causes a substantial perturbation of the Zeemann splitting. This perturbation is so large that other NMR nuclear spin interactions such as the scalar J coupling, the deuteron-proton and deuteron-deuteron dipole-dipole interaction, and the deuteron chemical shift anisotropy are negligible. As the quadrupolar interaction dominates, deuterium powder spectra for unoriented samples are quite broad and can be up to 250 kHz in width. If the electric field gradient is axially symmetric, the spectrum for a single deuteron consists of a doublet with a peak separation $\Delta\nu_q$ given by[33]

$$\Delta\nu_q = \frac{3e^2qQ}{4h} (3\cos^2\theta - 1) \qquad (4.3)$$

where $\frac{e^2qQ}{h}$ is the quadrupole coupling constant and θ specifies the orientation of the C-D field vector with respect to the magnetic field. The line shape reflects the probabilities of the various C-D bond orientations (different values for θ) with respect to the magnetic field[34]. This process is schematically shown in Figure 2a-c for a single transition. The two transitions are combined in Figure 2d to produce the Pake powder pattern[17]. According to equation (4.3), the 'steps' at the wings of the spectrum correspond to θ = 0°, and the central pair of peaks to θ = 90° and the mid point to the orientation with θ = 54°44' where the two peaks from the quadrupole splitting coalesce and the quadrupole interaction vanishes.

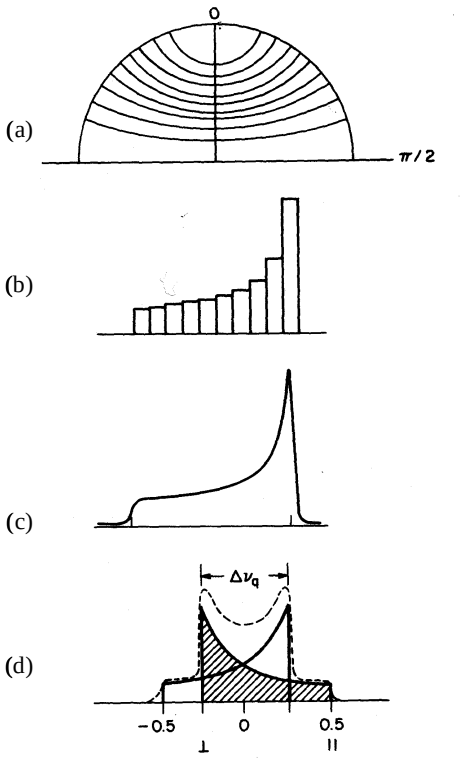

Figure 2 *The deuterium line shape and how it arises. (a) Consider a sphere divided into latitudes of equal frequency. 0 is the orientation when the C-D bond is parallel to the external magnetic field and π/2 is the perpendicular orientation. (b) A histogram of the areas in the equal frequency latitudes. (c) A smoothed version of (b). (d) Both transitions.*

If a single crystal or an oriented system is rotated in the magnetic field, different resonance lines are predicted to be obtained for each orientation. This orientation-dependent information can be used to determine the orientation of a specific group i.e. a C-D bond, in a polymer relative to a fiber drawn direction, for example. On the other hand, if the orientation of the C-D bond is changed because of internal molecular motions, the static powder pattern is averaged highly in a specific way. The line shape can therefore be used to determine the amplitude and frequency of molecular motions. The strategy is to first calculate a theoretical pattern for an

assumed motion and order. Then, the observed pattern is matched to the calculated pattern, thereby specifying the motion and order. Figure 3 shows some explicit line shapes for various types of motion that are often found in polymers.

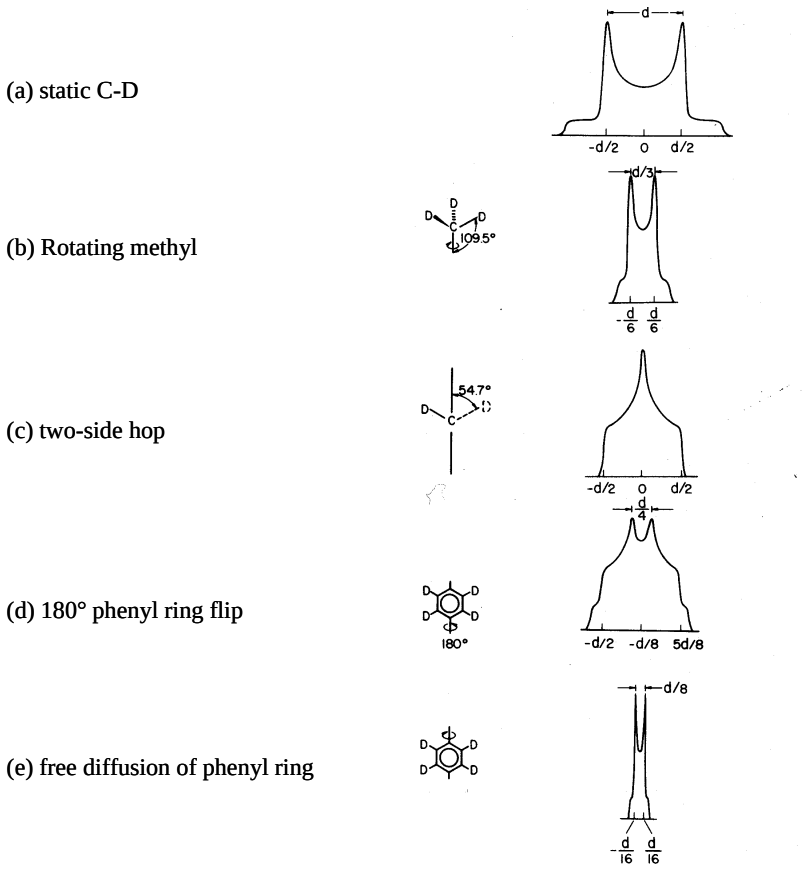

Figure 3 *Theoretical deuterium NMR line shapes for various types of anisotropic motions.*

Deuterium line shape analysis is sensitive to slow molecular motions with correlation times[35] of 10^{-3} to 10^{-7} s. It must be noted that polymers can rarely be isolated as large single crystals so they produce mostly a powder line shape. Although the deuterium NMR line shape provides information about the angular range of motion, it contains no further information about the rate of motion on the deuterium NMR time scale when motion is fast (correlation times of 10^{-6} to 10^{-10} s).

This information can be obtained from deuterium NMR relaxation experiments, most notably from T_1 measurements using the inversion-recovery pulse sequence followed by quadrupole echo detection (see further). As mentioned earlier, the quadrupole interaction provides also a very efficient mechanism for the spin-lattice relaxation. In addition, spin diffusion is very unefficient for deuterons (deuterium has a low natural abundance, lower than ^{13}C).

4.7 References

[1] a) Flory, P. J. *Principles of Polymer Chemistry* **1953**, Cornell University Press, Ithaca. b) Kroschwitz, J. I. *Concise Encyclopedia of Polymer Science and Technology* **1990**, Wiley, New York.

[2] Inglefield, P. T.; Amici, R. M.; O'Gara, J. F.; Hung, C.-C, Jones, A. A. *Macromolecules* **1983**, *261*, 193.

[3] Jelinski, L. W.; Dumais, J. J. ; Engel, A. K. *Macromolecules* **1983**, *16*, 492.

[4] Bovey, F. A.; Jelinsky, L. W. *J. Phys. Chem.* **1985**, *89*, 571.

[5] a) Torchia, D. A.; Szabo, A. *J. Magn. Reson.* **1982**, *49*, 107. b) Silvestri, R. L.; Koenig, J. L. *Macromolecules* **1992**, *25*, 2341.

[6] a) Schaefer, J.; Stejskal, E. O.; Buchdahl, R. *Macromolecules* **1977**, *10*, 384. b) Schaefer, J.; Stejskal, E. O.; Steger, T. R.; Sefcik, M. D.; McKay, R. A. *Macromolecules* **1980**, *13*, 1121.

[7] Carr, H. Y.; Purcell, E. M. *Phys. Rev.* **1954**, *94*, 630.

[8] a) Komoroski, R. A. *High Resolution NMR Spectroscopy of Synthetic Polymers in Bulk* **1986**, VCH: Florida. b) McBrierty, V. J.; Douglas, D. C. *J. Polym. Sci., Macromolec. Rev* **1981**, *16*, 295.

[9] Douglas, D. C.; Jones, G. P. J. J. *Chem. Phys.* **1966**, *45*, 956.

[10] Schmidt-Rohr, K.; Spiess, H. W. *Multidimensional solid state NMR and polymers* **1996**, Academic Press, 402.

[11] Laws, D. D.; Bitter, H-M. L, Jershow, A. *Angew. Chem. Int. Ed.* **2002**, *41*, 3096.

[12] Silvestry, R. L.; Koenig, J. L. *Anal. Chim. Acta* **1993**, *283*, 997.

[13] Ibbett, R. N. *NMR spectroscopy of Polymers* **1993**, Chapman & Hall, London, 161.

[14] Komoroski, R. A. *High Resolution NMR spectroscopy of Synthetic Polymers in Bulk* **1986**, VCH Publishers, Inc., 19.

[15] Bovey, F. A.; Jelinski, L. W. *J. Phys. Chem.* **1985**, *89*, 571.

[16] Komoroski, R. A. *High Resolution NMR spectroscopy of Synthetic Polymers in Bulk* **1986**, VCH Publishers, Inc., 247.

[17] Pake, G. E. *J. Chem. Phys.* **1948**, *16*, 327.

[18] Bloch, F. *Phys. Rev.* **1956**, *102*, 104.

[19] a) Andrew, E.R.; Bradbury, A.; Eades, R. G. *Nature* **1958,** *182*, 1659. b) Lowe, I. J. *Phys. Rev. Lett.* **1959**, *2*, 285. c) Schaefer, J.; Stejskal, E. O.; *J. Am. Chem. Soc.* **1976**, *98*, 1031.

[20] Pines, A.; Gibby, M. G.; Waugh, J. S. *J. Chem. Phys.* **1973**, *59*, 569.

[21] Hartmann, S. R.; Hahn, E. L. *Phys. Rev.* **1962**, *128*, 2042.

[22] Ricardo, N.; Lahtinen, M.; Price, C.; Heatley, F. *Polym. Int.* **2002**, *51*, 627.

[23] Geppi, M.; Kenwright, A. M.; Say, B. J. *Solid State Nuclear Magnetic Resonance* **2000**, *15*, 195.

[24] Ibbett, R. N. *NMR spectroscopy of Polymers* **1993**, Chapman & Hall, London, 231.

[25] Henrichs, P. M.; Linder, M.; Hewitt, J. M.; Massa, D.; Isaacson, H. V. *Macromolecules* **1984**, *17*, 2412.

[26] Slotfeldt-Ellingsen, D.; Resing, H. A. *J. Phys. Chem.* **1980**, *84*, 2204.

[27] Mathias, L. *Solid State NMR of Polymers* **1991**, Plenum Press, New York, 23.

[28] Ibbett, R. N. *NMR spectroscopy of Polymers* **1993**, Chapman & Hall, London, 275.

[29] Komoroski, R. A. *High Resolution NMR spectroscopy of Synthetic Polymers in Bulk* **1986**, VCH Publishers, Inc., 335.

[30] Simpson, J. H.; Liang, W.; Rice, D. M. ; Karasz, F. E. *Macromolecules* **1992**, *25*, 3068.

[31] Simpson, J. H.; Rice, D. M. ; Karasz, F. E. *Macromolecules* **1992**, *25*, 2099.

[32] Spiess, H. W. *Colloid Polym. Sci.* **1983**, *261*, 193.

[33] a) Abragam, A. *The principles of nuclear magnetism* **1961**, Oxford University Press, Oxford. B) Spiess, H. W. *NMR – Basic Principles and Progress* **1978**, vol. 15, Springer-Verlag, New York.

[34] Mehring, M. *High Resolution NMR in Solids* **1983**, second edition, Springer-Verlag, New York.

[35] a) Spiess, H. W.; Sillescu, H. *J. Magn. Reson.* **1981**, *42*, 381. b) Spiess, H. W. *Chem. Macromol. Symp.* **1989**, *26*, 197.

5. Chain dynamics and organization during the elimination process

5.1 Introduction

This study focuses on the thermal conversion of n-butyl sulphinyl MDMO-precursor polymers toward the conjugated state. Depending on the elimination or conversion temperature, the obtained polymer will be fully or partly conjugated. Uncomplete elimination induces various fluctuations in the properties of the final opto-electronic devices since the noneliminated groups act as sp^3 defects that will interrupt the π-conjugation. It has already been shown that a disruption of the conjugation has serious consequences with respect to the electrical conductivity[1], photo- and electroluminescence efficiency[2] and degree of chain organization[3]. Moreover, too high elimination temperatures will not only cause thermal degradation[4], but will also lead to unnecessary production costs. So, it is of utmost importance that this temperature can be kept as low as possible.

To get a reliable idea about the most efficient elimination temperature, several complementary techniques including in-situ ultraviolet visible spectroscopy (UV/Vis), fourier transform infrared spectroscopy (FT-IR) and ^1H wideline NMR spectroscopy are compared. We opted for studying the sulphinyl MDMO precursor polymers since they can easily be isolated and are stable at room temperature. Previously[5], the thermal conversion of n-alkyl-sulphinyl MDMO-PPV precursor polymers as a function of elimination temperature was studied by means of various analytical techniques. The temperature range in which the elimination and degradation processes take place could be derived from in-situ FT-IR and UV/Vis

spectroscopy. The thermal reaction of the elimination products, on the other hand, was investigated by X-ray photoelectron spectroscopy (XPS), electron spin resonance (ESR) and Raman spectroscopy. Up to now, however, the effect of elimination on polymer motion and organization (e.g. chain association) has never been studied.

A series of MDMO-PPV precursor polymers, synthesized according to the sulphinyl precursor route[6], was converted toward the conjugated state by thermal elimination in toluene during 90 min at 50, 60, 65, 70, 80, 90, 100 and 110 °C, respectively. In Figure 1 the thermal elimination step is depicted.

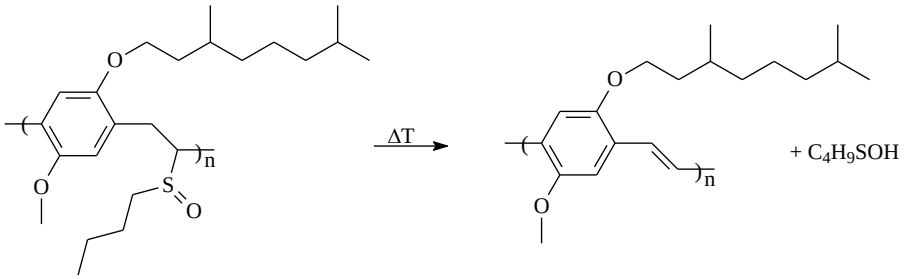

Figure 1 *The thermal conversion of the n-butyl sulphinyl MDMO-PPV precursor polymer.*

The elimination reaction is considered to proceed via a syn-elimination[7] in which sulphenic acids are expulsed as the double bonds are formed. First, the UV-Vis and FT-IR spectra will be discussed and interpreted, afterwards they will be related to the results of a ^{1}H wideline NMR relaxation time study.

5.2 Results and discussion

5.2.1 Ultraviolet visible spectroscopy (UV/Vis)

In-situ UV-Vis spectroscopy is an analytical technique by which the formation of the conjugation (red shift of λ_{max}) can be followed as a function of temperature. The UV-Vis absorption spectra of MDMO-PPV precursor polymers recorded with a ramp of 2 °C/ min starting from ambient temperature are shown for some temperatures in Figure 2. The absorption band at 301 nm originates from the MDMO-PPV precursor polymer and its absorbance decreases upon increasing the temperature. The absorption band at 374 nm on the other hand originates from the initial formation of rather short conjugated sequences. It disappears gradually as the elimination reaction proceeds (between 70 and 110 °C), while a new and broad absorption band is formed at longer wavelengths. The latter clearly shows a red shift upon increasing the elimination temperature, indicating that the effective conjugation length of the conjugated π-system increases. The position of this band is stable around 110 °C as no further bathochromic effects are noticed.

From these UV-Vis experiments, one can conclude that the elimination reaction gradually proceeds in the temperature range between 70 °C and 110 °C. However, one has to be cautious in interpreting such in-situ data since they are sometimes influenced by differences between the temperature in the oven and of the polymer sample. Slow heating rates (e.g. 2 ° C/ min) have therefore to be respected to avoid these discrepancies.

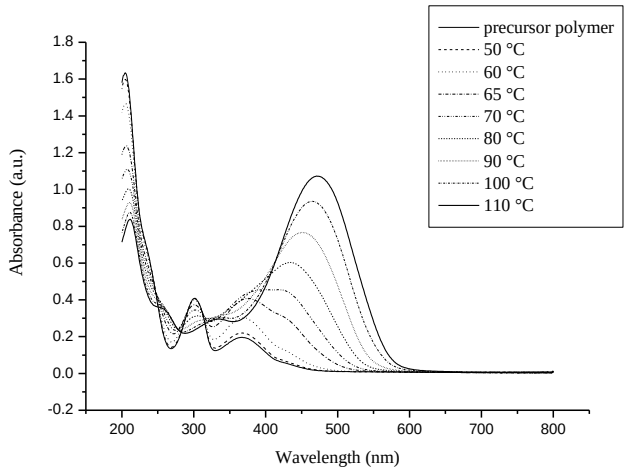

Figure 2 *In-situ UV-Vis absorption spectra of n-butyl sulphinyl MDMO-PPV precursor polymers at different temperatures.*

5.2.2 Fourier transform infra-red spectroscopy (FT-IR)

The FT-IR spectra of the MDMO-PPVs which have been eliminated for 90 min in toluene at different temperatures were recorded in the solid state. FT-IR spectroscopy allows to monitor the elimination process since both the decrease of the IR absorbance of the sulphoxide stretch vibration at 1038 cm^{-1} and the increase of the absorbance of the out-of-plane bend vibration of the trans double bond at 965 cm^{-1} can be followed as a function of the elimination temperature. Therefore, the summed integrated area of the absorbances at 1505 and 1465 cm^{-1}, attributed to stretchings of the phenylene ring, were used to normalize the integrated area of the double bond absorbance or of the S(O) stretch.

As a conclusion, it can be stated that the elimination reaction starts around 70 °C and seems to be completed only after elimination around 100 °C for 90 min (see Figure 3).

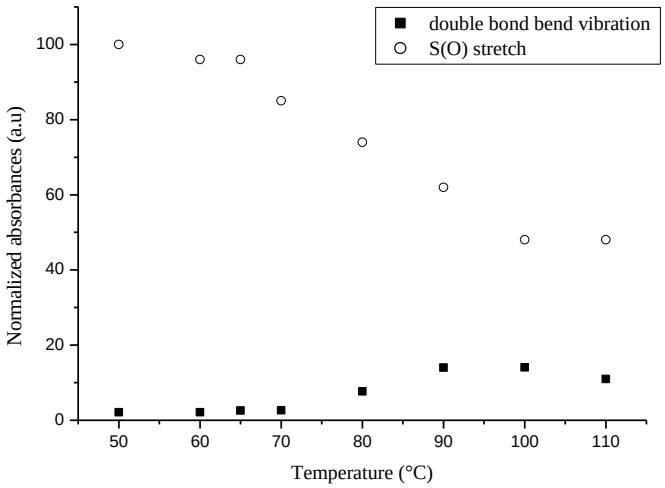

Figure 3 *Evolution of the normalized absorbance at 965 cm^{-1} (double bond bend vibration) and 1038 cm^{-1} (S(O) stretch vibration) as a function of the elimination temperature*.

5.2.3 ^{1}H wideline solid state NMR

^{1}H wideline solid-state NMR is a fast technique (in the order of a few minutes) that offers the possibility to study molecular chain mobility and phase morphology on the nanometer scale by means of a diverse set of relaxation decay times. The relaxation times of interest are the proton spin-lattice relaxation time T_{1H}, the proton spin-lattice time in the rotating frame $T_{1\rho H}$, and the proton spin-spin relaxation time T_{2H}. The decay times were measured for a series of precursor polymers that have been eliminated during 90 min at different temperatures before the NMR measurements.

5.2.3.1 The proton spin-lattice relaxation time (T_{1H})

Measurements at ambient temperature show a T_{1H} decay time that is independent of the elimination temperature, T_{elim}. As differential scanning calorimetry (DSC) measurements point out that the conjugated MDMO-PPV has a T_g around 55 °C, spin diffusion can take place efficiently at ambient temperature. So, a single T_{1H} decay of 0.65 s (efficient relaxation) is observed since the proton magnetization is averaged out efficiently between the rigid polymer backbone and the more mobile side chains (Table 1). In the solid state at temperatures below T_g, the T_{1H} relaxation is often dominated by the high frequency motions of mobile end groups and side chains[8] as expressed in the following equation:

$$\frac{1}{T_1} = \frac{x_{mobile}}{T_{1,mobile}} + \frac{x_{immobile}}{T_{1,immobile}} \qquad (5.1)$$

in which x_{mobile} and $x_{immobile}$ are the molar fractions of the mobile and immobile proton populations and $T_{1,mobile}$ and $T_{1,\,immobile}$ are the corresponding decay times.
Therefore, T_{1H} represents the average decay time of the mobile and immobile proton populations which is dominated by the fast motions of the mobile side chain ends, since the amount of protons in the rigid backbone ($x_{immobile}$) is small and $T_{1,immobile}$ is long.
Concerning the measurements at 57.5 °C, similar T_{1H} decay times are observed up to T_{elim} = 60 °C. A significant increase of T_{1H} is observed starting from a T_{elim} = 65 °C as a result of a decrease of the side chain mobility which indicates that the elimination reaction has started. The observed increase in T_{1H} can be explained by a decrease of the molar fraction of the mobile side chains (removal of the sulphinyl leaving group) and an increase of $T_{1,mobile}$ (τ_c of the side chains will increase upon elimination).

T_{elim} (°C)	T_{1H} (s)		$T_{1\rho H}^{S}$ (ms)/ M_o^{S}(%)	$T_{1\rho H}^{L}$(ms)/ M_o^{L}(%)	$T_{1\rho H}^{S}$(ms)/ M_o^{S}(%)	$T_{1\rho H}^{L}$(ms)/ M_o^{L}(%)
	20 °C	57.5 °C	20 °C		57.5 °C	
/	0.64	0.62	1.2/49	3.0/51	1.7/53	3.8/47
50	0.68	0.65	1.0/44	3.4/56	1.5/48	3.7/52
60	0.65	0.65	1.4/50	2.9/50	1.6/58	3.9/42
65	0.68	0.88	1.5/54	3.0/46	1.6/53	4.0/47
70	0.66	0.82	1.1/26	3.1/74	1.2/26	3.0/74
80	0.63	0.79	1.2/25	3.1/75	1.3/22	3.1/78
90	0.69	0.82	1.3/24	3.4/76	1.5/25	4.4/75
100	0.67	0.82	1.3/26	3.3/74	2.2/30	8.7/70
110	0.64	0.82	1.2/25	3.3/75	2.4/24	9.6/76

Table 1 *T_{1H} and $T_{1\rho H}$ relaxation times of the MDMO-PPV precursor polymers eliminated for 90 min at different temperatures. The average 95 % confidence limit for both T_{1H} and $T_{1\rho H}$ is about 5-8 %. The fractions of $T_{1\rho H}^{S}$ and $T_{1\rho H}^{L}$ are normalized to 100.*

5.2.3.2 The proton spin-lattice relaxation time in the rotating frame ($T_{1\rho H}$)

For all polymers, the $T_{1\rho H}$ relaxation behaves biexponentially, resulting in a short *($T_{1\rho H}^{S}$)* and long *($T_{1\rho H}^{L}$)* decay time. Table 1 presents the $T_{1\rho H}$ relaxation times and related proton fractions M_o for the polymers as a function of the elimination temperature.

Concerning the results at room temperature, it was found that both $T_{1\rho H}^{S}$ and $T_{1\rho H}^{L}$ remain unchanged upon increasing the elimination temperature. This indicates that the decay times are situated close around the minima of their log $T_{1\rho H}$ – log τ_c curves (Figure 5, chapter 2) due to an optimal spectral density of molecular motions in the kHz frequency range which causes relaxation to be highly efficient.

As the polymer backbone in contrast to the more mobile C_{10} side chain is characterized by a higher density of kHz motions, the $T_{1\rho H}$ relaxation will be more efficient leading to a shorter $T_{1\rho H}$ decay time. Therefore, the $T_{1\rho H}^{L}$ decay time can be assigned to the mobile protons of the dimethyloctyloxy side chains or C_{10} side chains, while $T_{1\rho H}^{S}$ represents the remaining less mobile protons.

Concerning the measurements at 57.5 °C, both decay times suddenly decrease at an elimination temperature of 70 °C, pass through the minimum of the log $T_{1\rho H}$ - log τ_c diagram (Figure 5, chapter 2) (notice that the values are now similar to those observed at ambient temperature), but start to increase again when $T_{elim} \geq 90$ °C. This implies that they shift to the right side of the correlation diagram (move to low frequency motions or longer τ_c, and so a drop in the spectral density of the kHz motions). This was further confirmed by measurements at a lower spin lock field for which lower values of the $T_{1\rho H}$ decay times were observed. This means that the polymer stiffness starts to enhance around 70 °C but keeps on enhancing up to 110 °C. Notice that the evolution of τ_c is less pronounced for the less mobile protons which explains why the changes observed for $T_{1\rho H}^{S}$ are less clear.

At ambient temperature as well as at 57.5 °C, an abrupt change of the corresponding fractions from 50/50 % to 25/75 % can be noticed around 70 °C when elimination of the sulphinyl groups starts to take place (see also UV/Vis and FT-IR measurements). A reasonable explanation of the data presented in Table 1 can be found in the UV/Vis experiments.
Below 65 °C, two absorption bands at 301 and 374 nm are observed which originate from the precursor polymer and the initial, random formation of very short conjugated sequences, respectively. Of special interest is the decrease of the latter between 70 and 90 °C while a new band is formed around 424 nm, indicating that the length of the conjugated blocks increases. At this stage, the polymer chain mainly consists of conjugated segments intermittent by non-conjugated segments.

This idea was further confirmed by recording a solution-state ^{13}C NMR spectrum of a ^{13}C-labeled polymer which was eliminated for 90 min at 70 °C. In this way, the intensity ratio of the backbone aliphatic carbons to the carbons of the double bonds could be derived as being 31 and 69 %, respectively indicating that elimination is still not complete, but that most of the sulphinyl groups are already removed. Above 90 °C, λ_{max} increases further upon increasing the elimination temperature and a main absorption band around 475 nm, typical for an extended conjugated π-system, is finally formed at 110 °C (Figure 2). Between 90 and 110 °C, most of the remaining sulphoxide groups are gradually removed leading to large conjugated sequence blocks that are only sporadically interrupted by noneliminated groups (sp^3 defects). This is a clear indication that the rather strong increase in $T_{1\rho H}^{L}$ (but also in $T_{1\rho H}^{S}$) for 90 °C ≤ T_{elim} ≤ 110 °C is pointing to a further enhancement of the conjugation length which limits the mobility of the backbone and the long C_{10} side chains. Although their presence can not be excluded, interchain interactions (aggregates) can not be demonstrated straightforward from these measurements. For MEH-PPV, a polymer similar in structure to MDMO-PPV the formation of aggregates was found by means of photoluminescence spectroscopy[9].

Recently[10], we synthesized an almost fully conjugated ^{13}C-labeled MDMO-PPV (labeled at the double bond carbon atoms; only 1 % of noneliminated groups) by means of a two-step elimination procedure (see Experimental Part) as was indicated by quantitative solution state ^{13}C NMR spectroscopy. Therefore, both $T_{1\rho H}$ decay times of this fully conjugated MDMO-PPV can be taken as representatives of a fully conjugated system (Table 2).

measuring temperature	T_{1H} (s)	$T_{1\rho H}^{S}$ (ms) /M_o^{S} (%)	$T_{1\rho H}^{L}$ (ms) /M_o^{L} (%)	T_{2H}^{S} (μs) /M_o^{S} (%)	T_{2H}^{L} (μs) /M_o^{L} (%)
20 °C	0.65	1.2/23	3.2/77	21/42	30/58
57.5 °C	0.81	3.0/24	10.4/76	24/23	42/77

Table 2 *T_{1H}, $T_{1\rho H}$ and T_{2H} relaxation times of fully conjugated MDMO-PPV. The average 95 % confidence limit is about 5% for T_{1H} and $T_{1\rho H}$, and 10 % for T_{2H}. The fractions of $T_{1\rho H}^{S}$ and $T_{1\rho H}^{L}$, and T_{2H}^{S} and T_{2H}^{L} are normalized to 100.*

From Table 2, it is clear that the values of $T_{1\rho H}^{S}$ and $T_{1\rho H}^{L}$ of this fully conjugated polymer as measured at 57.5°C, are still somewhat larger as compared to those mentioned in Table 1 for a polymer that is eliminated for 90 min at 110 °C. This indicates that the spectral density of kHz motions is further reduced for the two-step eliminated MDMO-PPV and means that segmental motions of the backbone and C_{10} side chains are further slowed down. The obtained results are in agreement with ^{13}C solution-state NMR spectrum for a ^{13}C labeled precursor polymer which is eliminated for 90 min at 110 °C (one-step elimination): 10 % of the sulphoxide groups has still not been eliminated.

5.2.3.3 The proton spin-spin relaxation time T_{2H}

In contrast to the T_{1H} and $T_{1\rho H}$ relaxation times, the spin-spin relaxation time T_{2H} can be interpreted straightforward in terms of molecular chain dynamics (no minimum in the correlation diagram): a longer T_{2H} relaxation time always indicates a higher segmental chain mobility (see Figure 5, chapter 2). Also the T_{2H} relaxation analysis results in two time constants for all MDMO-PPV polymers as presented in Table 3.

T_{elim} (°C)	T_{2H}^S (µs)/ M_o^S(%)	T_{2H}^L (µs)/ M_o^L (%)	T_{2H}^S (µs)/ M_o^S (%)	T_{2H}^L(µs)/ M_o^L(%)
	20 °C		57.5 °C	
/	25/22	63/78	29/22	125/78
50	23/20	70/80	32/21	117/79
60	24/21	63/79	34/20	120/80
65	24/21	63/79	28/21	69/79
70	21/44	32 /56	26/31	59/69
80	22/40	33/60	27/32	65/68
90	21/40	30/60	23/28	42/72
100	21/42	31/58	24/27	42/73
110	21/44	29/56	24/25	41/75

Table 3 *T_{2H} relaxation times of the MDMO-PPV precursor polymers eliminated for 90 min at different temperatures. The average 95 % confidence limit for T_{2H} is about 10 %. The fractions of T_{2H}^S and T_{2H}^L are normalized to 100.*

At room temperature, both T_{2H}^S and T_{2H}^L decay times show a rather discrete jump toward shorter values at T_{elim} = 70 °C (more clear for T_{2H}^L) which indicates that the polymer system becomes more rigid. This observation is confirmed by a sudden change of the corresponding fractions which can be understood on the basis of the assignment of the proton fractions: below 70 °C, T_{2H}^S (ca 20 %) can be roughly assigned to the protons of the polymer backbone (high density of low frequency motions), while T_{2H}^L (ca 80 %) represents the protons of the sulphoxide groups and C_{10}-side chains (lower density of low frequency motions). However, at $T_{elim} \geq 70$ °C a proton distribution of 40/60 % was found instead of the expected 25/75 %.

This can be attributed to the start of the elimination reaction: due to the stiffening of the system upon elimination (formation of the conjugated system), the protons of the side chain carbons closest to the backbone will become strongly immobilized and will end up in the T_{2H}^{S} fraction.

When measured at 57.5 °C, both T_2 decay times decrease as a function of T_{elim} and show two discrete jumps around 65 and 90 °C, respectively. These jumps are somewhat less pronounced for T_{2H}^{S} and correspond to the formation of conjugated segments intermittent by non-conjugated segments, and the large conjugated sequence blocks, respectively. This observation is completely in agreement with the $T_{1\rho H}$ decay time observation. At a measuring temperature close to T_g the proton fractions at T_{elim} = 110 °C (25/75 %) clearly represent the main chain and C_{10} side chain protons in contrast with the results at room temperature

5.3 Conclusion

The chain dynamics of MDMO-PPV precursor polymers have been studied as a function of the elimination temperature to obtain more insight into the elimination process. In-situ UV/Vis, FT-IR and ^{1}H wideline solid state NMR spectroscopy have proven to be complementary techniques as all three techniques show that the elimination reaction starts around 70 °C. However, the end phase of elimination is difficult to detect by FT-IR probably since quantification of IR signals can be rather complex, especially for the trans double bond bend vibration which has a low respons. Although λ_{max} also becomes less sensitive toward the final phase of elimination, in-situ UV/Vis has shown to be indispensable for the study of the elimination processes in PPV derivatives: the technique is fast, informative, sensitive and no overestimation of T_{elim} (due to the fast heating ramp) seems to occur for thin films. Although the quantification of the double bonds at

intermediate stages can neither be determined by ^{1}H wideline NMR (^{13}C solution-state NMR is probably the only quantitative technique for this purpose), the $T_{1\rho H}$ decay time seems to be extremely sensitive toward the detection of the final stage of elimination in the solid state (cf. differences in $T_{1\rho H}^{L}$ for the one and two step elimination procedure at 110 °C). $T_{1\rho H}^{L}$ measurements at temperatures close to T_g are indicating to be fast, sensitive and reliable substitutes for labour-intensive and time consuming ^{13}C liquid state NMR measurements on ^{13}C labeled specimens toward the detection of the completion of elimination (constant decay time indicates complete conversion). Both T_{2H} and $T_{1\rho H,}$ especially when measured at temperatures close to T_g, are furthermore sensitive toward the detection of the intermediate stage of the elimination process: initial, random formation of double bonds below 70 °C, blocks of conjugated/non-conjugated segments between 70 and 90 °C, and finally the formation of large conjugated blocks above 90°C.

As a final and general conclusion, it can be stated that ^{1}H wideline NMR is a very fast (about 30 min) and sensitive technique (only a few spincoated films of 100-200 nm in thickness are needed) for the study of the chain dynamics (and eventually phase separation) in opto-electronic devices based on conjugated polymers such as LEDs, organic transistors and solar cells.

5.4. References

[1] a) Basescu, N.; Liu, Z. X.; Moses, D.; Heeger, A. J.; Naarmann, H.; Theophilou, N. *Nature* **1987**, 327,403. b) Gelinck, G. H.; Warmann, J. M. *J. Phys. Chem.* **1996**, *100*, 20035.

[2] a) Staring, E. G. J.; Demandt, R. C.; Braun, D.; Rikken, G. L. J.; Kessener, Y. A.; Venhuizen, A. H. J.; Wynberg, H.; ten Hoeve, W.; Spoelstra, K. J. *Adv. Mat.* **1994**, *6*, 934. b) Braun, D.; Staring, E. G. J.; Demandt, R. C.; Rikken, G. L. J.; Kessener, Y. A.; Venhuizen, A. H. J. *Synth. Met.* **1994**, *66*, 75.

[3] Wong, K. F.; Skaf, M. S.; Yang, C-Y.; Rossky, P. J.; Bagchi, B.; Hu, D.; Yu, J; Barbara, P.F. *J. Phys. Chem. B.* **2001**, *105*, 6103.

[4] a) Papadimitrakopoulos, F.; Yan, M.; Rothberg, L. J.; Katz, H. E.; Chandross, E. A.; Galvin, M. E. *Mol. Cryst. Liq. Cryst.* **1994,** 256, 663. b) Rothberg, L. J.; Yan, M.; Papadimitrakopoulos, F.;Galvin, M. E.; Kwock, E. W.; Miller, T. M. *Synt. Met.* **1996**, 80, 41.

[5] Kesters, E.; Lutsen, L.; Vanderzande, D.; Gelan, J.; Nguyen, T. P.; Molinié, P. *Thin Solid Films* **2002**, *403-404*, 120-125.

[6] a) Louwet, F.; Vanderzande, D.; Gelan, J.; Mullens, J. *Macromolecules* **1995**, *28*, 1330. b Issaris, A.; Vanderzande, D.; Gelan, J. *J. Polymer* **1997**, *38*, 2571

[7] a) Janssen, J. W. A. M.; Kwart, H. *J. Org. Chem.* **1977**, *42*, 1530. b) Kwart, H.; George, T. J.; Louw, R.; Ultee, W. *J. Am. Chem. Soc.* **1978**, 3927.

[8] Lauprette, F. *Prog. Polym. Sci* **1990**, *15*, 425.

[9] Nguygen, T.; Martini, I. B.; Liu, J.; Schwarz, B. J. *J. Phys. Chem.* **2000**, *104*, 237.

[10] Roex, H.; Adriaensens, P.; Vanderzande, D.; Gelan, J. *Macromolecules* **2003**, *36 (15)*, 5613.

6. Molecular dynamics and ordering in sulphinyl and Gilch MDMO-PVV

6.1 Introduction

As mentioned before, one of the parameters that will affect to a great extent the efficiency of the opto-electronic devices is the morphology of the polymer layer. The final morphology may depend on several factors: the polymerization method, the molecular ordering and dynamics of the polymer chains, the casting conditions and the casting solvent[1] etc. In this chapter we want to examine whether the polymerization defects and the synthetic procedure (sulphinyl versus Gilch precursor route) will affect the molecular ordering and if so, to which extent. Only an integral optimization of these variables will lead to a better device performance since the presence of ordered domains (pseudo-ordered or crystalline) and/or disordered domains (amorphous) can heavily influence their working. Consequently, the search for suitable analytical techniques that provide information about the phase morphology (molecular ordering and miscibility) of polymers in the active layer of the opto-electronic devices has been the main goal of this chapter. T_{1H} and $T_{1\rho H}$ relaxation time measurements can be used to determine the degree of phase separation and to estimate the size of phase separated domains for block-copolymers and blends if the conditions for efficient spin diffusion (see 4.2) are fulfilled: T_{1H} and $T_{1\rho H}$ relaxation of abundant nuclei (protons), relative slow molecular motions or short correlation times (working below T_g) and long relaxation times (time is needed to transfer magnetization). As a result, only the T_{1H} and $T_{1\rho H}$ decay times are suitable. The T_{2H} relaxation time on the other hand, provides information about ultra slow, local molecular motions since the decay

time is too short to allow magnetization transfer. Furthermore it is known that long range ordering can be examined by means of T_{1C} relaxation time studies, whereas ^2H solid state line shape analyses can give information about the local molecular ordering. WAXS and DSC on the other hand are valuable to study the degree of crystallinity. It must be noted that in contrast to the other experimental chapters, this chapter has to be considered as an extended feasibility study rather than an completed study. So, only preliminary conclusions have been drawn.

6.2 ^2H wideline NMR

6.2.1 ^2H line shape studies

Deuterium wideline NMR provides a powerful way to study local molecular motions in polymers. These motions are capable to average partially the quadrupolar interaction leading to a change in the line shape which reflects the orientation distribution. This information about the chain conformational mobility can be used for a better understanding of the opto-electronic behaviour of conducting polymers. Consequently, adequate solutions can be taken into account for further improvement of the operating mechanism of the devices.

Previously, solid state deuterium NMR has already contributed to a better understanding of the electro-optical properties of PPV. Solid state ^2H line shapes of both unstretched and stretched phenylene ring-deuterated PPV (PPV-d_4) have shown that portions of the PPV chains undergo 180 ° rotational jumps about the 1,4 ring axis ("ring flips") with a rate constant $k > 10^6$ s^{-1} at 25 °C [2]. For polymers, ring flips have previously been associated exclusively with disordered, amorphous domains or boundary regions of crystalline domains[3]. For PPV however, it is suggested that this motion is related to the disorder within the crystalline structure of PPV, referred to as paracrystallinity[4]. Direct information about the backbone

motion was obtained by replacing the vinylene protons of PPV with deuterium (PPV-d_2). The ^2H line shape spectra have shown that portions of the PPV chain undergo a 180 ° rotational jump about the chain axis[5] at 225 °C with a rate constant k of 10^5-10^7 s^{-1}. These findings are in agreement with other techniques such as X-ray diffraction[4].

As the MDMO-PPV is frequently used as the active layer in lots of applications and as it is more easily to process than PPV, it is interesting to examine the chain dynamics and ordering of this polymer too. The synthesis of the MDMO-PPV-d_2 via the Gilch and the sulphinyl precursor route is described in detail in the Experimental Section (see Chapter 7). Figure 1 shows the structure of MDMO-PPV-d_2 in which the vinylene protons have been replaced by deuterium.

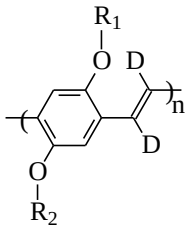

$R_1 = C_{10}H_{21}$,$R_2 = CH_3$

Figure 1 *Structure of the MDMO-PPV-d_2.*

The deuterium line shapes of all three polymers at low temperatures are typically broad Pake patterns, resulting from static, random orientations of the C-D bonds (Figure 2, 3, 4). The measured quadrupole splitting, $\Delta\upsilon_q$, is 128 kHz. By increasing the temperature from 20 °C to 160 °C, the spectra consist of a narrow isotropic peak superimposed on the rigid Pake pattern above a certain temperature. The narrow peak represents rapidly rotating (amorphous) chain segments of which the intensity gradually increases as the temperature is raised due to an increase of molecular chain motion. It is assumed that the isotropic peak is related to the motions of small conjugated segments enclosed on both sides by structural sp^3

defects. Notice that the temperature at which this isotropic peak appears, $T_{isotropic}$, is different for the three polymers. This means that the three polymers are featured by a difference in rotational jump frequencies around the chain axis. Figure 2 and 3 show the change in line-shape as a function of temperature for the standard and two-step eliminated sulphinyl MDMO-PPV, respectively. Below the glass-transition temperature, the glassy polymer is very rigid which explains why no isotropic line is observed. By increasing the temperature, however, the glassy, amorphous phase will be converted to a rubbery phase and this is reflected by the appearance of the sharp isotropic line resonance. By comparing the solid state deuterium NMR spectra of standard and two-step eliminated sulphinyl MDMO-PPV-d_2, it can be noticed that both have a different $T_{isotropic}$ (Figure 2 and 3). This can be explained on the basis of their different amount of sp^3 defects (see Chapter 3). As the standard sulphinyl MDMO-PPV has more sp^3 defects, the fast rotations of enclosed chains fragments around the chain axis is already observed at lower temperatures (80 °C) as compared to two-step eliminated MDMO-PPV (95 °C).

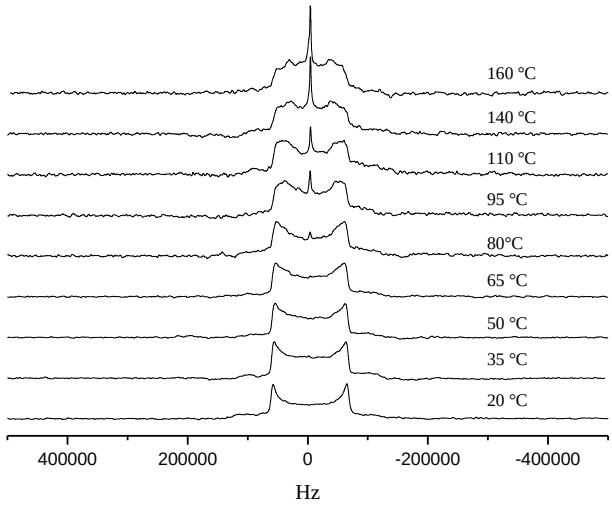

Figure 2 *^{2}H NMR spectra of standard sulphinyl MDMO-PPV as a function of temperature.*

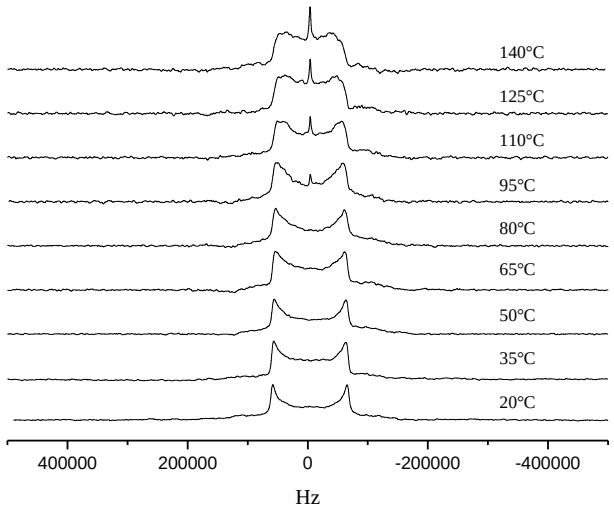

Figure 3 *^{2}H NMR spectra of two-step eliminated sulphinyl MDMO-PPV as a function of temperature.*

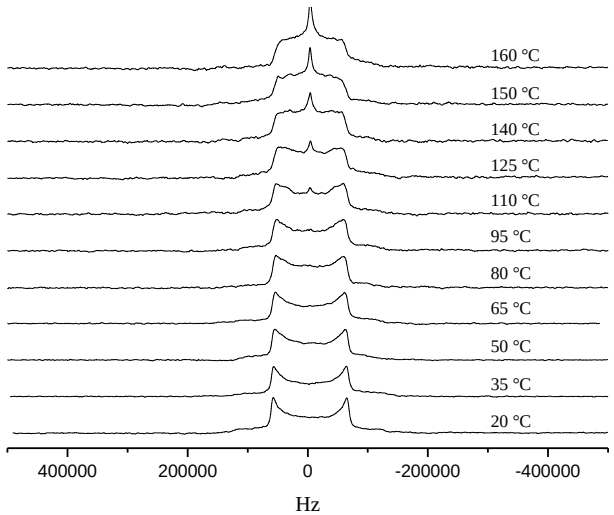

Figure 4 *^{2}H NMR spectra of Gilch MDMO-PPV as a function of temperature.*

Concerning the Gilch MDMO-PPV-d_2, the isotropic peak appears around $T_{isotropic}$ = 110 °C (Figure 4). As there are more structural defects in the Gilch MDMO-PPV, a lower $T_{isotropic}$ was expected with respect to the sulphinyl MDMO-PPVs. This since it was supposed that a higher amount of structural defects should imply that fast rotational jumps of entrapped chain segments would become possible at lower temperatures. Obviously there must be some other reasons for the higher $T_{isotropic}$. To examine further this surprising phenomenon, the three polymers were subjected to WAXS, DSC and rheology measurements.

6.2.2 Measurement of ^2H spin-lattice relaxation time

Figure 5 shows a plot of T_1 versus temperature for the Gilch, the standard and the two-step eliminated sulphinyl MDMO-PPV-d_2, respectively. Relaxation is dominated by the fluctuations of the electric field gradient due to the non-spherical charge distribution (quadrupolar interaction). The three polymers are characterized by approximately the same relaxation decay times, which decrease with increasing temperature due to an enhanced mobility of the polymer chain segments. Below T_g the spectral density of high frequency motions will not be different for a glassy or crystalline phase. Although it should be confirmed by duplo measurements, it seems that above T_g the T_1 of the Gilch polymer is somewhat retarded with respect to the sulphinyl polymers probably due to limitations in high frequency motions. On the other hand, it is clear that the deuterium spin-lattice relaxation decay time is not the most suitable parameter to confirm the differences observed in the ^2H line shape studies.

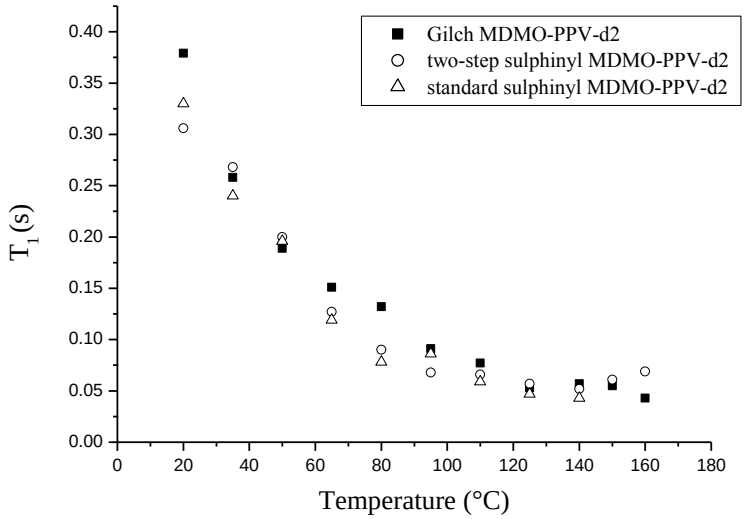

Figure 5 *T_1 as a function of temperature for the standard sulphinyl, two-step eliminated sulphinyl and Gilch MDMO-PPV.*

6.3 ^{13}C wideline NMR

6.3.1 ^{13}C line shape studies

The change in line shape of the ^{13}C solid state NMR spectra could also be another source of information about segmental polymer motions. Figure 6 (bottom) shows the spectrum of Gilch MDMO-PPV with ^{13}C in natural abundance. The signals at 50 and 140 ppm are assigned to the aliphatic, and the double bond and aromatic carbon atoms, respectively. The line shape is broad since it is dominated by the ^{1}H-^{13}C dipolar interactions and the chemical shift anisotropy.

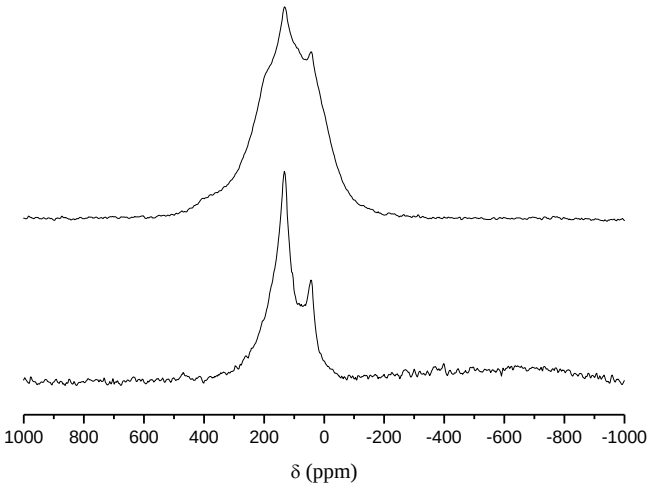

Figure 6 *^{13}C solid state NMR spectra of non-labeled (bottom) and ^{13}C labeled (top) Gilch MDMO-PPV.*

By ^{13}C-labeling the double bond carbon atoms, the spectrum is considerably broadened due to the ^{13}C-^{13}C dipolar interaction (Figure 6 – top). Spectra recorded at temperatures as high as 160 °C are essentially the same as those acquired at

room temperature (see Figure 7), except that at high temperature, the peaks become somewhat sharper due to an increase in segmental chain mobility which partially average out the dipolar interaction and CSA. As the line shape predominantly remains the same upon increasing the temperature, it is assumed that even at 160 °C the segmental chain mobility is rather limited. This will be confirmed later by the still very short T_{2H} decay time of about 120 μs We remark that the same conclusion can be drawn for the standard and two-step eliminated sulphinyl MDMO-PPV (figures not shown) and that there are no significant differences in the line shape evolution as a function of temperature for the three polymers.

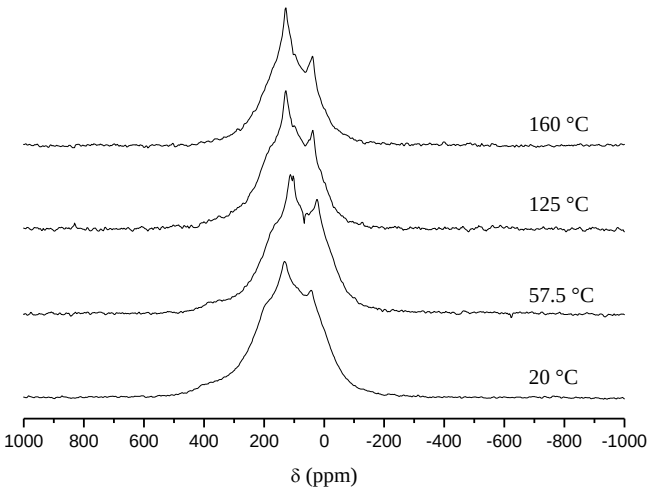

Figure 7 *Solid state ^{13}C NMR spectra of ^{13}C-labeled Gilch MDMO-PPV as a function of temperature.*

6.3.2 Measurement of the ^{13}C spin-lattice relaxation time

The T_{1C} relaxation time is sensitive toward motions in the MHz frequency regime and is mainly influenced by the dipolar relaxation mechanism. As the vinylene carbon atoms are labeled with ^{13}C, the study of the behaviour of the T_{1C} relaxation times can give specific information about the polymer backbone motions. Moreover, it has been shown that T_{1C} strongly depends on the degree of crystallinity or molecular ordering[6]: the higher the degree of organization, the longer the T_{1C} decay time. In Figure 8 the T_{1C} relaxation decay times as a function of temperature are shown. In contrast to the deuterium T_1 relaxation times, the T_{1C} relaxation behaviour up to 80 °C is clearly different for the three polymers. Regarding the Gilch MDMO-PPV, the longer T_{1C} decay time as compared to this of standard and two-step eliminated sulphinyl MDMO-PPV is pointing to a higher degree of molecular organization. The longer T_{1C} decay time of standard sulphinyl MDMO-PPV compared to the two-step sulphinyl MDMO-PPV probably indicates also a higher degree of ordering in the former. As similar T_{1C} decay times were obtained by means of magic angle spinning (MAS) experiments in which the resonance of the labeled vinylene carbons are resolved, the T_{1C} decay times represent undoubtly the chain dynamics of the double bonds.

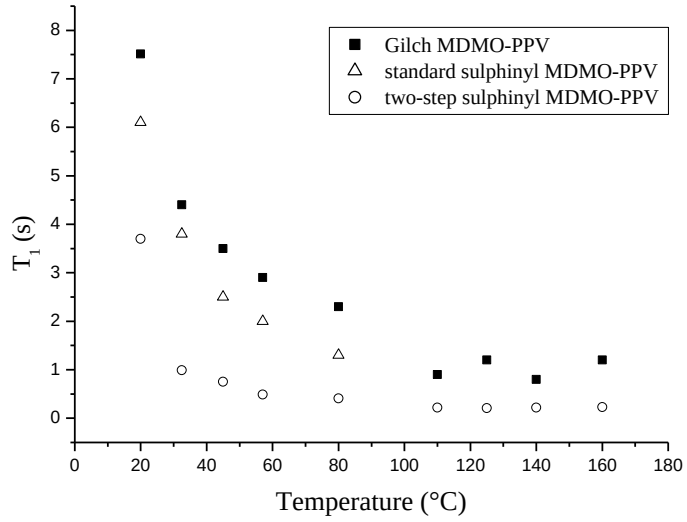

Figure 8 *T_{1C} as a function of temperature for the standard sulphinyl, two-step eliminated sulphinyl and Gilch MDMO-PPV.*

6.4 Wide angle X-ray scattering

Wide angle X-ray scattering (WAXS) is a technique by which the degree of crystallinity in polymers can be determined. The WAXS spectra of standard and two-step eliminated sulphinyl MDMO-PPV recorded at room temperature are shown in Figure 9 and 10, respectively. Both WAXS patterns are very similar and consist of two broad amorphous halos centred at $2\theta = 19.0°$ and 43.5° for the standard sulphinyl MDMO-PPV, and at $2\theta = 20.1°$ and 42.9° for the two-step eliminated sulphinyl MDMO-PPV. Besides the amorphous diffraction peaks, there are also some small diffraction maxima in front of the amorphous halos. These peak intensities are centred at $2\theta = 3.7°$, 5.8° and 12° for the standard sulphinyl polymer, and at $2\theta = 3.9°$, 5.5° for the two-step sulphinyl polymer. These small diffraction maxima might be attributed to a pseudo-ordered structure. It must be

noted that the mass fraction of the pseudo-ordered phase is three times higher for the standard sulphinyl polymer compared to the two-step sulphinyl polymer (see Table 1). The longer T_{1C} decay time of standard sulphinyl MDMO-PPV compared to the two-step eliminated sulphinyl MDMO-PPV is consistent with the higher amount of the pseudo-ordered phase. It is proposed that the higher amount of sp^3 defects in the standard sulphinyl polymer results in an enhanced chain flexibility that allows some kind of low order chain organization, but also explains the lower $T_{isotropic}$ observed in the deuterium solid state spectra. The higher degree of chain stiffness in the two-step eliminated MDMO-PPV was previously confirmed by means of ^1H wideline NMR measurements (see Chapter 5) and will hinder the polymer chain organization.

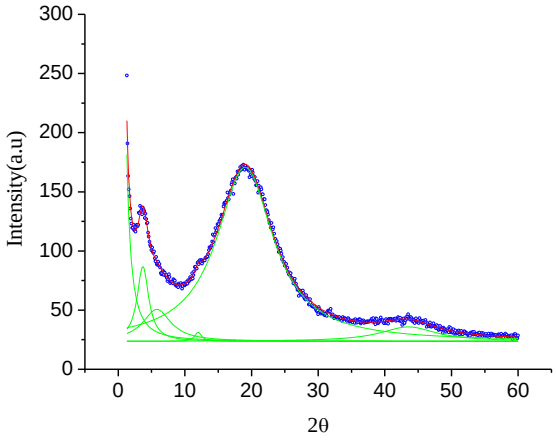

Figure 9 *WAXS pattern of standard sulphinyl MDMO-PPV at room temperature.*

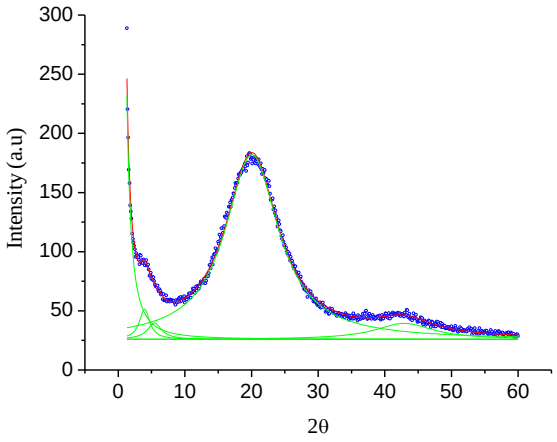

Figure 10 *WAXS pattern of two-step eliminated sulphinyl MDMO-PPV at room temperature.*

The main difference between both sulphinyl MDMO-PPVs and the Gilch MDMO-PPV is the presence of sharp diffraction maxima at well defined Bragg angles in the latter (2θ = 28.3°, 40.5°, 50.1°, 58.6 °) (compare Figure 9, 10 and 11), indicating that crystalline domains are present in this particular Gilch MDMO-PPV. This finding was unexpected since all three MDMO-PPVs were assumed to be predominantly amorphous. Moreover, we want to remark that at this moment it is not investigated yet whether other Gilch polymers are also characterized by a crystalline phase. For the particular Gilch MDMO-PPV under study, it is likely that the crystalline domains strongly restrict the segmental motions of the polymer chains is only possible in the interface of the crystalline and amorphous domains and even in the amorphous parts. This explains the higher $T_{isotropic}$ in the deuterium solid state NMR spectra and longer T_{1C} decay times compared to both sulphinyl MDMO-PPVs. Notice that the amorphous and pseudo-ordered phases are also present in the Gilch MDMO-PPV polymer.

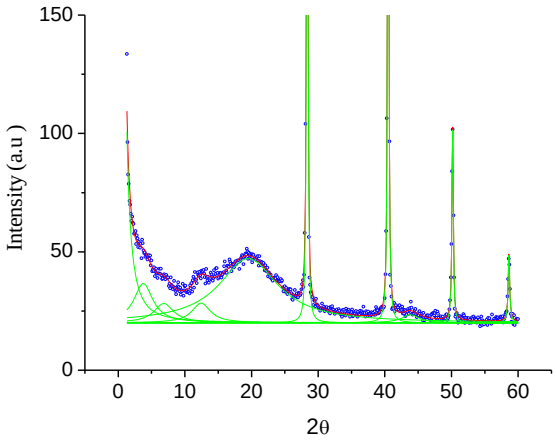

Figure 11 *WAXS pattern of Gilch MDMO-PPV(polymerized in dioxane) at room temperature*

polymer	solvent	w (%) amorphous	w (%) crystalline	w (%) pseudo-ordered
standard sulphinyl	toluene	85	/	15
two-step sulphinyl	toluene	95	/	5
Gilch	dioxane	49	32	19
Gilch	toluene	93	/	7

Table 1 *The weight fractions of the amorphous, crystalline and pseudo-ordered phases in sulphinyl and Gilch MDMO-PPV.*

Whether the crystalline phase in the Gilch MDMO-PPV is due to the different type and amount of defects present (see Chapter 3) or to the polymerization method i.e. the difference in solvent (toluene versus dioxane for sulphinyl and Gilch precursor route, respectively) was still not clear. Therefore, the Gilch polymer was dissolved

in toluene, heated to 110 °C, cooled down to 50 °C, and precipitated in methanol (cf. sulphinyl elimination treatment) to eliminate the influence of the solvent. The resulting WAXS pattern is now similar to the WAXS pattern of both sulphinyl polymers, indicating that the crystallization circumstances i.e. the solvent, heavily influence the final morphology of the polymer chains (see Figure 12). Without doubt, further research is necessary to find out more about the parameters (temperature, time, etc) leading to this different morphology.

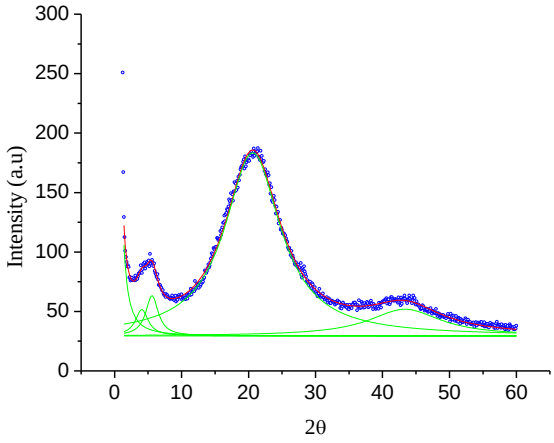

Figure 12 *WAXS pattern of Gilch MDMO-PPV(redissolved in toluene) at room temperature.*

6.5 Differential scanning calorimetry

The DSC measurements were recorded at a heat rate of 20 °C/min and confirm the presence of a crystalline phase in the Gilch MDMO-PPV since a melting endotherm was present around 127 °C (Figure 13). As both sulfinyl polymers are mainly amorphous, no melting peaks were observed (Figure 14 and 15). The DSC plot of the Gilch MDMO-PPV redissolved in toluene is in agreement with the WAXS pattern since no melting peak can be observed (Figure 16). We further want

to remark that the change in heat flow observed around 50-60 °C is not due ot the T_g since it does not appear in the second run.

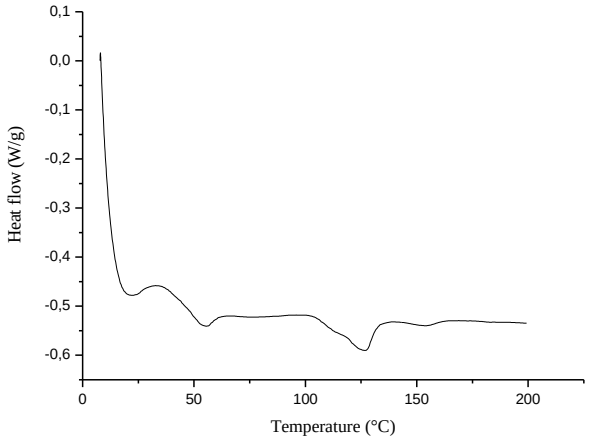

Figure 13 *DSC spectrum of Gilch MDMO-PPV polymerized in dioxane.*

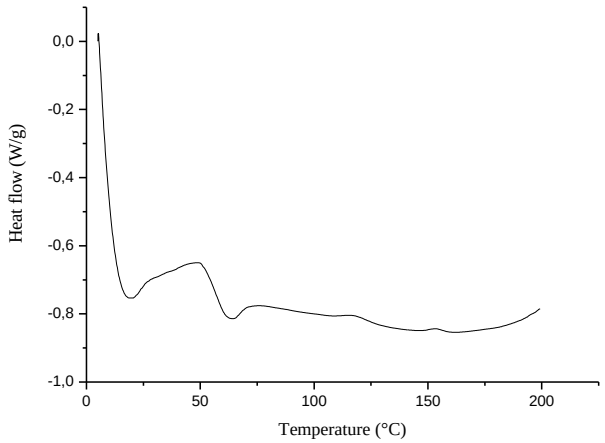

Figure 14 *DSC spectrum of standard sulphinyl MDMO-PPV.*

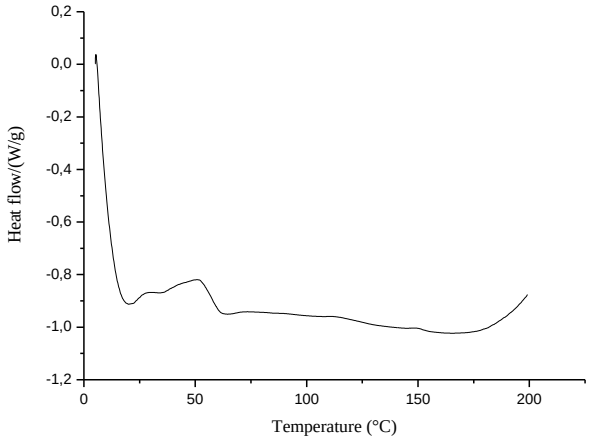

Figure 15 *DSC spectrum of two-step eliminated sulfphinyl MDMO-PPV.*

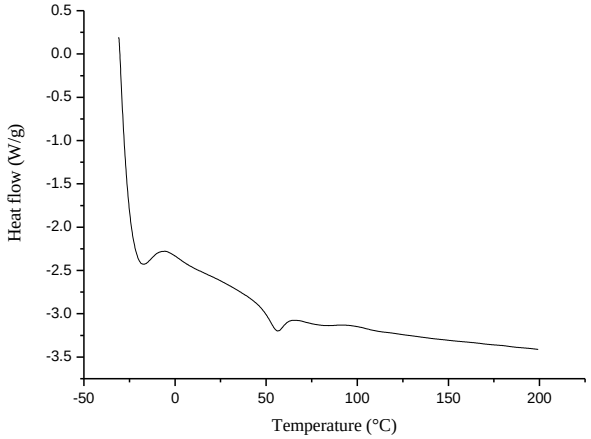

Figure 16 *DSC spectrum of Gilch MDMO-PPV redissolved in toluene.*

6.6 Rheology

The gelation behaviour of the three polymers was studied as a function of decreasing temperature: starting from 55 °C, the solutions were cooled at a rate of 3 °C/min to minus 20 °C. The obtained gelation temperatures are listed in Table 2.

polymer	gelation point (°C)
standard sulphinyl	33
two-step sulphinyl	24
Gilch	20

Table 2 *Gelation temperatures of the standard, two-step eliminated and Gilch MDMO-PPV.*

As the amount of structural defects is higher in the standard sulphinyl MDMO-PPV as compared to the two-step eliminated MDMO-PPV, the former has a higher gelation point which might correspond with the formation of pseudo-ordered phase. The Gilch MDMO-PPV has the lowest gelpoint.

6.7 ^{1}H wideline NMR

^{1}H wideline NMR relaxation measurements were performed on the non-labeled sulphinyl and Gilch MDMO-PPVs to obtain additional information about the mobility of the polymer chains. We want to remark that the interpretation of the proton wideline relaxation data is more complex compared to the previously described techniques. This since a ^{1}H wideline solid state NMR spectrum consists of a single broad resonance line due to the strong ^{1}H-^{1}H dipolar interactions. Consequently the analysis can be rather complex, especially when more relaxation

decay times are present of which the corresponding fractions are often difficult to assign to specific protons.

6.7.1 The proton spin-lattice relaxation time T_{1H}

The study of the spin-lattice relaxation times as a function of temperature is less informative as all three polymers show a similar relaxation behaviour (Table 3). As no differences in the spectral density of motions in the MHz frequency regime seem to be present, it can be concluded that the T_{1H} relaxation time is not a suitable parameter to study segmental chain motions. Single decay times are observed due to efficient spin diffusion between the rigid polymer backbone protons and the more mobile side chains protons.

	T_{1H} (s)				
polymer	kT	57.5°C	80°C	140°C	160°C
standard sulphinyl	0.7	0.8	0.9	1.2	1.5
two-step sulphinyl	0.7	0.8	0.9	1.6	1.9
Gilch	0.6	0.7	0.8	1.2	1.5

Table 3 *T_{1H} (in s) as a function of temperature for the standard, two-step eliminated and Gilch MDMO-PPV. The average 95 % confidence limit for T_{1H} is about 2 %.*

6.7.2 The proton spin-spin relaxation time T_{2H}

As mentioned before, interpreting the T_{2H} decay times is straightforward since a shorter T_{2H} decay time always implies slower segmental chain motions (see Figure 5, chapter 2). From Table 4, it can be concluded that for each polymer system both

T_{2H}^S and T_{2H}^L decay times increase with increasing temperature, indicating that the system becomes more mobile. In general it can be stated that the Gilch as well as the sulphinyl MDMO-PPVs are very rigid since the T_{2H} decay times are in the order of tens of μs (cf. rubbers for which T_{2H} is in the order of ms).

Up to 57.5 °C, all three polymers show a similar relaxation time behaviour as they are all below their glass transition temperature. As expected, no difference in T_{2H} behaviour is observed for an amorphous and crystalline phase.

Since around 55 °C a glass-rubber transition takes place, a decrease of the rigid proton fraction is noticed by going from room temperature to 80 °C. Starting from 57.5 °C, a fraction distribution of 25/75 % is observed which can be assigned to backbone and side chain protons, respectively. At 80 °C, there is still no significant difference between the relaxation decay times of the three polymers.

	T_{2H}^S/T_{2H}^L (μs) M_0^S/M_0^L (%)				
polymer	kT	57.5°C	80°C	140°C	160°C
standard sulphinyl	21/29 44/56 %	24/41 25/75 %	26/53 32/68%	35/89 32/68%	35/94 30/70%
two-step sulphinyl	21/30 42/58%	25/41 24/76%	25/50 25/75%	32/79 25/75%	32/79 22/78%
Gilch	21/30 42/58 %	25/48 25/75 %	26/55 26/74%	37/111 28/72%	38/121 25/75%

Table 4 *T_{2H}^S and T_{2H}^L decay times(in μs) as a function of temperature for the standard, two-step eliminated and Gilch MDMO-PPV. The average 95 % confidence limit is about 7 % for T_{2H}. The fractions of T_{2H}^S and T_{2H}^L are normalized to 100.*

On the other hand, at 140 °C, both T_{2H}^S and T_{2H}^L decay times are clearly different for the three polymers. The difference is most pronounced for the T_{2H}^L decay times, representing the more mobile proton population of the C_{10} side chain. Concerning

the Gilch MDMO-PPV, both T_{2H}^{S} and T_{2H}^{L} decay times are longer than those of standard and two-step eliminated sulphinyl MDMO-PPV, indicating that the polymer chains are more mobile. Above 140 °C the crystallinity is destroyed and only the structural defects will be responsible for the differences in chain mobility. Therefore, the higher mobility of the Gilch MDMO-PPV compared to standard and two-step eliminated sulphinyl MDMO-PPV can be attributed to the higher amount of structural defects (see Chapter 3). As both sulphinyl MDMO-PPVs have a lower amount of structural defects compared to Gilch MDMO-PPV their overall chain mobility will be lower. Due to the lower amount of sp^3 defects in two-step eliminated sulphinyl MDMO-PPV, its chain mobility will be lower and consequently its T_{2H} decay times will be the shortest.

6.7.3 The proton spin-lattice relaxation time in the rotating frame $T_{1\rho H}$

Below the glass transition temperature no significant differences in the $T_{1\rho H}^{S}$ and $T_{1\rho H}^{L}$ decay times between the three polymers can be observed (Table 5). Around the glass transition temperature (50 °C–70 °C) the fraction associated with $T_{1\rho H}^{S}$ for Gilch MDMO-PPV, which represents the immobile protons, is significantly higher (46%) due to the presence of the crystalline phase. This indicates that for the Gilch MDMO-PPV a part of the C_{10} side chains is rather immobilized. Between 57.5 °C and 140 °C, the fractions of both decay times of the Gilch MDMO-PPV remain unchanged as not all crystallites have been melted yet (T_m = 127 °C). For both sulphinyl MDMO-PPVs all restrictions are removed in this temperature range meaning that the chain mobility depends only on the amount of structural defects. As the two-step eliminated sulphinyl MDMO-PPV is characterized by the longest $T_{1\rho H}^{L}$ it is the most immobile. Above 140 °C, the crystallites in the Gilch MDMO-PPV are melted (decrease of fraction of $T_{1\rho H}^{S}$). As all restrictions are removed now, it allows to compare the mobility of the three polymers. It can be concluded that above 140 °C the Gilch MDMO-PPV is the most mobile (shortest $T_{1\rho H}$ decay time)

due to the higher amount of defects (higher density of kHz motions). The two-step eliminated sulphinyl MDMO-PPV on the other hand, is characterized by the longest $T_{1\rho H}^{L}$ decay time indicating that this polymer is the most rigid (lower density of kHz motions). The mobility of standard sulphinyl MDMO-PPV is in between.

	$T_{1\rho H}^{S}$/ $T_{1\rho H}^{L}$ (ms) M_0^{S}/M_0^{L} (%)				
polymer	kT	57.5°C	80°C	140°C	160°C
standard	1.2/3.3	2.4/9.6	3.4/12.3	4.0/18.1	5.0/24.6
sulphinyl	25/75%	24/76%	29/71%	25/75%	30/70%
two-steps	1.2/3.1	3.7/11.5	3.2/14.6	4.0/23.9	5.0/26.3
sulphinyl	22/78%	24/76 %	25/75%	25/75%	24/76%
Gilch	1.5/3.6	3.0/9.0	2.9/9.5	3.6/17.7	4.2/20.8
	34/66%	46/54%	43/57%	38/62%	32/68%

Table 5 *$T_{1\rho H}^{S}$ and $T_{1\rho H}^{L}$ (in ms) as a function of temperature for the standard, two-step eliminated and Gilch MDMO-PPV. The average 95 % confidence limit for $T_{1\rho H}$ is about 5%. The fractions of $T_{1\rho H}^{S}$ and $T_{1\rho H}^{L}$ are normalized to 100.*

6.8 Conclusion

In general we can state that ^{2}H line shape and ^{13}C relaxation time studies are very useful to gain information about the molecular ordering in MDMO-PPVs, whereas ^{1}H relaxation time studies are more suitable for gaining information about the chain dynamics.

^{2}H line shape studies as a function of temperature have proven to be the most sensitive toward rotational jumps of chain segments enclosed by structural defects since no changes could be observed in the ^{13}C and ^{1}H solid state NMR spectra. Moreover, the appearance of the isotropic peak at different temperatures for the

three polymers as well as the differences in the T_{1C} decay times were found to be related to a different segmental chain and dynamics chain organization. Additional information concerning the organization of the polymer chains was provided by means of WAXS and DSC measurements. From the WAXS patterns of both sulphinyl polymers it was found that the amount of pseudo-ordered phase was three times higher for the standard sulphinyl MDMO-PPV as compared to two-step eliminated polymer. The WAXS pattern of the Gilch MDMO-PPV on the other hand was completely different in that also crystalline domains were present next to amorphous and pseudo-ordered phase. The appearance of a melt endotherm in the DSC plot confirmed the WAXS results.

From the T_{2H} and $T_{1\rho H}$ ^{1}H wideline results, it could be concluded that at $T \geq 80$ °C the segmental chain motion of Gilch MDMO-PPV is higher compared to both sulphinyl polymers and this allows the formation of the ordered domains. The higher degree of ordering in the Gilch polymer was reflected in the higher $T_{isotropic}$ in the solid state deuterium NMR spectra and the longer T_{1C} decay times. Furthermore it was confirmed by means of ^{1}H wideline NMR that at $T \geq 80$ °C the two-step eliminated sulphinyl MDMO-PPV is the most rigid as was expected on the basis of its lower amount of structural defects resulting in an almost completely amorphous structure (shortest T_{1C} decay time). The higher chain stiffness compared to standard sulphinyl MDMO-PPV was represented in the higher $T_{isotropic}$ in the solid state deuterium NMR spectra. Moreover, on the basis of the ^{1}H wideline measurements of MDMO-PPVs we can attribute proton populations to the observed relaxation times and fractions. This will absolutely be a help for the further interpretation of the relaxation times found for blends of e.g MDMO-PPV and PCBM, as used in opto-electronic devices.

6.9 References

[1] a) Martens, T.; D'Haen, J.; Munters, T.; Goris, L.; Beelen, Z.; Manca, J.; D'Olieslaeger, M.; Vanderzande, D.; De Schepper, L.; Andriessen, R. *Mat. Res. Soc. Symp. Proc.* **2002**, *725*, 7.11.1. b) Shaheen, S. E., Brabec, C. J.; Saricifci, N. S. Padinger, F.; Fromherz, T.; Hummelen, J. C. *Appl Phys. Lett.* **2001**, *78 (6)*, 841.

[2] a) Simpson, J. H.; Egger, N.; Masse, M. A. ; Rice, D. M. ; Karasz, F. E. *J. Polym. Sci. Part B : Polym. Phys.* **1990**, *28*, 1859. b) Simpson, J. H.; Rice, D. M. ; Karasz, F. E. *J. Polym. Sci. Part B : Polym. Phys.* **1992**, *30*, 11.

[3] Jelinski, L. W. *High Resolution NMR Spectroscopy of Synthetic Polymers in Bulk*, **1986**, VCH, Weinheim.

[4] Granier, T.: Thomas, E. L.; Karasz, F. E. *J. Polym. Sci. Part B : Polym. Phys.* **1989**, *27*, 469.

[5] Simpson, J. H.; Liang, W.; Rice, D. M. ; Karasz, F. E. *Macromolecules* **1992**, *25*, 3068.

[6] Pollers, I. *Ph. D. Dissertation* **1996**, Limburgs Universitair Centrum, Diepenbeek, Belgium.

7. Experimental section

7.1 Synthesis of ^{13}C-labeled monomers and polymers

7.1.1 Synthesis of the ^{13}C-labeled Gilch monomer and polymer[1]

7.1.2 Synthesis of the ^{13}C-labeled sulphinyl monomer and polymer

Preparation of 1-(3,7-dimethyloctyloxy)-4-methoxybenzene, 1. In a three-neck round-bottom flask 10 g p-methoxyphenol (80.3 mmol), 4.92 g KOH (87.8 mmol) and 1.2 g sodium iodide (8.06 mmol) were dissolved in 34 ml ethanol. During refluxing 1-chloro-3,7-dimethyloctane (14.9 g, 84.6 mmol) was added dropwise. After stirring for 62 h, the mixture was cooled, decanted and extracted with chloroform (3x 200 ml) and 10 % NaOH. The organic phases were combined, dried over $MgSO_4$ and evaporated under reduced pressure. A yield of 13.7 g (52 %) of **1** was obtained. ^{1}H NMR (300 MHz, $CDCl_3$): δ = 6.8 (4H, H_{arom}); 3.9 (2H, OCH_2); 3.7 (s, 3H, OCH_3); 1.8(1H); 1.7 (1H); 1.6 (2H); 1.4 (2H); 1.3 (1H); 1.2 (3H); 1.0 (d, J=6.6Hz, 3H, CH_3); 0.9 (d, J=6.7Hz, 6H; 2 x CH_3). MS (EI, m/z, rel.int. (%)): 264.

Preparation of 2,5-bis(chloro-^{13}C-methyl)-1-(3,7-dimethyloctyloxy)-4-methoxybenzene, 2. A 3.26 g (0.012 mol) of **1** and 1 g (0.033 mol) of paraformaldehyde-^{13}C (isotopic purity of 99 %, Cambridge Isotope Laboratory, Inc., Andover) were placed in a 100 ml three-neck round bottom flask. After adding 6.5 g (0.066 mol) of 37 % HCl under N_2, a 12.25 g (0.12 mol) of acetic anhydride was added dropwise at such a rate that the internal temperature did not exceed 70 °C. After

stirring for 3.5 h at 75 °C, the mixture was cooled and a light colored solid crystallised at 30 °C. Afterwards, the reaction mixture was admixed with 11 ml of cold-saturated sodium acetate solution, followed by a dropwise addition of 25 % NaOH (8 ml). The mixture was heated to 52 °C and subsequently cooled in an ice bath while stirring. The cream-colored solid was filtered off, washed with water (7 ml) and dissolved in hexane (24 ml). After extraction with water, the yellowish organic phase was dried over $MgSO_4$, filtered and evaporated. After crystallization, a 3.78 g (87 %) of **2** was isolated. By ^{1}H NMR an isotopic purity of 99.2 % was determined. Melting point: 65°C. ^{1}H NMR (300 MHz, $CDCl_3$), δ = 6.9 (m, 2H, H_{ar}); 4.9 +4.4 (s, 4H, CH_2Cl, ^{1}J= 152 Hz); 4.0 (m, 2H, OCH_2); 3.8 (s,3 H, OCH_3); 1.9 (1H); 1.7 (1H); 1.6 (2H); 1.4 (2H); 1.3 (1H); 1.2 (3H); 1.0 (d, J=6.6Hz, 3H, CH_3); 0.9 (d, J=6.7Hz, 6H; 2 x CH_3). ^{13}C NMR (100 MHz, $CDCl_3$), δ = 19.8 (1C); 22.6 (2C); 24.6 (1C); 27.9 (1C); 30.2 (1C); 36.6 (1C); 37.4 (1C); 39.2 (1C); 41.2 (2C); 56.4 (1C); 67.9 (1C); 113.2 (1C); 114.3 (2C); 127.0 (2C); 151.4(2C). MS(CI, m/z, rel.int. (%)): 362 $[M+1]^+$.

Preparation of bis-tetrahydrothiopheniumsalt of 2,5-bis(chloro-^{13}C-methyl)-1-(3,7-dimethyl-octyloxy)-4-methoxybenzene, 3. A solution of 3.7 g (0.01 mol) of **2** and 3.7 g (0.04 mol) of tetrahydrothiophene in MeOH (10 ml) was stirred for 70 h at ambient temperature. After precipitation in aceton (100 ml), the precipitate was washed with hexane. The product (4 g, 72 %) was dried under reduced pressure at room temperature. ^{1}H NMR (300 MHz, D_2O) δ = 7.1 (d, 2H, H_{ar}); 4.6+4.2 (d, 4H, CH_2S, ^{1}J=149Hz); 4.0 (m, 2H, OCH_2); 3.8 (s, 3H, OCH_3); 3.4 (m, 8H, $S(\underline{CH_2})_2(CH_2)_2$); 2.2 (m, 8H, $S(CH_2)_2(\underline{CH_2})_2$); 1.8 (1H); 1.7 (1H); 1.6 (2H); 1.4 (2H); 1.3 (1H); 1.2 (3H); 1.0 (d, J=6.6Hz, 3H, CH_3); 0.9 (d, J=6.7Hz, 6H; 2 x CH_3). ^{13}C NMR (100 MHz, D_2O) δ = 21.3 (1C); 24.31/24.39 (2C); 26.4 (1C); 29.6 (1C); 30.7 (1C); 31.3 (1C); 37.6 (1C); 38.7 (1C); 40.9 (1C); 43.9 (2C); 45.5 (1C); 58.6 (1C); 70.0 (1C); 117.8/118.6 (2C); 121.9/122.4 (2C); 153.7/154.3 (2C).

Preparation of 2-(^{13}C-butylsulphanyl)methyl)-5-(^{13}C-chloromethyl)-1-(3,7-dimethyloctyloxy)-4-methoxybenzene, 4. A mixture of NaO*t*Bu (0.69 g, 7.18 mmol) and n-butanethiol (0.64 g, 7.18 mmol) in MeOH (12 ml) was stirred for 30 min at room temperature. The clear solution was added in one portion to a stirred solution of **3** (4 g, 7.18 mmol). After one hour the reaction mixture was neutralised with aqueous HCl, if necessary, and concentrated in vacuo. The crude product was diluted with $CHCl_3$ (21 ml), the precipitate was filtered off and the solvent was evaporated. The obtained oil was diluted with petroleumether (boiling range 100-140 °C) and concentrated to remove the tetrahydrothiophene. This sequence was repeated three times to afford a light yellow viscous oil. A 2.6 g (6.19 mmol) of crude product was formed. ^{1}H NMR (300 MHz, $CDCl_3$) δ = 6.89/6.87 (d, 2H, H_{ar}); 4.88/4.87+4.37/4.36 (dd, 2H, ^{1}J=152 Hz, CH_2Cl); 4.0 (m, 2H, OCH_2); 3.9/3.5 (dd, 2H, ^{1}J=144 Hz, $CH_2S(R)$); 2.5 (m, 2H, $SCH_2(CH_2)_2CH_3$); 1.9-1.2 (14H, $H_{alif.}$); 1.0 (3H, CH_3); 0.9 (9H, 3xCH_3). MS(CI, m/z, rel.int. (%)): 417 $[M+1]^+$.

Preparation of 2-(^{13}C-butylsulphinyl)methyl)-5-(^{13}C-chloromethyl)-1-(3,7-dimethyloctyloxy)-4-methoxybenzene, 5. An aqueous (35 wt%) solution of H_2O_2 (1.2 g, 12.4 mmol) was added dropwise to a solution of crude thioether **4** (6.19 mmol), TeO_2 (0.12 g, 0.74 mmol) and three drops of concentrated HCl in 1,4-dioxane (24 ml). The reaction was followed on TLC (time: 2.5 h) and as soon as the overoxidation took place, it was quenched by a saturated aqueous NaCl solution (30 ml). After extraction with $CHCl_3$ (3 x 30 ml), the organic layers were dried over $MgSO_4$ and concentrated in vacuo. The reaction mixture was purified by column chromatography (SiO_2, eluent hexane/ethylacetate 60/40) to give pure **5** (1.74 g, 65 %) starting from tetrahydrothiofeniumsalt as a light yellow viscous oil. ^{1}H NMR (300 MHz, $CDCl_3$) δ = 6.9 (d, 1H, H_{ar}); 6.8 (d, 1H, H_{ar}); 4.8/4.3 (d, 2H, ^{1}J=152Hz, CH_2Cl); 4.3/4.1 + 3.8/3.6 (dd, 2H, ^{1}J = 130 Hz, $CH_2S(O)R$); 3.9 (m, 2H, OCH_2); 3.8 (s,3H, OCH_3); 1.9 (1H); 1.7 (1H); 1.6 (2H); 1.4 (2H); 1.3 (1H); 1.2 (3H); 1.0 (d, J=6.6Hz, 3H, CH_3); 0.9 (d, J=6.7Hz, 6H; 2 x CH_3). ^{13}C NMR (100

MHz, $CDCl_3$) δ = 13.5 (1C); 19.8 (1C); 22.1 (1C); 22.6 (2C); 24.6 (2C); 27.9 (1C); 30.2 (1C); 36.6 (1C); 37.4 (1C); 39.2 (1C); 41.3 (1C); 49.7 (1C); 52.5 (1C); 56.4 (1C); 67.9 (1C); 112.8 (1C); 115.7 (1C); 119.7(1C); 127.0 (1C); 151.4 (2C). MS(CI, m/z, rel.int. (%)): 433 $[M+1]^+$.

Preparation of precursor polymer of 2-(^{13}C-butylsulphinyl)methyl-5-(^{13}C-chloromethyl)-1-(3,7-dimethyloctyloxy)-4-methoxybenzene, 6 according the SULPHINYL route. A solution of 0.5 g monomer **5** (1.15 mmol) in 2-butanol (8 ml) and a solution of 0.14 g NaO*t*Bu (1.5 mmol) in 2-butanol (5 ml) was degassed for 1 h at 30 °C by passing through a continous stream of nitrogen. The base solution was added in one portion to the stirred monomer solution. After one hour the reaction mixture was poured dropwise in a well stirred amount of ice water (115 ml), neutralised with aqueous hydrogen chloride, extracted with $CHCl_3$ (3 x 50ml) and the combined organic layers were concentrated in vacuo. A 0.36 g of precursor **6** (77 %) was obtained. ^{1}H NMR (400 MHz, $CDCl_3$), δ = 6.9-6.2 (br m, 2H, H_{ar}); 4.9/4.6 (br d, 1H, Ar-CHS(O)R); 4.0-2.9 (br m, 7H, OCH_2, OCH_3, Ar-CHS(O)R-CH_2-Ar); 2.7-2.1 (br d, 2H, -S$CH_2(CH_2)_2CH_3$); 1.9-1.0 (br m, 14H, $H_{aliph.}$); 1.0-0.8 (m, 9H, CH_3). ^{13}C NMR (100 MHz, $CDCl_3$): δ = 151.4 (C_{3+6}, 2C); 127.0 (C_{1+4}, 2C); 110.5 (C_{2+5}, 1C); 67.9 (C_{10}, 1C); 59.1/55.1 (C_8, 1C); 56.4 (C_9, 1C); 39.2 (C_{15}, 1C); 37.4 (C_{13}, 1C); 36.6 (C_{11}, 1C); 32.1/29.1 (C_7, 1C); 30.2 (C_{12}, 1C); 27.9 (C_{16}, 1C); 24.6 (C_{14}, 1C); 22.6 (C_{17}, 2C); 19.8 (C_{18}, 1C); 49.7 ($C_{1'}$, 1C); 24.6 ($C_{2'}$, 1C); 21.9 ($C_{3'}$, 1C); 13.5 ($C_{4'}$, 1C).

Thermal conversion of precursor polymer 6 to conjugated polymer, 7. A solution of **6** (0.35 g) in toluene (22 ml) was degassed for 1 h passing through a continuous stream of nitrogen. The solution was heated to 110 °C and stirred for 3 h. After cooling to 50 °C, the resulting orange-red solution was precipitated dropwise in methanol in a ratio toluene/methanol 1/10. The polymer was filtered off, washed with methanol and dried at room temperature under reduced pressure. The polymer

was purified by dissolving it in 25 ml THF (68 °C), cooling the solution to 40 °C and precipitating dropwise in methanol (45 ml). A 0.2 g (0.69 mmol, 77 %) of **7** was obtained as a red, fibrous polymer. ^{1}H NMR (400 MHz, $C_2D_2Cl_4$) δ = 7.5 (br, 2H, $H_{olef.}$); 7.2 (br, 2H, H_{ar}); 5.2 (d weak, ^{1}J = 134 Hz , Ar-CHS(O)R-CH_2-Ar); 4.6-3.2 (br m, 5H, OCH_2, OCH_3 + (3.7 ppm, Ar-CHS(O)R-CH_2-Ar)); 2.1-0.6 (br m; 19H; $H_{aliph.}$). ^{13}C NMR (100MHz, $CDCl_3$): 151.4 (C_{3+6}, 2C); 127.0 (C_{1+4}, 2C), 123.3 (C_{7+8}, 2C); 110.5 (C_2, 1C); 108.8 (C_5, 1C); 67.9 (C_{10}, 1C); 56.4 (C_9, 1C); 39.2 (C_{15}, 1C); 37.4 (C_{13}, 1C); 36.6 (C_{11}, 1C); 30.2 (C_{12}, 1C); 27.9 (C_{16}, 1C); 24.6 (C_{14}, 1C); 22.6 (C_{17}, 2C); 19.8 (C_{18}, 1C). (2.7 g, 7.75 mmol, 78 %). Molecular weight determination by SEC in THF against polystyrene standards gave a M_w = 426 000 g/mol and a polydispersity of 4.7. The unlabeled polymer was prepared analogously.

7.2 Synthesis of the model compounds

Preparation of 1,4-bis(butylsulphanyl)benzene, 8. A mixture of n-butanethiol (12 g, 0.14 mol.) and NaO*t*BuO (13.1 g, 0.14 mol) was dissolved in methanol/THF (1/3) and in one portion added to a stirred solution of 6 g (0.034 mol) dichloro-p-xylene in THF (30 ml). The mixture was heated to reflux and after 2 h the reaction was finished. The mixture was cooled to room temperature. The salts were filtered off and the liquid was concentrated in vacuo. A 9.6 g of 1,4-bis(butylsulphanyl)benzene (0.03 mol, 98 %) was obtained as a yellow oil. ^{1}H NMR (300MHz, $CDCl_3$) δ = 7.2 (s, 4H, H_{ar}); 3.6 (s, 4H, Ar-CH_2-SR); 2.4 (t, 4H, Ar-CH_2-S-CH_2-$(CH_2)_2CH_3$); 1.5 (m, 4H, -S-CH_2-CH_2-CH_2-CH_3); 1.3 (m, 4H, -S-CH_2-CH_2-CH_2-CH_3); 0.9 (m, 6H; 2xCH_3). MS(EI, m/z, rel.int. (%)): 250.

Preparation of 1,4-bis(butylsulphinyl)benzene, 9. An aqueous (35wt%) solution of H_2O_2 (8.5 g, 0.085 mol) was added dropwise to a solution of 0.4 g 1,4-bis(butyl-

sulphanyl)benzene, TeO_2 (1.3 g; 8 mmol) and three drops of concentrated HCl in 128 ml 1,4-dioxane. The reaction was followed on TLC (19/1 dichloro-methane/methanol) and as soon as the overoxidation took place, the reaction was quenched by a saturated aqueous NaCl solution (150 ml). The reaction mixture was extracted with $CHCl_3$ (3x200ml), the combined organic layers were dried over $MgSO_4$ and concentrated in vacuo. The reaction mixture was purified by column chromatography (SiO_2, eluent dichloromethane/mehtanol 19/1) to give pure 1,4-bis(butylsulphinyl)benzene (6.3 g, 0.02 mol, 60 %) which appear as white crystals after evaporation of the solvent. ^{1}H NMR (300MHz, $CDCl_3$) δ = 7.3 (s, 4H, H_{ar}) ; 3.9 (s, 4H, Ar-CH_2-SR); 2.5 (t, 4H, Ar-CH_2-S-$\underline{CH_2}$-$(CH_2)_2CH_3$); 1.7 (m, 4H, -S-CH_2-$\underline{CH_2}$-CH_2-CH_3); 1.4 (m, 4H, -S-CH_2-CH_2-$\underline{CH_2}$-CH_3); 0.9 (m, 6H; 2xCH_3). ^{13}C NMR (100MHz, $CDCl_3$) δ = 13.5 (2C); 21.9(2C); 24.6 (2C); 49.7 (1C); 57.6 (1C); 130.5 (1C); 137.8 (1C); 128.7 (2C); 129.0 (2C). MS(EI, m/z, rel.int. (%)): 282. T_m = 192°C.

Preparation of 1,4-bis(butylsulphinyl)-4'-chlorobenzene, 10. A 1.3 g of N-chloro-succinimide (0.01 mol) was added portion wise as a solid to a solution of 3 g 1,4-bis(butyl-sulphinyl)benzene (0.01 mol) in 50 ml dichoromethane (time: 30 min). The solution was stirred at room temperature. The mixture was extracted with water (3 x 50ml) and dried over $MgSO_4$. After column chromatography (SiO_2, chloroform/methanol 19/1) the product could be isolated as white crystals (2.7 g, 7.75 mmol, 78 %). ^{1}H NMR (300MHz, $CDCl_3$); δ = 7.5 (m, 2H, H_{ar}); 7.4 (m, 2H, H_{ar}); 5.54 (d, 1H, CHClS(O)R); 4.0 (s,2H, CH_2S(O)R); 2.6 (m, 2H, S(O)$\underline{CH_2}(CH_2)_2CH_3$); 2.4 (m, 2H, S(O)$\underline{CH_2}(CH_2)_2CH_3$); 1.7 (m, 2H, S(O)$CH_2\underline{CH_2}CH_2CH_3$), 1.4 (m, 2H, S(O)CH2-CH2$\underline{CH2}$CH3); 0.9 (m, 6H, 2xCH_3). ^{13}C NMR (100MHz, $CDCl_3$); δ = 13.5 (2C); 21.9 (2C); 24.6 (2C); 49.7 (1C); 51.1 (1C); 57.6 (1C); 74.7-73.1 (1C); 130.5 (1C); 137.8 (1C); 128.6 (2C); 129.0 (2C). MS(CI,m/z, rel.int. (%)): 349 $[M+1]^+$. T_m = 143 °C.

Preparation of poly(p-phenylene-1,2-bis(butylsulphinyl)ethylene) according the SULPHINYL route, 11. A solution of 0.4 g of monomer **10** (1.15 mmol) in THF (9 ml) and a solution of NaO*t*Bu (0.14 g, 1.5 mmol) in THF (5 ml) was degassed for 1 h at 40 °C by passing through a continous stream of nitrogen. The base solution was added in one portion to the stirred monomer solution. After one hour the reaction mixture was poured dropwise in a well stirred amount of ice water (150 ml). The mixture was neutralised with aqueous hydrogen chloride and extracted with $CHCl_3$ (3 x 50ml). The combined organic layers were concentrated in vacuo. The obtained polymer was purified by precipitating it in an ice cold mixture of hexane/diethyleter 1/1. A 0.15 g of yellow, viscous polymer (0.48 mmol, 40 %) was isolated and dried under reduced pressure at ambient temperature.

^{1}H NMR (300MHz, $CDCl_3$) δ = 7.5-7.1 (br m, 4H, H_{ar}); 3.9/3.7 (br m, 2H, Ar-CHS(O)R-CHS(O)R-Ar); 2.7/2.5 (br m, 4H, S(O)$CH_2$$(CH_2)_2CH_3$); 1.7 (br m, 4H, S(O)$CH_2CH_2CHCH_3$); 1.4 (br m, 4H, S(O)$CH_2CH_2CH_2CH_3$); 0.9/0.8 (b, 6H, CH_3). ^{13}C NMR (400MHz, d-acetone) δ = 14.1 (2C, C_{10}); 22.6 (2C, C_9); 25.2 (2C, C_8); 50.9/51.5 (2C, C_{5+6}); 51.9 (2C, C7); 58.3 (C_{11}); 130-138 (6C, C_{1-4}). M_w = 1592; polydispersity = 1.5.

7.3 Synthesis of ^{2}H-labeled monomers and polymers

7.3.1 Synthesis of the ^{2}H-labeled Gilch monomer and polymer

Preparation of 2,5-bis(chloro-^{2}H-methyl)-1-(3,7-dimethyloctyloxy)-4-methoxy-benzene, 12. A 3.26 g (0.012 mol) of **1** and 1 g (0.033 mol) of paraformaldehyde-^{2}H (isotopic purity of 99 %, Cambridge Isotope Laboratory, Inc., Andover) were placed in a 100 ml three-neck round bottom flask. After adding 6.5 g (0.066 mol) of 37 % HCl under N_2, a 12.25 g (0.12 mol) of acetic anhydride was added dropwise at such a rate that the internal temperature did not exceed 70 °C. After

stirring for 3.5 h at 75 °C, the mixture was cooled and a light colored solid crystallises at 30 °C. Afterwards, the reaction mixture was admixed with 11 ml of cold-saturated sodium acetate solution, followed by a dropwise addition of 25 % NaOH (8 ml). The mixture was heated to 52 °C and subsequently cooled in an ice bath while stirring. The cream-colored solid was filtered off, washed with deuterated water (7 ml) and dissolved in hexane (24 ml). After extraction with water, the yellowish organic phase was dried over $MgSO_4$, filtered and evaporated. After crystallization, a 3.78 g (87 %) of **12** was isolated. Melting point: 65°C. ^{1}H NMR (300 MHz, $CDCl_3$), δ = 6.9 (m, 2H, H_{ar}); 4.0 (m, 2H, OCH_2); 3.8 (s, 3 H, OCH_3); 1.9 (1H); 1.7 (1H); 1.6 (2H); 1.4 (2H); 1.3 (1H); 1.2 (3H); 1.0 (d, J=6.6 Hz, 3H, CH_3); 0.9 (d, J=6.7Hz, 6H; 2 x CH_3). ^{2}H NMR (61.5 MHz, $CDCl_3$), δ = 4.6 ppm. ^{13}C NMR (100 MHz, $CDCl_3$), δ = 19.8 (1C); 22.6 (2C); 24.6 (1C); 27.9 (1C); 30.2 (1C); 36.6 (1C); 37.4 (1C); 39.2 (1C); 41.2 (2C); 56.4 (1C); 67.9 (1C); 113.2 (1C); 114.3 (2C); 127.0 (2C); 151.4(2C). MS(CI, m/z, rel.int. (%)): 365 $[M+1]^+$.

Preparation of poly(2-(3,7-dimethyloctyloxy)-5-methoxy-p-phenylenevinylene 13 according to the GILCH precursor route.

In a three-neck round-bottom flask fitted with a reflux condenser and a septum 1 g (2.7 mmol) of **12** was dissolved in dry dioxane and flushed with N_2 for 15 min. Afterwards, a balloon filled with N_2 was placed on top of the condenser. After heating to 98 °C, 8 ml of a K*t*BuO solution (7.1 mmol) was added drop wise with a syringe while stirring. During this addition the solution turned from colorless to yellow. After 5 min, 6 ml of a K*t*BuO solution (5.4 mmol) was added and the solution colored orange. After stirring for 2 h at 98 °C, the solution was cooled down to 50 °C and neutralized with acetic acid. Finally, the polymer was precipitated in methanol (200 ml), filtered off, washed and dried under reduced pressure at room temperature.

The polymer was purified by dissolving it in 60 ml THF (68 °C), cooling the solution to 40 °C and precipitating drop wise in methanol (70 ml). A 0.8 g (2.0 mmol, 74 %) of **13** was obtained as a red, fibrous polymer. A net deuteration of 99 % as determined by ^{1}H NMR was achieved. ^{1}H NMR (400 MHz, $C_2D_2Cl_4$) δ = 7.2 (br, 2H, H_{ar}); 5.2 (d weak, ^{1}J = 134 Hz , Ar-CHS(O)R-CH_2-Ar); 4.6-3.2 (br m, 5H, OCH_2, OCH_3 + (3.7 ppm, Ar-CHS(O)R-CH_2-Ar)); 2.1-0.6 (br m; 19H; $H_{aliph.}$).

7.3.2 Synthesis of the ^{2}H-labeled sulphinyl monomer and polymer

Preparation of bis-tetrahydrothiopheniumsalt of 2,5-bis(chloro-^{2}H-methyl)-1-(3,7-dimethyl-octyloxy)-4-methoxybenzene, 14. A solution of 7.8 g (0.02 mol) of **12** and 7.4 g (0.08 mol) of tetrahydrothiophene in MeOD (15 ml) was stirred for 70 h at ambient temperature. After precipitation in aceton (100 ml), the precipitate was washed with hexane. The product (4.9 g, 45 %) was dried under reduced pressure at room temperature. ^{1}H NMR (300 MHz, D_2O) δ = 7.1 (d, 2H, H_{ar}); 4.0 (m, 2H, OCH_2); 3.8 (s, 3H, OCH_3); 3.4 (m, 8H, $S(CH_2)_2(CH_2)_2$); 2.2 (m, 8H, $S(CH_2)_2(CH_2)_2$); 1.8 (1H); 1.7 (1H); 1.6 (2H); 1.4 (2H); 1.3 (1H); 1.2 (3H); 1.0 (d, J=6.6Hz, 3H, CH_3); 0.9 (d, J=6.7Hz, 6H; 2 x CH_3). ^{2}H NMR (61.5 MHz, D_2O), δ = 4.2 ppm. ^{13}C NMR (100 MHz, D_2O) δ = 21.3 (1C); 24.31/24.39 (2C); 26.4 (1C); 29.6 (1C); 30.7 (1C); 31.3 (1C); 37.6 (1C); 38.7 (1C); 40.9 (1C); 43.9 (2C); 45.5 (1C); 58.6 (1C); 70.0 (1C); 117.8/118.6 (2C); 121.9/122.4 (2C); 153.7/154.3 (2C).

Preparation of 2-(^{2}H-butylsulphanyl)methyl)-5-(^{2}H-chloromethyl)-1-(3,7-di-methyloctyloxy)-4-methoxybenzene, 15. A mixture of NaO*t*Bu (0.86 g, 8.9 mmol) and n-butanethiol (0.8 g, 8.9 mmol) in MeOD (20 ml) was stirred for 30 min at room temperature. The clear solution was added in one portion to a stirred solution of **14** (4.9 g, 8.9 mmol). After one hour the reaction mixture was neutralized with

aqueous HCl, if necessary, and concentrated in vacuo. The crude product was diluted with $CHCl_3$ (21 ml), the precipitate was filtered off and the solvent was evaporated. The obtained oil was diluted with petroleumether (boiling range 100-140 °C) and concentrated to remove the tetrahydrothiophene. This sequence was repeated three times to afford a light yellow viscous oil. A 3.7 g (8.9 mmol) of crude product was formed. ^{1}H NMR (300 MHz, $CDCl_3$) δ = 6.89/6.87 (d, 2H, H_{ar}); 4.0 (m, 2H, OCH_2); 2.5 (m, 2H, $SCH_2(CH_2)_2CH_3$); 1.9-1.2 (14H, $H_{alif.}$); 1.0 (3H, CH_3); 0.9 (9H, 3xCH_3). ^{2}H NMR (61.5 MHz, $C_2D_2Cl_4$), δ = 4.6 (-CD_2Cl); 4.0/3.8 (-CD_2SR). MS(CI, m/z, rel.int. (%)): 421 $[M+1]^+$.

Preparation of 2-(^{2}H-butylsulphinyl)methyl)-5-(^{2}H-chloromethyl)-1-(3,7-dimethyloctyloxy)-4-methoxybenzene, 16. An aqueous (35 wt%) solution of H_2O_2 (1.3 g, 13.4 mmol) was added dropwise to a solution of crude thioether **16** (8.9 mmol), TeO_2 (0.17 g, 1.1 mmol) and three drops of concentrated HCl in 1,4-dioxane (34 ml). The reaction was followed on TLC (time: 2.5 h) and as soon as the overoxidation took place, it was quenched by a saturated aqueous NaCl solution (30 ml). After extraction with $CHCl_3$ (3 x 30 ml), the organic layers were dried over $MgSO_4$ and concentrated in vacuo. The reaction mixture was purified by column chromatography (SiO_2, eluent hexane/ethylacetate 60/40) to give pure **16** (1.74 g, 65 %) starting from tetrahydrothiofeniumsalt as a light yellow viscous oil. ^{1}H NMR (300 MHz, $CDCl_3$) δ = 6.9 (d, 1H, H_{ar}); 6.8 (d, 1H, H_{ar}); 4.3/4.1 + 3.8/3.6 $CDCl_3$) δ = 6.9 (d, 1H, H_{ar}); 6.8 (d, 1H, H_{ar}); 4.3/4.1 + 3.8/3.6 (dd, 2H, ^{1}J = 130 Hz, $CH_2S(O)R$); 3.9 (m, 2H, OCH_2); 3.8 (s,3H, OCH_3); 1.9 (1H); 1.7 (1H); 1.6 (2H); 1.4 (2H); 1.3 (1H); 1.2 (3H); 1.0 (d, J=6.6Hz, 3H, CH_3); 0.9 (d, J=6.7Hz, 6H; 2 x CH_3). ^{2}H NMR (61.5 MHz, $C_2D_2Cl_4$), δ = 4.6 (-CD_2Cl); 4.0/3.8 (-CD_2SR).^{13}C NMR (100 MHz, $CDCl_3$) δ = 13.5 (1C); 19.8 (1C); 22.1 (1C); 22.6 (2C); 24.6 (2C); 27.9 (1C); 30.2 (1C); 36.6 (1C); 37.4 (1C); 39.2 (1C); 41.3 (1C); 49.7 (1C); 52.5 (1C); 56.4 (1C); 67.9 (1C); 112.8 (1C); 115.7 (1C); 119.7 (1C); 127.0 (1C); 151.4 (2C). MS(CI, m/z, rel.int. (%)): 437 $[M+1]^+$.

Preparation of precursor polymer of 2-(^{2}H-butylsulphinyl)methyl-5-(^{2}H-chloro-methyl)-1-(3,7-dimethyloctyloxy)-4-methoxybenzene, 17 according the SULPHINYL route. See before.

Thermal conversion of precursor polymer to conjugated polymer, 18. See before.

7.4 NMR measurements

7.4.1 Liquid state NMR experiments

^{1}H spectra of the monomers and conjugated polymers were acquired in a dedicated 5 mm probe on a Varian Inova 400 MHz (9.4 T) spectrometer in $CDCl_3$ and $C_2D_2Cl_4$ respectively. The ^{13}C spectra were obtained at 100 MHz with a dedicated carbon 10 mm probe at 40 °C. Typical acquisition parameters are: a spectral width of 21344 Hz, a filter band width equal to the spectral width, a pulse width of 13 μs, an acquisition time of 0.7 sec., a processing line broadening of 7.5 Hz. For both monomers and polymers, a solution of 46.5 mg in 3.5 ml $CDCl_3$, containing 30 mg (25 mM) chromium(III)-acetylacetonate to reduce the T_{1C} decay times, was used. According to this procedure a pulse preparation delay of only 5 s needs to be respected between consecutive pulses in order to obtain fully quantitative results. Inversed Gated Decoupling was used to avoid unequal NOE's. ^{1}H and ^{13}C chemical shifts were referenced relative to tetramethylsilane. For proton NMR, both standard 1D and 2D COSY spectra[2] were performed. For carbon NMR, fully quantitative 1D spectra, APT[3] (Attached Proton Test) and DEPT[4] (Distortionless Enhancement by Polarization Transfer) spectra were used. Carbon-proton 2D-heteronuclear correlation spectra HETCOR[5] were recorded using an evolution time corresponding to an average direct coupling $^1J_{CH}$ value of 140 Hz.

7.4.2 Solid state NMR experiments

7.4.2.1 ^{1}H wideline NMR

All proton wideline measurements were carried out on a Varian Inova 400 MHz spectrometer equipped with a wideline probe with a 5 mm coil. A spectral width of 2 MHz was used and a preparation delay time equal to 5 times the longest T_{1H} relaxation time was always maintained between successive pulses. The T_{2H} relaxation times were obtained by applying the solid echo pulse sequence[6]: ($90°_{x'}$ - $\tau/2$ - $90°_{y'}$ - $\tau/2$ - acquire) with an echo delay (τ) of 8 μs. The Free Induction Decays (FIDs) were analysed by means of the following equation: $M(t) = M_o^S \exp(-1/2\ (t/T_{2H}^S)^2) + M_o^L \exp(-t/T_{2H}^L)$, where T_{2H}^S is the decay time for a fast decaying component (Gaussian term) and T_{2H}^L for the slow decaying component (exponential term). M_o^S and M_o^L are the corresponding fractions of T_{2H}^S and T_{2H}^L, respectively.

The T_{1H} relaxation times were measured by means of a modified solid echo pulse sequence in which an inversion recovery filter was placed in front of the solid echo part: ($180°_{x'} – t_i$ - $90°_{x'}$ - $\tau/2$ - $90°_{y'}$ - $\tau/2$ – acquire). The following equation was used for the analysis of the integrated signals: $M(t) = M_\infty - (M_\infty - M_o) \exp(-t_i / T_{1H})$ where M_∞ is the intensity at equilibrium, M_o the intensity of the resonance at time t = 0, t_i is the variable delay time and T_{1H} is the proton spin-lattice relaxation time in the laboratory frame.

The $T_{1\rho H}$ decay times were measured by applying a spin-lock field (45 kHz) of variable duration after the initial $90°_{x'}$ pulse ($90°_{x'}$ – spin-lock - $\tau/2$ - $90°_{y'}$ - $\tau/2$ - acquire). For the analysis of the $T_{1\rho H}$ decay times, a sum of two exponential functions was used to describe the relaxation during the variable spin-lock time t_i. This is expressed in the following equation: $M(t) = \sum M_{0,j} \exp(-t_i / T_{1\rho H,j})$.

Data were analysed by non-linear least squares fitting methods employing the Levenberg-Marquardt algorithm[7] and Origin 6.1.

7.4.2.2 ^{13}C CP/MAS

The solid state relaxation measurements by means of cross polarization[8] and magic angle spinning[6,9] (CP/MAS) were recorded on an Inova 400 Varian spectrometer operating at 100 MHz. Magic angle spinning was performed at 6.0 kHz, making use of ceramic Si_3N_4 rotors. The aromatic signal of hexamethylbenzene was used to determine the Hartmann-Hahn condition for cross polarization and to calibrate the carbon chemical shift scale (132.1 ppm). For decoupling of the protons during acquisition a power of 65 kHz is used. The T_{1C} decay times were obtained by means of a standard inversion recovery pulse sequence (without CP) with decoupling of the protons during the acquisition. Other spectral parameters used were: a pulse width of 5.2 μs, an acquisition time of 20 ms and a spectral width of 50 kHz. A preparation delay time equal to 5 times the longest T_{1H} relaxation time was always maintained between successive pulses.

7.4.2.3 ^{13}C wideline NMR

^{13}C line shape studies were carried out an Inova 400 Varian spectrometer operating at 100 MHz by applying the solid echo pulse sequence: ($90°_{x'}$ - $\tau/2$ - $90°_{y'}$ - $\tau/2$ - acquire) with an echo delay (τ) of 5 μs without decoupling of the protons during acquisition. The T_{1C} decay times were obtained using the following pulse sequence: ($180°_{x'}$ – t_i - $90°_{x'}$ - $\tau/2$ - $90°_{y'}$ - $\tau/2$ – acquire).

7.4.2.4 ^{2}H wideline NMR

^{2}H NMR line shape spectra were obtained on an Inova 400 Varian spectrometer operating at 61.5 MHz using the quadrupole echo NMR pulse sequence[10] ($90°_{x'}$ - $\tau/2$ - $90°_{y'}$ - $\tau/2$ - acquire) with an echo delay (τ) of 15 μs. Measurements of the spin-lattice relaxation time T_1 were obtained with an inversion-recovery quadrupolar echo pulse sequence ($180°_{x'} – t_i$ - $90°_{x'}$ - $\tau/2$ - $90°_{y'}$ - $\tau/2$ – acquire).

7.5 Other measurements

7.5.1 Size exclusion chromatography

Molecular weights and molecular weight distributions were determined relative to polystyrene standards with a narrow polydispersity (Polymer Labs) by Size Exclusion Chromatography (SEC). Separation to hydrodynamic volume was obtained using light scattering experiments on a Spectra Series P100 (Spectra Physics) equipped with two mixed-B columns (10 μm, 2 x 30 cm x 7.5 mm, Polymer Labs) and a refractive index detector (Shodex) at 40 °C. SEC samples were filtered through a 45 μm filter. HPLC grade THF (p.a.) was used as the eluent at a constant flow of 1.0 ml/min.. Toluene is used as flow rate marker. Only for product **11,** a different GPC column (5 μm, 100 °A, 300 x 7.5 mm) had to be used.

7.5.2 Direct insertion probe mass spectroscopy

Direct Insertion Probe Mass Spectroscopy (DIP-MS) analyses were carried out on a Finnigan TSQ 70. Either chemical ionisation with isobutane as reagent gas, mass range 90-600 and heated at 120 °C/min from 30 to 650 °C or electron impact

mode, mass range 35-350 and an inter scan time of 2 s, were applied. The electron energy was 70 eV.

7.5.3 Ultraviolet visible spectroscopy

The in-situ UV/Vis spectra of the polymers were recorded on a Cary 500 UV-Vis-NIR spectrophotometer (interval 1 nm, scan rate 600 nm/min, continuous run from 200 to 800 nm). The precursor polymer was spincoated from a chloroform solution (6 mg/ml) on a quartz disc (diameter 25 mm, thickness 3 mm) at 1000 rpm. A non-isothermal heating experiment with a ramp of 2 °C/min and starting from ambient temperature up to 300 °C was carried out under a continuous flow of nitrogen in a Harrick High Temperature Cell (Safir).

7.5.4 Fourier Transform InfraRed spectroscopy

IR spectra were recorded on a FT-IR spectrometer (Perkin Elmer Spectrum One Spectrometer). The MDMO-PPV polymers, obtained after elimination in toluene at 50, 60, 65, 70, 80, 90, 100, 110 °C for 90 min, were spincoated at 500 rpm on a KBr pellet from a chloroform solution (6 mg/ml).

7.5.5 Wide angle X-ray scattering

Wide angle X-ray scattering measurements (WAXS) were carried out at room temperature on a URD-6 Seifert diffractometer equipped with a graphite monochromator. A Cu target X-ray tube was used as radiation source (λ = 1.542 Å), operating at a voltage of 40 kV and a current of 30 mA. The scattering angle 2θ was gradually increased from 1° to 60° with 0.1°. The WAXS patterns were resolved into Gaussian shape diffraction maxima by using the Levenberg-Marquardt non-linear fitting procedure implemented on the ORIGIN 6.1 software.

The amount of a given phase in the sample was calculated as the intensity ratio of the diffraction maxima of the phase concerned to the total WAXS pattern.

7.5.6 Rheology

The gelation behavior of the MDMO-PPV polymers in pure toluene (concentration 5 mg/ ml) was studied as a function of temperature using a CSL 2 – 500 (TA instruments). Starting from 55 °C, the solutions were cooled at a rate of 3 °C/min to minus 20 °C. The viscosity was measured continuously at a shear rate of 20 $s^{-1.}$

7.5.7 Differential Scanning Calorimetry

DSC measurements were recorded on a DSC 2920 (TA instruments) at a heating rate of 20 °C/min going from 20 °C to 200 °C

7.6 References

[1] Becker, H.; Spreitzer, H.; Ibrom, K.; Kreuder, W. *Macromolecules* **1999**, *32*, 4925-4932.

[2] Martin, G. ; Zektzer, A. S. *Two dimensional NMR methods for establishing molecular connectivity* **1988**, VCH Publishers, Inc.: Weinheim, Germany, 58-96.

[3] Patt, L.; Shoolery, J. N. *J. Magn. Resonance* **1982**, *46*, 535-539.

[4] Braun, S.; Kalinowski, O.S.; Berger, S. *100 and more basic NMR experiments* **1996**, VCH Publishers, New York, 150-154.

[5] Atta-ur-Rahman; *Nuclear Magnetic Resonance* **1986**, Springer-Verlag Inc.: New York, 260-271.

[6] Schaefer, J.; Stejskal, E. O. *J. Am. Chem. Soc.* **1976**, 98, 1031.

[7] D.W. Marquardt, *J. Soc. Ind. Appl. Math.* **1963**, 431.

[8] a) Pines, A.; Gibby, M. G.; Waugh, S. J. *J. Chem. Phys.* **1973**, 59,569. b) Stejskal, E. O.; Schaefer, A. J.; Waugh, S. J. *J. Magn. Reson.* **1977**, *28*, 105.

[9] a) Andrew, E.R.; Bradbury, A.; Eades, R. G. *Nature* **1958,** *182*, 1659. b) Lowe, I. J. *Phys. Rev. Lett.* **1959**, *2*, 285.

[10] a) Solomon, I. *Phys. Rev.* **1958**, *110*, 61. b) Davis, J. H.; Jeffrey, K. R.; Bloom, M.; Valic, M. I.; Higgs, T. P. *Chem. Phys. Lett.* **1976**, *42*, 390.

8. Summary, conclusion and perspectives

In the field of plastic electronics, further advancements to enhance the performance (e.g. lifetime, efficiency) of opto-electronic devices are needed to obtain realistic applications based on conductive polymers. As the polymer structure and morphology are two parameters that may affect the final device performance, understanding the relation between the polymer synthesis, polymer defects and morphology has been the main aim of this research project. The diversity of NMR experiments in both the liquid and solid state offers the possibility to elucidate not only the polymer structure, but also to obtain information about the molecular ordering and dynamics of polymer chains. The polymer of interest in this work is poly(2-methoxy-5-(3,7-dimethyloctyloxy)-1,4-phenylene vinylene) or MDMO-PPV, which is often used as active layer in opto-electronic devices.

In chapter one a short overview of the various factors which could influence the opto-electronic properties is presented. Besides typical applications in which conjugated polymers are used, the requirements that have to be fulfilled to obtain a high device performance are also described.

The physical basis of nuclear magnetic resonance (NMR) spectroscopy and relaxometry is summarized in chapter two.

In chapter three, the nature and amount of the structural defects in MDMO-PPV, synthesized by different precursor routes namely the Gilch and sulphinyl route, were examined to clarify the role of synthesis in their introduction. As the defect concentration was expected to be low, the polymers were selectively ^{13}C-labeled in

the main chain and studied by means of 1D and 2D liquid state NMR techniques. The amount of structural defects was derived from quantitative ^{13}C NMR spectra. As a major defect in eliminated Gilch MDMO-PPV a tolane-bisbenzyl (TBB) unit (11.2 %) due to head-to-head and tail-to-tail additions was found. Also the presence of non-eliminated groups (1.8 %) as well as chloro-vinyl bonds (ca 1.4%) were demonstrated.

The most remarkable distinction between Gilch and sulphinyl polymers is the absence of TBB moieties in the latter since only a considerable amount of noneliminated groups (6.9 %) was found in the standard sulphinyl MDMO-PPV. By increasing the elimination time or temperature the amount of noneliminated groups could be reduced to 2.0 % and 2.4 %, respectively. However, a two-step elimination procedure was shown to be the most efficient and results in a polymer with less than 0.5 % of noneliminated groups referred to as two-step eliminated MDMO-PPV. Furthermore, it was found that the observed aldehyde functionalities represent the end groups since oxygen clearly affects the termination reaction of the growing oligomers. In conclusion, the polymerization reaction via the sulphinyl precursor route in contrast to the Gilch precursor route is characterized by a very regular propagation step, which is attributed to the different chemistry used in both routes.

Chapter four describes the various solid state NMR techniques used to examine the chain ordering and dynamics of sulphinyl and Gilch MDMO-PPV in the solid state. The following techniques are briefly discussed: high resolution ^{13}C cross-polarization and magic angle spinning NMR with high-power proton decoupling (^{13}C CP/MAS), ^{1}H wideline, ^{2}H wideline and ^{13}C wideline NMR spectroscopy.

MDMO-PPV precursor polymers as a function of the elimination temperature were studied in chapter 5 to obtain a profound insight into the elimination process, but also into the chain dynamics. In-situ UV/Vis, FT-IR and ^{1}H wideline solid state

NMR spectroscopy have proven to be complementary techniques as all three techniques show that the elimination reaction starts around 70 °C. Both T_{2H} and $T_{1\rho H,}$ especially when measured at temperatures close to T_g, have shown to be sensitive toward the detection of the intermediate stages of the elimination process: initial, random formation of double bonds below 70 °C, blocks of conjugated/non-conjugated parts between 70 and 90 °C, and finally the formation of large conjugated sequences above 90°C. Especially the $T_{1\rho H}$ decay time seems to be extremely sensitive toward the detection of the final stage of elimination (cf. differences in $T_{1\rho H}^{L}$ for the one and two step elimination procedure at 110 °C) and shows that two-step eliminated MDMO-PPV has the lowest segmental chain motion. In that way $T_{1\rho H}^{L}$ measurements can be used toward the detection of the completion of elimination (constant decay time indicates complete conversion) instead of labour-intensive and time consuming ^{13}C liquid state NMR measurements on ^{13}C labeled polymers.

In chapter six the differences in the molecular ordering (morphology) and dynamics of sulphinyl and Gilch MDMO-PPV were studied by means of various analytical techniques. Although this study has not been completed yet, some interesting conclusions can already be drawn. ^{2}H line shape studies as a function of temperature have shown to be the most efficient toward the observation of rotational jumps of chain segments enclosed by structural sp^3 defects since no changes could be observed in the ^{13}C and ^{1}H solid state NMR spectra. An indication for the different chain organization and segmental chain dynamics between the three polymers was found in the difference in temperature of the appearance of the isotropic peak in the deuterium line shape spectra as well as in the differences in the T_{1C} relaxation decay times. WAXS and DSC measurements on the other hand provided confirmative information about the organization of the polymer chains. From the WAXS patterns of both sulphinyl polymers it was found that the amount of pseudo-ordered phase was three times higher for the standard

sulphinyl MDMO-PPV as compared to two-step eliminated polymer. The WAXS pattern of the Gilch MDMO-PPV on the other hand was completely different in that also crystalline domains were present next to amorphous and pseudo-ordered phase. The appearance of a melt endotherm in the DSC plot confirmed the WAXS results.

Concerning the T_{2H} and $T_{1\rho H}$ ^{1}H wideline results, it was found that the segmental chain motion of Gilch MDMO-PPV was higher compared to both sulphinyl polymers above 80 °C. This can explain the formation of the ordered structures in cooling down the polymerization solutions before precipitation. The higher degree of molecular ordering in the Gilch polymer is reflected both in the higher $T_{isotropic}$ in the solid state deuterium NMR spectra and the longer T_{1C} decay times. Furthermore it was found that above 80 °C the two-step eliminated sulphinyl MDMO-PPV was the most rigid as was expected on the basis of its lower amount of structural sp^3 defects resulting in an almost completely amorphous structure (shortest T_{1C} decay time). The higher chain stiffness compared to standard sulphinyl MDMO-PPV was represented in the higher $T_{isotropic}$ in the solid state deuterium NMR spectra.

As mentioned before, chapter six is still in progress and allows to work out further some interesting perspectives. Concerning the crystallinity of Gilch MDMO-PPV, it is preferred that some duplo syntheses and measurements are performed. If duplo experiments confirm the existence of a crystalline phase, the precipitation circumstances e.g. the duration of the cooling-down period and cooling rate, have to be studied in more detail. Furthermore, it would be interesting to carry out some WAXS measurements as a function of temperature to study the disappearance of the ordered domains. These experiments will learn us if there is relation between the disappearance of the ordered phase and the appearance of the isotropic peak in the ^{2}H solid state Pake patterns. Finally, photoluminescence spectroscopy may offer the possibility to verify whether the pseudo-ordered phase is formed by intermolecular interactions (aggregates).

In general, liquid state NMR spectroscopy has shown to be a unique tool for identifying polymerization defects, especially when present in low (< 5%) amounts. This since by isotopic labeling, the nuclei of interest can almost be studied exclusively as the intensity of the labeled nuclei is much enhanced with respect to the other resonance lines. Moreover, it allows quantitative measurements so that the amount of structural defects could be determined accurately. Besides structural information, the molecular dynamics and ordering can also be studied by means of a variety of solid state NMR experiments: ^{2}H line shape and ^{13}C relaxation decay time studies have been shown to be very useful to gain information about the molecular ordering, whereas ^{1}H relaxation time studies are more suitable for obtaining information about the segmental chain dynamics. Finally, this project has shown that the different analytical techniques employed provide complimentary information towards a more complete picture of the polymer morphology.

9. Samenvatting, besluit en perspectieven

Vooraleer opto-elektronische devices op basis van geconjugeerde polymeren praktische toepassing vinden, zijn er toch nog een aantal ontwikkelingen nodig om de performantie (levensduur, efficiëntie, enz.) van deze devices te verhogen. Twee factoren die bepalend zijn voor de performantie zijn enerzijds de polymeer-structuur en anderzijds de morfologie van de polymeerketens. Daarom is het verwerven van een dieper inzicht in de relatie tussen polymeersynthese, polymeer-defecten en morfologie onontbeerlijk. Om deze relatie te onderzoeken hebben we geöpteerd voor het poly(2-methoxy-5-(3,7-dimethyloctyloxy)-1,4-fenyleen vinyleen) of kortweg MDMO-PPV vermits dit polymeer gebruikt wordt als aktieve laag in tal van opto-elektronische devices.
Het uitgestrekt gamma aan nucleaire magnetische resonantie (NMR) experimenten in de vloeibare en vaste toestand laat niet alleen toe om de polymeerstructuur te bepalen, maar ook om de moleculaire dynamica en ordening van de polymeerketens te bestuderen.

In hoofdstuk één wordt er een kort overzicht gegeven van de verschillende factoren die de opto-elektronische eigenschappen kunnen beïnvloeden. Daarnaast worden er een aantal typische toepassingen op basis van geconjugeerde polymeren besproken, alsook de criteria die vervuld moeten worden om een hoge device performantie te bekomen.

De fysische basis van de NMR spectroscopie en relaxometrie is weergegeven in hoofdstuk twee.

Om de invloed van de polymerisatiemethode op het ontstaan van defecten te onderzoeken werd in hoofdstuk drie de aard van en hoeveelheid aan structurele

defecten bestudeerd in MDMO-PPV dat gesynthetiseerd werd via twee verschillende precursorroutes namelijk de Gilch en sulfinyl precursorroute. Aangezien verwacht werd dat de hoeveelheid structurele defecten laag was en dus niet detecteerbaar in de ^{13}C NMR spectra, werden er selectief ^{13}C-labels ingebouwd op de plaats van de dubbele binding en vervolgens werden de polymeren bestudeerd met 1D en 2D vloeibare toestand NMR spectroscopie. Op basis van kwantitatieve ^{13}C NMR spectra, kon de hoeveelheid aan structurele defecten bepaald worden. In het Gilch MDMO-PPV werden volgende structurele defecten gevonden: een tolaan-bisbenzyl eenheid als gevolg van kop-kop en staart-staart addities (11.2 %), niet-geëlimineerde groepen (1.8 %) en chlorovinyl bindingen (1.4 %). Het sulfinyl MDMO-PPV daarentegen werd enkel gekenmerkt door een onvolledige eliminatie: 6.9 % niet-geëlimineerde groepen. Door het verhogen van de eliminatietijd en -temperatuur kon de hoeveelheid aan niet-geëlimineerde groepen verminderd worden tot respectievelijk 2.0 en 2.4 %. Een zogenaamde twee-staps eliminatie procedure gaf aanleiding tot een polymeer met minder dan 0.5 % niet-geëlimineerde groepen. Zowel in het Gilch als het in sulfinyl polymeer kwamen aldehydegroepen voor die, zoals aangetoond, de eindgroepen van het polymeer voorstellen In het algemeen kunnen we besluiten dat de polymerisatie-reactie volgens de sulfinyl precursorroute leidt tot een meer regelmatige ketenopbouw ten opzichte van de Gilch precursorroute.

Hoofdstuk vier beschrijft de verschillende vaste stof NMR technieken zoals ^{13}C CP/MAS, ^{1}H wideline, ^{2}H wideline en ^{13}C wideline NMR spectroscopie, die aangewend werden om de moleculaire dynamica en ordening van de MDMO-PPVs te bestuderen.

In hoofdstuk vijf werden MDMO-PPV precursorpolymeren bestudeerd in functie van de eliminatietemperatuur om meer inzicht te verkrijgen in enerzijds het eliminatieproces en anderzijds in de mobiliteit van ketendelen. In-situ UV-Vis, FT-IR and ^{1}H wideline NMR spectroscopie toonden aan dat de eliminatiereactie start rond 70 °C. Zowel de T_{2H} als $T_{1\rho H}$ relaxatietijden waren geschikt om de verschillende stappen van het eliminatieproces te volgen: de vorming van initiële

dubbele bindingen beneden 70 °C, afwisselend geconjugeerde en niet-geconjugeerde sequenties tussen 70 en 90 °C, en uiteindelijk de vorming van een groot geconjugeerd systeem boven 90 °C. Vooral de $T_{1\rho H}$ relaxatietijd was gevoelig voor het vaststellen van het eindpunt van de eliminatie (zie ook de verschillen in $T_{1\rho H}{}^{L}$ voor één- en twee-staps geëlimineerd MDMO-PPV bij 110 °C). Hieruit bleek ook dat het twee-staps geëlimineerd MDMO-PPV de laagste segmentale ketenmobiliteit vertoont. Bovendien kunnen de $T_{1\rho H}$ metingen gebruikt worden als alternatief voor de tijdrovende ^{13}C NMR op ^{13}C-gelabelde polymeren.

In hoofdstuk zes werd het verschil in moleculaire ordening en dynamica van de sulfinyl en Gilch polymeren bestudeerd met verschillende analytische technieken. Hoewel dit hoofdstuk nog niet volledig is afgerond, kunnen er toch een aantal conclusies getrokken worden. In tegenstelling tot ^{1}H en ^{13}C wideline NMR spectra bleken ^{2}H line shape studies in functie van de temperatuur, uiterst geschikt voor het observeren van rotationele jumps van ketensegmenten ingesloten door structurele sp^3 defecten. Zowel het verschil in temperatuur waarbij de isotrope piek verschijnt in de ^{2}H wideline NMR spectra, $T_{isotroop}$, als de verschillende T_{1C} relaxatietijden, wezen op een verschillende ketenorganisatie en -mobiliteit. Bijkomende informatie over de morfologie van de polymeren werd verkregen met behulp van WAXS en DSC metingen. Uit het WAXS patroon van beide sulfinyl polymeren blijkt dat de gewichtsfractie aan pseudo-geordende fase drie maal zo hoog was voor het standaard sulfinyl MDMO-PPV. Het WAXS patroon van het Gilch MDMO-PPV daarentegen was totaal verschillend vermits er ook kristallijne gebiedjes voorkomen. Dit werd bevestigd door het verschijnen van een smelt-endotherm in de DCS plot. Uit de T_{2H} and $T_{1\rho H}$ ^{1}H wideline metingen boven 80 °C kon afgeleid worden dat het Gilch MDMO-PPV gekenmerkt wordt door een hogere segmentale keten mobiliteit ten opzichte van beide sulfinyl polymeren. De hogere graad van moleculaire ordening werd weerspiegeld in de hogere $T_{isotroop}$ in de ^{2}H solid state NMR spectra en de langere T_{1C} relaxatietijd. De hogere ketenimmobiliteit van het twee-staps geëlimineerd MDMO-PPV werd ook bevestigd door ^{1}H wideline metingen boven 80 °C en resulteert bijgevolg in een bijna volledig amorfe fase. De

hogere ketenstijfheid ten opzichte van het standaard sulfinyl MDMO-PPV kwam eveneens tot uiting in de hogere $T_{isotroop}$ in de ^2H solid state NMR spectra.
Zoals eerder vermeld, is hoofdstuk zes nog niet volledig afgerond en biedt het nog interessante perspectieven. Zo zullen er nog een aantal duplo syntheses en metingen moeten gebeuren om er zeker van te zijn dat in alle Gilch MDMO-PPVs een kristallijne fase voorkomt. Indien deze bevestigend zijn, zullen de parameters zoals afkoelsnelheid, temperatuur, enz. die aanleiding zouden kunnen geven tot het vormen van een kristallijne fase, onderzocht moeten worden.
Daarnaast loont het ook de moeite om WAXS metingen in functie van de temperatuur uit te voeren om vast te stellen of er een relatie is tussen het verdwijnen van de geordende fase en het verschijnen van de isotrope piek in de ^2H solid state NMR spectra. Om te zien of de pseudo-geordende fase een gevolg is van intermoleculaire interacties kunnen er ook nog fotoluminescentie metingen uitgevoerd worden.

Over het algemeen kunnen we stellen dat NMR spectroscopie in de vloeibare toestand een uniek middel is om polymerisatiedefecten op te sporen, vooral bij lage hoeveelheden (< 5%). Dit kan gerealiseerd worden door isotoopverrijking zodat bepaalde specifieke kernen bijna individueel bestudeerd kunnen worden omdat hun intensiteit zodanig verhoogd wordt ten opzichte van de andere resonantiesignalen van het spectrum. Daarenboven biedt het de mogelijkheid om kwantitatief te werken zodat de hoeveelheid aan structurele defecten nauwkeurig bepaald kan worden. Door het enorm gamma aan vaste stof NMR experimenten kan ook de moleculaire dynamica en ordening bestudeerd worden. ^2H wideline line shape studies en T_{1C} relaxatietijden bleken geschikt te zijn voor het bestuderen van de moleculaire ordening. ^1H wideline NMR studies daarentegen zijn ideaal voor het bestuderen van de segmentale ketenmobiliteit. Bovendien werd er aangetoond dat door een combinatie van analytische technieken, die complementair bleken te zijn, de polymeermorfologie bestudeerd kan worden.

10. List of abbreviations

γ	gyromagnetic ratio
μ	magnetic moment
θ	pulse angle
ω_1	frequency of the r. f. generator
τ_c	correlation time
$\theta_{I,S}$	angle between the internuclear vector and the main magnetic field B_o
ω_L	Larmor frequency
τ_p	pulse duration
AFM	atomic force microscopy
AM	air mass
APT	attached proton test
B_1	alternating radiofrequency field with frequency ω_1
B_o	external, static magnetic field
$C_2D_2Cl_4$	1,1,2,2 –tetrachloroethane – d_2
C_{60}	buckminsterfullerene
CB	conduction band
$CDCl_3$	chloroform-d
CP/MAS	cross-polarization and magic angle spinning
CSA	chemical shift anisotropy
D/A	donor/acceptor
DD	dipolar decoupling
DEPT	distortionless enhancement by polarization transfer
E_g	bandgap
EL	electroluminescence

Chapter 10

ESR	electron spin resonance
FET	field effect transistor
FID	free induction decay
FT-IR	fourier transform infra-red spectroscopy
h	Planck's constant
HETCOR	heteronuclear correlation
HOMO	highest occupied molecular orbital
I	nuclear spin
INADEQUATE	incredible natural abundance double quantum transfer experiment
ITO	indium tin oxide
J(ω)	spectral density function
L	path length over which spin diffusion can occur
LCD	liquid crystal display
LUMO	lowest unoccupied molecular orbital
M	magnetic quantum number
MDMO-PPV	poly(2-methoxy-5-(3,7-dimethyloctyloxy)-1,4-phenylene vinylene
MEH-PPV	poly(2-methoxy-5-(2'ethylhexoxy)-1,4- phenylene vinylene
M_o	macroscopic magnetization of the sample in the static field B_o
MS	mass spectroscopy
NMR	nuclear magnetic resonance spectroscopy
NOE	nuclear overhauser enhancement
OTFT	organic thin film transistor
P	nuclear angular momentum
PATs	poly(3-alkylthiophenes)
PCBM	(6,6)-phenyl-C_{61}-butyric acid

PET	polyethylene terephtalate
PL	photoluminescence
PLED	polymer light emitting diode
PPP	poly(*p*-phenylene)
PPV	poly(*p*-phenylene vinylene)
PR-TRMC	pulse radiation time-resolved microwave conductivity
R&D	research and development
$r_{I,S}$	internuclear distance
T_1	spin-lattice or longitudinal relaxation time
$T_{1\rho}$	relaxation time in the rotating frame
T_2	spin-spin or transverse relaxation time
TBB	tolane-bisbenzyl
TEM	transmission electron microscopy
TMPV	2,3,5,6-tetramethyl-1,4-phenylenevinylene
UV/Vis	ultraviolet visible spectroscopy
VB	valence band
WAXS	wide angle X-ray scattering
XPS	X-ray photoelectron spectroscopy